ELECTRON TUNNELING THROUGH THIN FILMS OF ALUMINUM NITRIDE

Thesis by

George W. Lewicki

In Partial Fulfillment of the Requirements
for the Degree of
Doctor of Philosophy

California Institute of Technology
Pasadena, California
1966
(Submitted March 28, 1966)

ACKNOWLEDGMENTS

The author wishes to express his indebtedness to his advisor, Dr. Carver A. Mead, for the guidance, encouragement, and patience given within the course of this work. The financial support of the Hughes Aircraft Company through a Howard Hughes Fellowship is gratefully acknowledged. The encouragement and aid of the author's wife, Bettina, who helped tangibly in the preparation of this manuscript is also appreciatively noted.

ABSTRACT

Thin film structures involving Aluminum as the base electrode, Aluminum Nitride as the insulating layer, Magnesium, Aluminum or Gold as the counterelectrodes were fabricated by nitriding a freshly deposited Aluminum film in a Nitrogen glow discharge with the thickness of the insulator varying from some thirty to ninety Angstroms with the express purpose of studying currents arising from the tunneling of electrons through the forbidden band of the insulator. Currents understood on the basis of the presently existing tunneling theory were observed for structures having thinner insulating regions. For structures having thicker insulating regions a temperature independent excess current was observed which could not be accounted for by the present tunneling theory.

The usual analysis of tunneling assumes the energy momentum relation of the insulator forbidden band to be parabolic and the shape of the barrier separating the two metal electrodes to be trapezoidal. Any deviation from the current voltage characteristic predicted by this model is normally attributed to the lack of validity in the assumption concerning the barrier shape. Data obtained in this research indicated that the barriers of the structures investigated were trapezoidal but that the insulator energy momentum relationship was non-parabolic. Consequently, the analysis was extended to cover the case of a trapezoidal

barrier with a semi-arbitrary energy momentum relationship. Greater freedom was obtained for the current voltage characteristics but certain relations between these characteristics and the insulator thickness were retained which could be used to determine whether or not the barrier of a particular structure was trapezoidal. These same relations also suggested a means of experimentally determining the insulator energy momentum relationship if the barrier could be considered trapezoidal.

The analysis was applied to the experimental data and a complete self consistent model for electron tunneling through thin insulating layers of Aluminum Nitride was obtained.

TABLE OF CONTENTS

Page

Abstract...i
Acknowledgements.......................................ii
Introduction...1

I. Models for electron tunneling through thin film structures.......................................3
1.1 Tunneling equations...................................6
1.1.1 Tunneling probability.........................6
1.1.2 Tunneling current...............................9
1.2 Barrier shape..11
1.3 Trapezoidal barrier with parabolic energy momentum relationship..........................16
1.3.1 Integration of tunneling equation...........17
1.3.2 Current voltage characteristics for a trapezoidal barrier...21
1.4 Trapezoidal barrier with arbitrary energy momentum relationship..........................27
1.4.1 Tunneling current equation.................28
1.4.2 Coefficients B(V), C(V), D(V)...........30
1.4.3 Dependence of characteristics on insulator thickness..36
1.5 Conclusion...40

II. Sample preparation and measurement procedures......43
2.1 Sample preparation......................................44
2.1.1 Substrate preparation..........................44
2.1.2 Evaporation of base electrode..............45
2.1.3 Nitridization of the base electrode..........45
2.1.4 Counterelectrodes.................................51
2.2 Measurement procedures................................56

III. Presentation of experimental results...............58
3.1 Properties of structures with Magnesium counterelectrodes...59
3.1.1 Current voltage characteristics..............59
3.1.2 Barrier geometry and insulator energy momentum relationship.......................75
3.2 Properties of structures with Aluminum counterelectrodes...92
3.2.1 Barrier geometry and insulator energy momentum relationship.......................93
3.2.2 Excess current voltage characteristics......97
3.3 Properties of structures with Gold counterelectrodes...112

INTRODUCTION

At sufficiently low temperatures, the current transfer through a sufficiently thin insulating film sandwiched between metal electrodes will be primarily by electron tunneling. The tunneling current voltage characteristic of a thin film structure, as it is determined by the tunneling probability of electrons within the metals incident upon the barrier presented by the insulator, is related to the forms of the wave solutions within the insulator forbidden band and thus to the insulator energy momentum relationship and the shape of the barrier.

Recent experimental investigations of tunneling through a variety of insulating materials sandwiched between various metal electrodes have been based on a model assuming a parabolic energy momentum relationship for the insulator and a trapezoidal barrier shape modified by the effects of image forces. It has been found in some cases that relatively poor agreement exists between current voltage characteristics observed experimentally and those expected on the basis of this model. The discrepancy has been attributed to a barrier deviating from a trapezoidal shape to an extent greater than that expected from the effect of image forces.

This work is a report of an experimental investigation of electron tunneling through thin insulating films of Aluminum Nitride

based on the possibility that the model appropriate to the thin film structures involves an essentially trapezoidal barrier characterized by a semi-arbitrary energy momentum relationship.

In Chapter I, the technique introduced by Stratton for the determination of current voltage characteristics of thin film structures based on a model assuming a parabolic energy momentum relationship for the insulator will be reproduced. This technique will be expanded to cover the case of a trapezoidal barrier with a semi-arbitrary energy momentum relationship. It will be seen that even though the tunneling current voltage characteristics acquire greater freedom certain relations between the insulator thickness and the shape of these characteristics are retained. These relations can be used to determine experimentally whether or not the barriers of particular structures can be considered trapezoidal. It will also be seen that once the barrier has been determined as trapezoidal, certain procedures exist which allow the determination of the barrier heights at the metal insulator interfaces and the energy momentum relationship characterizing the insulator forbidden band.

Chapter II describes the procedures used for the fabrication of thin film structures with AlN insulating films. Chapter III presents the results relevant to the anlysis carried out in Chapter I obtained from the experimental investigation of the structures Al-AlN-Mg; Al; Au.

CHAPTER I

MODELS FOR ELECTRON TUNNELING IN THIN FILM STRUCTURES

Current flow through thin film structures is limited by a barrier separating the electrons within the conduction bands of the two metals. This barrier is the result of the conduction band edge of the insulator lying above the fermi level of the structure. Transport of electrons can take place in either one of two ways, (see Figure I.1). Electrons having sufficient energy to overcome the barrier can propagate through the conduction band of the insulator, whereas less energetic electrons have a finite probability of tunneling through the forbidden band. The first process is commonly referred to as thermionic emission; the second process is known as tunneling. When the insulating region of a thin film structure is sufficiently thin, tunneling is expected to predominate.

The probability of an electron making a tunneling transition is related to the transmission of an electron wave through the forbidden band of the insulator and consequently to the form of the wave solutions within this band. Any attempt to predict the tunneling current voltage characteristics of a thin film structure must involve some assumption concerning the form of these wave solutions. In this work it will be assumed that the structure of

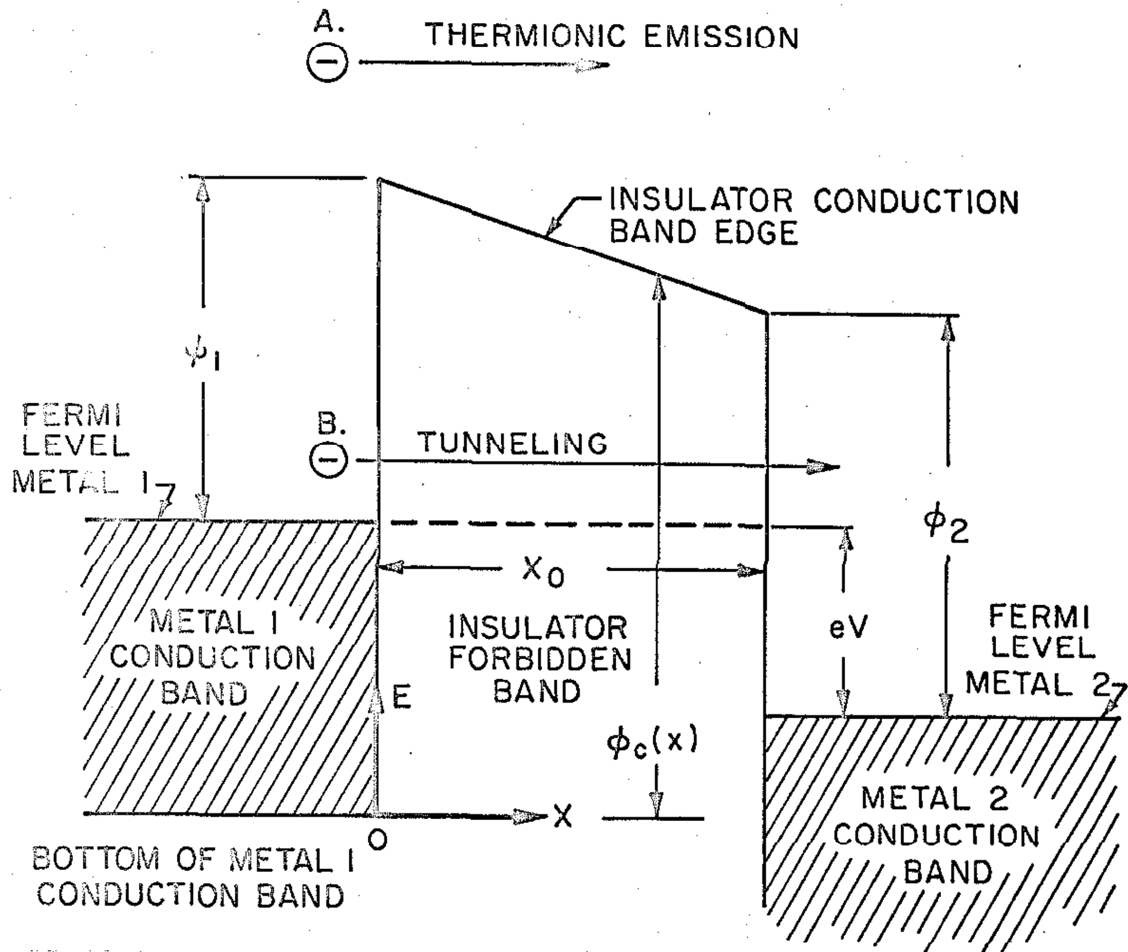

Figure 1.1 Energy band representation for thin film structure with positive voltage V applied to metal 2. Metal 2 is also referred to as the counterelectrode. Energy is referenced to bottom of metal 1 conduction band. Position is referenced to metal 1 insulator interface.

the insulator is uniform throughout its width and that as a result the wave solutions in the forbidden band are characterized by the energy momentum relationship of the insulator material. This assumption of structure uniformity also implies that the only factors governing the shape of the barrier presented by the insulator are the contact potentials at the two metal interfaces, the effect of image forces, and the possible existence of appreciable space charge within the insulator.

The tunneling current voltage characteristics based on 1) a trapezoidal barrier with a parabolic energy momentum relationship, and 2) a trapezoidal barrier with a semi-arbitrary energy momentum relationship will be presented in this chapter. The first model leads to a definite characteristic which in principle can be fitted to an experimental result to yield the relevant parameters associated with the model. It is presented mainly for historical reasons. An observed characteristic which can not be thus fitted can be the result of either a deviation of the barrier from a trapezoidal shape, a non-parabolic energy momentum relationship within the insulator forbidden band, or a combination of these two possibilities. The first possibility was found not to be applicable to the results obtained in the author's research and thus will not be considered. The second possibility was applicable; consequently the relations between the characteristics and a semi-arbitrary energy momentum relation-

ship for the case of a trapezoidal barrier will be developed. It will be seen that even though the second model gives the current voltage characteristics greater freedom, certain relations between these characteristics and their dependence upon the insulator thickness are retained which can be used to experimentally determine whether the barrier of a particular structure can be considered trapezoidal. Furthermore, these same relations allow the experimental determination of the energy momentum relationship characterizing the insulator forbidden band of a particular structure.

The following discussion will be based on the energy band representation of the thin film structure given in Figure 1.1. Unless it is specified otherwise all expressions leading towards current voltage relationships will correspond to a positive voltage applied to metal 2.

1.1 TUNNELING EQUATIONS

1.1.1 Tunneling Probability

An electron wave propagating in the conduction band of the first metal towards the insulator will be partially reflected at the metal insulator interface and partially transmitted to the conduction band of the opposite metal or the conduction band of the insulator. If the incident wave can be represented by the function $A \exp\left(\frac{i}{\hbar}\vec{p}_1 \cdot \vec{r}\right)$ and the transmitted wave by the function

$I \exp(\frac{i}{\hbar} \vec{p}_2 \cdot \vec{r})$, the transmission coefficient, given by the ratio $(\frac{I}{A})^2$, represents the probability that an electron incident on the barrier with a momentum $\vec{p}_1$ will make a tunneling transition, assuming that there is an unoccupied state available for transition. In the notation just used $\vec{r}$ is a vector denoting spatial position, $\vec{p}$ a vector denoting electron momentum and $\hbar$ is Planck's constant divided by 2π. Relating the tunneling probability to the transmission coefficient is justified in view of the fact that the function $A \exp(i \frac{\vec{p}_1 \vec{r}}{\hbar})$ can be considered to represent a stream of electrons flowing in the direction given by $\vec{p}_1$ with a density proportional to A^2.

The transmission coefficient can be determined by obtaining with the use of the W.K.B. approximation the forms of the wave solutions within the metals and insulator which correspond to a particular incident wave and by relating the amplitudes of these waves to the amplitude of the incident wave with the use of the W.K.B. connection formulae[1]. Continuity considerations require that the component of the wave momentum parallel to the metal insulator interfaces be equal for the wave solutions in all three regions. Conservation of energy requires that the energies associated with the wave solutions also be equal.

For an incident wave within the first metal given by $A \exp(\frac{i}{\hbar} (p_{1x}x + p_{1y}y + p_{1z}z))$, the corresponding wave solutions within all three regions of the thin film structure are:

$$F \exp\left[-\frac{i}{\hbar}(p_{1x} + p_{1y} + p_{1z})\right] \qquad (1.1)$$

representing the reflected wave within the conduction band of the first metal,

$$G \exp\left[\frac{i}{\hbar}\left(\int_{x_1}^{x} p_{x\,ins}(x)\,dx + p_{1y}y + p_{1z}z\right)\right] + H \exp\left[-\frac{i}{\hbar}\left(\int_{x_2}^{x} p_{x\,ins}(x)\,dx - p_{1y}y + p_{1z}z\right)\right] \qquad (1.2)$$

representing the incident and reflected waves within the forbidden band of the insulator and

$$I \exp\left[\frac{i}{\hbar}(p_{2x}x + p_{1y}y + p_{1z}z)\right] \qquad (1.3)$$

representing the transmitted wave within the conduction band of the opposite metal. The integral representation of the waves within the forbidden band (equation (1.2)) are the result of the W.K.B. approximation; the limits on this integral, x_1 and x_2, represent the turning points of the barrier. A constant energy level in the forbidden band does not necessarily involve a constant value of p_{ins}; this parameter, in general complex, is a function of position in that the forbidden band is normally distorted as a result of the existence of a macroscopic potential variation within the insulator arising from image forces, space charge, and internal or applied fields.

The W.K.B. connection formulae relate to each other the amplitudes of the wave solutions within all three regions of the thin film structure and thus allow the determination of the transmission coefficient. As a result, the probability that an electron incident on the barrier will make a tunneling transition, assuming that there is an unoccupied state available for the transition, can be expressed as

$$P(p_t, E) = \exp\left[-\frac{2}{\hbar}\int_{x_1}^{x_2} \mathrm{Im}\, p_{x\,ins}(x)\,dx\right] = \exp\left[-\frac{2}{\hbar}(x_2 - x_1)\,\overline{\mathrm{Im}\, p_{x\,ins}}\right] \qquad (1.4)$$

if the absolute value of the exponent in the exponential is much greater than unity and where $\overline{\mathrm{Im}\, p_{x\,ins}} = \frac{1}{x_2 - x_1}\int_{x_1}^{x_2} \mathrm{Im}\, p_{x\,ins}(x)\,dx$

The tunneling probability is a function of the transverse momentum and energy E of the incident electron and the shape of the barrier presented by the insulator in as much as Im p_{ins} is obtained from the energy momentum relationship characterizing the forbidden band with the conditions that transverse momentum and energy be conserved during a transition.

1.1.2 Tunneling Current.

The expression for the current resulting from the tunneling of electrons between conduction region 1 and conduction region 2 which are separated by a forbidden band can be arrived at in a straightforward manner. The number of electrons incident on the barrier in conduction region 1 per unit second per unit

area with momentum components within the usual infinitesimal limits and with unoccupied states available for transition is given by

$$dN_1 = \frac{2}{h^3} dp_{x1}\, dp_y\, dp_z \frac{\partial E}{\partial p_{x1}} \{f_1(E)[1-f_2(E)]\} \qquad (1.5)$$

where $f_1(E)$ and $f_2(E)$ are the Fermi - Dirac distribution functions in conducting reflons 1 and 2. An analogous expression holds for incident electrons in conducting region 2.

$$dN_2 = \frac{2}{h^3} dp_{x2}\, dp_y\, dp_z \frac{\partial E}{\partial p_{x2}} \{f_2(E)[1-f_1(E)]\} \qquad (1.6)$$

Multiplying (1.5) and (1.6) by the tunneling probability and the electron charge, subtracting (1.6) from (1.5), and integrating over all possible momenta yields the tunneling current density in the direction corresponding to flow of electrons from region 1. to region 2. The integration over p_{x1} and p_{x2} can be replaced by an integration over energy as a result of the velocity factors $\frac{\partial E}{\partial p_{x1}}$ and $\frac{\partial E}{\partial p_{x2}}$. Thus the current is more conveniently expressed as

$$J = \frac{2e}{h^3} \int \{f_1(E) - f_2(E)\} \{\int P(E, p_y, p_z)\, dp_y\, dp_z\}\, dE \qquad (1.7)$$

where the integration within the second bracketed term is carried out with energy E kept constant. The limits in the integrations are defined by the conditions that the transverse momenta and energy be conserved during a tunneling transition. A

more rigorous derivation of this result can be found in the paper presented by Harrison[2]. Throughout the remainder of this work current density will be referred to as current.

Before (1.7) can be used for predicting current voltage characteristics of a thin film structure the energy momentum relationships within the metal and insulator regions and the distortion of the forbidden band (barrier shape) must be postulated.

1.2 BARRIER SHAPE

If the effects of image forces and space charge can be neglected, the barrier will be trapezoidal and characterized by the barrier energies (contact potentials) at the two metal insulator interfaces. Barrier energies at metal insulator interfaces can in some cases be related to the difference between the work function or electronegativity of the metal and the electron affinity of the insulator depending on whether the bonding within the insulator is predominantly covalent or ionic[3]. On the other hand, the existence of high densities of surface states at the metal insulator interface can result in an effective shielding of the insulator leading to a barrier energy independent of the metal used for contact[4]. The important point is that the use of different metals for counterelectrodes may lead to different barrier energies at one of the metal insulator interfaces of a thin film structure.

A positive potential applied to the second metal electrode

will depress the fermi level of this electrode with respect to that of the first electrode by an energy eV. The energy of the insulator conduction band edge referenced to the conduction band of the first metal can then be expressed as

$$\phi_c(x) = \phi_1 - (\phi_1 - \phi_2)\frac{x}{x_0} - eV\frac{x}{x_0} + E_{f1} \qquad (1.8)$$

where ϕ_1 and ϕ_2 are the barrier energies at the metal insulator interfaces and E_{fl} is the fermi energy of metal l.

An electron within the insulator will induce charge on the two metal electrodes and thus experience a force resulting from the electric field generated by the induced charge. Use of image methods leads to a series solution for the potential lowering expected from this effect[5].

$$\Delta\phi_{IM} = \frac{-e^2}{8\pi K_0 \epsilon_0 x_0}\left[\sum_{n=0}^{n=\infty}\frac{2(2n+1)}{(2n+1)^2 - 4(\frac{x}{x_0}-\frac{1}{2})^2} - \sum_{n=1}^{n=\infty}\frac{1}{n}\right] \qquad (1.9)$$

In the above expression ϵ_0 represents the permitivity of free space and K_0 the optical dielectric constant of the insulator. The series is awkward to handle and can be approximated by a function which upon expansion has coefficients very near in value to those of the series

$$\Delta\phi_{IM} \approx -\frac{e^2}{8\pi K_0 \epsilon_0 x_0}\left\{\ln 2 + 2\frac{(2x/x_0 - 1)^2}{1-(2x/x_0-1)^2}\right\} \qquad (1.10)$$

The classical electrostatic solution is expected to be valid only for distances away from the metal electrodes greater than those of the order of atomic spacings[6,7] (a few Angstroms). Thus the infinite potential lowering at the metal insulator interfaces predicted by (1.9) can be ignored. The usual procedure for describing the potential near the interfaces involves joining the barrier height, which includes the effects of the image forces, to a line which then leads the barrier height to the bottom of the conduction band of the metal[7] or to the fermi level of the metal[6].

The effect of image forces is to lower the barrier and to decrease its width; the effect becomes more pronounced for lower insulator thicknesses and barrier heights. It must be pointed out that for values of insulator thicknesses and barrier heights encountered in this particular investigation of tunneling, the potential lowering resulting from image forces can be considered as a very small second order effect. The value for the optical dielectric constant of Aluminum Nitride as reported in the literature is 4.41[8]; the thinnest insulating region for the structures experimentally investigated was in excess of 30 Å. For the purpose of showing the magnitude of the effect of image forces, the shape of a rectangular barrier of height 1.5 eV and thickness 30 Å is given in Figure 1.2 with and without the image potential lowering. There it can be seen that the barrier

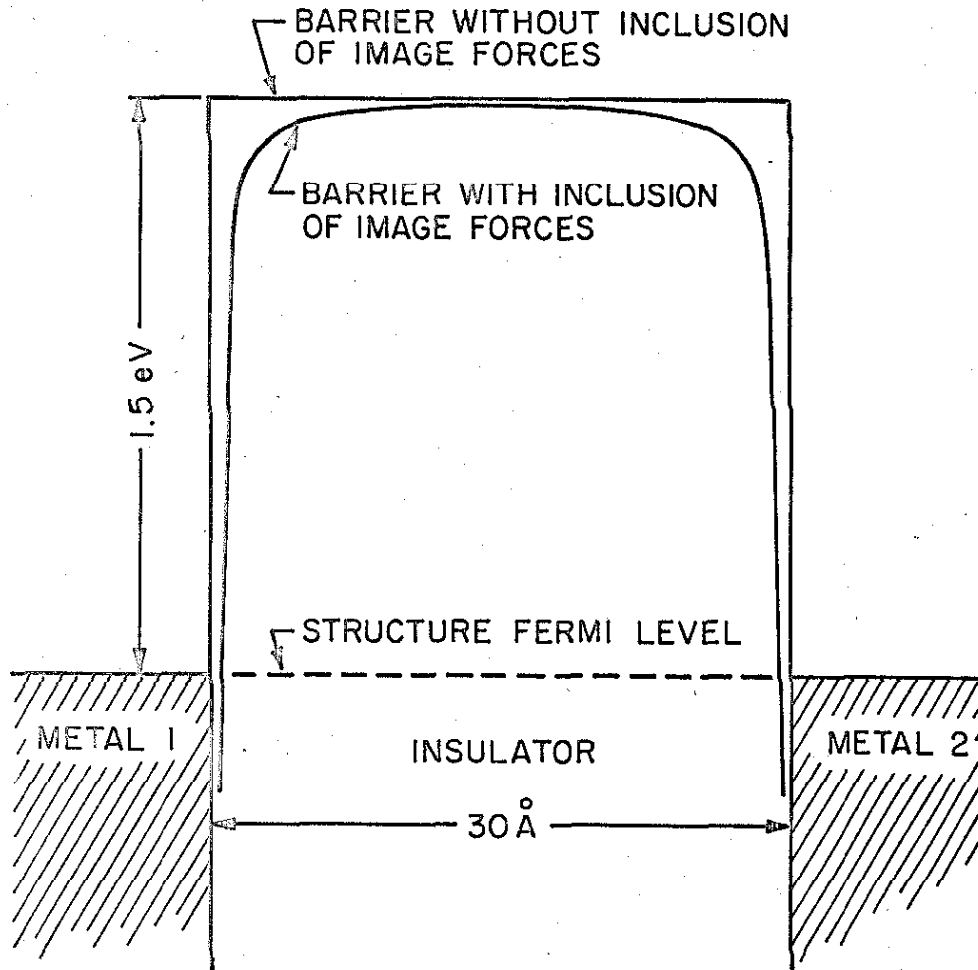

Figure 1.2 Rectangular barrier with barrier energy of 1.5 eV and thickness 30 Å with and without potential lowering expected from image forces. The value of the optical dielectric constant is assumed to be 4.41

essentially retains its trapezoidal shape; the potential lowering midway between the counterelectrodes is approximately 37 millivolts, the reduction in barrier thickness at the fermi level of the structure is approximately 2 Å.

The inclusion of the image force potential lowering in the equations describing the tunneling current leads to expressions which can only be solved numerically. This last consideration, the essentially zero order nature of the tunneling theory, and the magnitude of the image force potential lowering as shown in Figure 1.2 lead to the conclusion that a detailed analysis of the effect of image forces on the current voltage characteristics is not warranted.

Appreciable space charge within the insulator will also distort the shape of the barrier. Negative charge in acceptor type states below the fermi level will tend to raise the barrier; positive charge resulting from empty donor type states above the fermi level will tend to lower the barrier. If the space charge density throughout the insulator is uniform and independent of applied voltage, the barrier shape becomes

$$\phi_c = E_{f_1} + \phi_1 + (\phi_1 - \phi_2)\frac{x}{x_0} - V\frac{x}{x_0} + \frac{N_s e^2}{2k_s\epsilon_0}\frac{x}{x_0}\left(1 - \frac{x}{x_0}\right) - \Delta\phi_{IM} \qquad (1.11)$$

where k_s is the static dielectric constant of the insulator. This expression is valid only if the fermi level lies at least a few kT above or below the energy levels of the acceptor or donor type

states responsible for the space charge. (k represents Boltzmann's constant and T absolute temperature).

For the potential lowering or increase midway between the two metal electrodes resulting from a uniformly distributed space charge to be comparable to the magnitude of the barrier heights, (in the order of 1 eV) for an insulator thickness of 50Å, N_s would have to be in the order of $10^{20}/cm^3$ assuming a static dielectric constant of 8.5 for the insulator. (This value of the static dielectric constant is the one reported in the literature for bulk Aluminum Nitride[9].) The density of states just obtained is high, but of course not entirely out of the realm of possibility when it is realized that most insulators used in thin film structures are essentially amorphous.

The conclusion to be reached from the preceeding discussion is that if the thin film structures investigated in this research can be separated into three physically separate regions, the shape of the barrier separating the electrons in the conduction bands of the two metals is expected to be essentially trapezoidal if the space charge density within the insulator is less than $10^{19}/cm^3$.

1.3 TRAPEZOIDAL BARRIER WITH A PARABOLIC ENERGY MOMENTUM RELATIONSHIP.

Relatively simple expressions can be obtained for the tunneling current if the energy momentum relationship within all three regions of a thin film structure is assumed to be parabolic, that

is

$$E - E_c = \frac{p^2}{2m^*} \qquad (1.12)$$

where E_c is the energy of the conduction band edge of either of the metals or the insulator depending on the region of the thin film structure under consideration and m^* is an effective mass. For E-E_c, p will be equal to zero; for $E<E_c$, p will be imaginary.

1.3.1 Integration of Tunneling Equation

If the insulator conduction band edge referenced to the bottom of the conduction band of metal 1 is given by $\phi_c(x)$, the imaginary value of $p_{x\ ins}$ becomes

$$Im\ p_{INS}(x) = (2m^*)^{1/2}\left[\phi_c(x) - E + \frac{p_y^2 + p_z^2}{2m^*}\right]^{1/2} \qquad (1.13)$$

and the tunneling probability

$$P(E,p_\perp) = P(E_x) = exp\left[\frac{-2(2m^*)^{1/2}}{\hbar}\int_{x_1}^{x_2}(\phi_c(x) - E_x)^{1/2}dx\right] \qquad (1.14)$$

where E_x represents the x component of the energy of the incident electron. The form of (1.14) allows a change of variables from $dp_y\ dp_z$ to dE_x in the tunneling current equation (1.7) which becomes

$$J = \frac{4\pi m^* e}{h^3}\int_0^\infty\{f_1(E) - f_2(E)\}\{\int_0^E P(E_x)dE_x\}dE \qquad (1.15)$$

Integrating by parts leads to the simpler expression

$$J = \frac{4\pi m^* e}{h^3} \int_0^\infty P(E_x) \left\{ kT \ln \frac{1+\exp[(E_{f_1}-E_x)/kT]}{1+\exp[(E_{f_1}-eV-E_x)/kT]} \right\} dE_x \quad (1.16)$$

where V represents the positive voltage applied to metal 2.

Stratton[10] points out that a similar result is obtained if the effective mass m_i^* characterizing the parabolic energy momentum relationship of the insulator is smaller than the effective mass m_m^* appropriate to the energy momentum relationships of the metals. The current is given by an expression identical to (1.16) with the exception that m^* is replaced by m_i^*

Exact integration of (1.16) is not possible even for the simplest barrier shapes. Two approximate techniques are available.[10,11] The one reproduced here will be that first applied to this particular problem by Stratton. The bracketed term in (1.16), commonly referred to as the supply function, has the major part of its distribution below the fermi level of the first metal. For the purpose of visulaizing its form, the supply function can be approximated by the sum of two simple distributions, one temperature dependent and one temperature independent.

$$S_0(E_x) + S_T(E_x, kT) = kT \ln \frac{1+\exp[(E_{f_1}-E_x)/kT]}{1+\exp[(E_{f_1}-E_x-eV)/kT]} \quad (1.17)$$

where

$$S_0(E_x) = \begin{cases} 0 & \text{for } (E_{fl}-E_x) < 0 \\ (E_{fl}-E_x) & \text{for } 0 < (E_{fl}-E_x) < eV \\ eV & \text{for } E_{fl}-E_x > eV \end{cases} \qquad (1.18)$$

$$S_T(E_x, kT) = kT \ln 2 \{\exp[-[(E_{fl}-E_x)/kT]] - \exp[-[(E_{fl}-E_x-eV)/kT]]\} \qquad (1.19)$$

Since the exponent of the tunneling probability rapidly becomes more negative with increasing $(E_{fl}-E_x)$ it is expected that for sufficiently low temperatures the majority of the integrand of (1.12) will be in the vicinity of the fermi energy E_{fl}. This suggests the expansion of the exponent of the tunneling probability in powers of x directed energy about this fermi level. Using the notation of Stratton, the expansion is given as

$$-\ln P(E_x) = b + c(E_{fl}-E_x) + f(E_{fl}-E_x)^2 + \cdots \qquad (1.20)$$

If the temperature is sufficiently low, $ckT \ll 1$, and the variation of the tunneling probability exponent with $(E_{fl}-E_x)$ sufficiently rapid, then only the first two terms of the expansion are necessary for a satisfactory evaluation of (1.12). The integration can be carried out to yield

$$J = \frac{4\pi m_i^* e}{h^3} \frac{\pi c k T}{\sin \pi c k T} \frac{1-\exp(-ceV)}{c^2} \exp[-b] \quad (1.21)$$

The temperature dependent term may be represented by only the first two terms of an expansion in powers of ckT since (1.17) is only valid for $ckT \ll 1$.

$$J = \frac{4\pi m_i^* e}{h^3} \left\{1 + \frac{\pi^2}{6}(ckT)^2\right\} \frac{1-\exp(-ceV)}{c^2} \exp[-b] \quad (1.22)$$

The tunneling current resulting from the application of a positive voltage to metal I, under appropriate conditions, is seen to be proportional to the product of the tunneling probability corresponding to an incident electron with zero transverse momentum and an energy equal to the fermi energy of metal I and an effective number of tunneling electrons incident on the first metal insulator interface per unit area per second. The increase in current with increasing voltage is related to the variation of the two terms of this product. At low voltages, $ceV \ll 1$, the effective number of tunneling electrons is limited by the number of unoccupied states within the conduction band of the opposite metal available for transition. The effective number of tunneling electrons increases linearly with voltage while the tunneling probability remains essentially constant. Thus for $ceV \ll 1$

$$J \approx V\frac{4\pi m_i^* e^2}{h^3 c}\left\{1+\frac{\pi^2}{6}(ckT)^2\right\}\exp\left[-b(0)\right] \qquad (1.23)$$

For $ceV \gtrsim 1$ an increase in voltage effects an increase in the number of available states only for incident electrons with x directed energies too far below the fermi energy of metal I to lead to a significant increase in the tunneling current. Consequently, the effective number of tunneling electrons is determined by the rate of variation of the tunneling probability with $(E_{fI}-E_x)$ and the current is approximately given by

$$J \approx \frac{4\pi m_i^* e}{h^3 c^2}\left\{1+\frac{\pi^2}{6}(ckT)^2\right\}\exp\left[-b(V)\right] \qquad (1.24)$$

1.3.2 Current Voltage Characteristics for a Trapezoidal Barrier.

For an arbitrary barrier shape, the coefficients b(V) and c(V) are defined by the following relations

$$b(V) = \alpha\int_{x_1}^{x_2}\left[\phi_c(x,V)-E_{fI}\right]^{1/2}dx \qquad (1.25)$$

and

$$c(V) = \frac{\alpha}{2}\int_{x_1}^{x_2}[\phi_c(x,V) - E_f]^{-1/2}dx \qquad (1.26)$$

where $\alpha = \frac{2}{\hbar}\sqrt{2m_c^*} = 1.025\sqrt{\frac{m_c^*}{m}}\ [eV]^{-1/2}[\text{Å}]^{-1}$

and m = free electron mass.

For the trapezoidal barrier given by (1.8), the integrals in (1.25) and (1.26) can be solved exactly to yield

$$b_{+,-}(V) = \alpha x_0 \frac{\{\phi_{1,2}^{3/2} - (\phi_{2,1} - eV)^{3/2}\}}{3/2\{\phi_{1,2} - \phi_{2,1} + eV\}} \quad \text{for } eV < \phi_{2,1} \qquad (1.27)$$

$$b_{+,-}(V) = \frac{2}{3}\alpha x_0 \frac{\phi_{1,2}^{3/2}}{\phi_{1,2} - \phi_{2,1} + eV} \quad \text{for } eV > \phi_{2,1} \qquad (1.28)$$

$$c_{+,-}(V) = \alpha x_0 \frac{\{\phi_{1,2}^{1/2} - (\phi_{2,1} - eV)^{1/2}\}}{\{\phi_{1,2} - \phi_{2,1} + eV\}} \quad \text{for } eV < \phi_{2,1} \qquad (1.29)$$

$$c_{+,-}(V) = \alpha x_0 \frac{\phi_{1,2}^{1/2}}{\phi_{1,2} - \phi_{2,1} + eV} \quad \text{for } eV > \phi_{2,1} \qquad (1.30)$$

where the subscripts "+" and "-" are used to designate the coefficients corresponding to positive voltages applied to metals 1 and 2 respectively and x_o is the insulating region thickness.

The tunneling current has two characteristic regions. The

first of these corresponds to electron tunneling from the vicinity of the fermi level of one of the metals to the conduction band of the other metal which occurs for voltages smaller than $\frac{\phi_2}{e}$ or $\frac{\phi_1}{e}$ depending on whether the positive voltage is applied to metal 2 or metal 1 respectively; the second region corresponds to tunneling of electrons from the vicinity of the fermi level of one of the metals to the conduction band of the insulator which occurs for voltages greater than $\frac{\phi_2}{e}$ or $\frac{\phi_1}{e}$ depending on the polarity of applied voltage.

As has already been mentioned, for $ceV \ll 1$, the current varies linearly with voltage. For higher applied voltages, or $ceV \gtrsim 1$, the increase in current becomes essentially proportional to the increase in tunneling probability since the variation of the normalized coefficient $\frac{c(0)}{c(V)}$ is small when compared to the variation of the tunneling probability if $b(0)$ is sufficiently large. The coefficient $b(V)$ is a slowly decreasing function of voltage with a negative second derivative for voltages corresponding to electrode to electrode tunneling. Consequently, for $ceV \gtrsim 1$ and $V < \phi_{2,1}/e$, the current will rise with voltage more rapidly than at a constant exponential rate. For $V \gtrsim \phi_{2,1}/e$, $b(V)$ continues to decrease but its second derivative with respect to voltage becomes positive and the current increases with voltage at a slower than exponential rate.

In asymmetric barriers the current is also asymmetric.

For voltages $V_{+,-} < \frac{\phi_{2,1}}{e}$, the current will be greater for a positive voltage applied to the metal having the lower barrier energy when compared to the current resulting from the same voltage applied to the metal with the higher barrier energy. For voltages effecting electrode to insulator tunneling the current asymmetry becomes opposite to that at lower voltages.

The general features of the current voltage characteristic predicted by a trapezoidal barrier with a parabolic energy momentum relationship are shown in Figure 1.3 where the barrier parameters chosen are barrier energies of 1.5 and 2 eV and an insulator thickness and effective mass defined by the product $\alpha x_o = 25$.

The applicability of the model involving a trapezoidal barrier with a parabolic energy momentum relationship to a thin film structure is judged as to how well an observed current voltage characteristic fits that predicted on the basis of three arbitrary parameters (ϕ_1, ϕ_2 and the product αx_0) and as to the plausibility of the magnitudes of the parameters. Further verification of the model is also provided if the observed temperature dependence of a tunneling current has the form predicted by (1.22) and as to whether the coefficient c(V) experimentally obtained in this manner agrees with that expected on the basis of the values for the barrier energies and the product αx_o deduced from the observed tunneling current voltage characteristic.

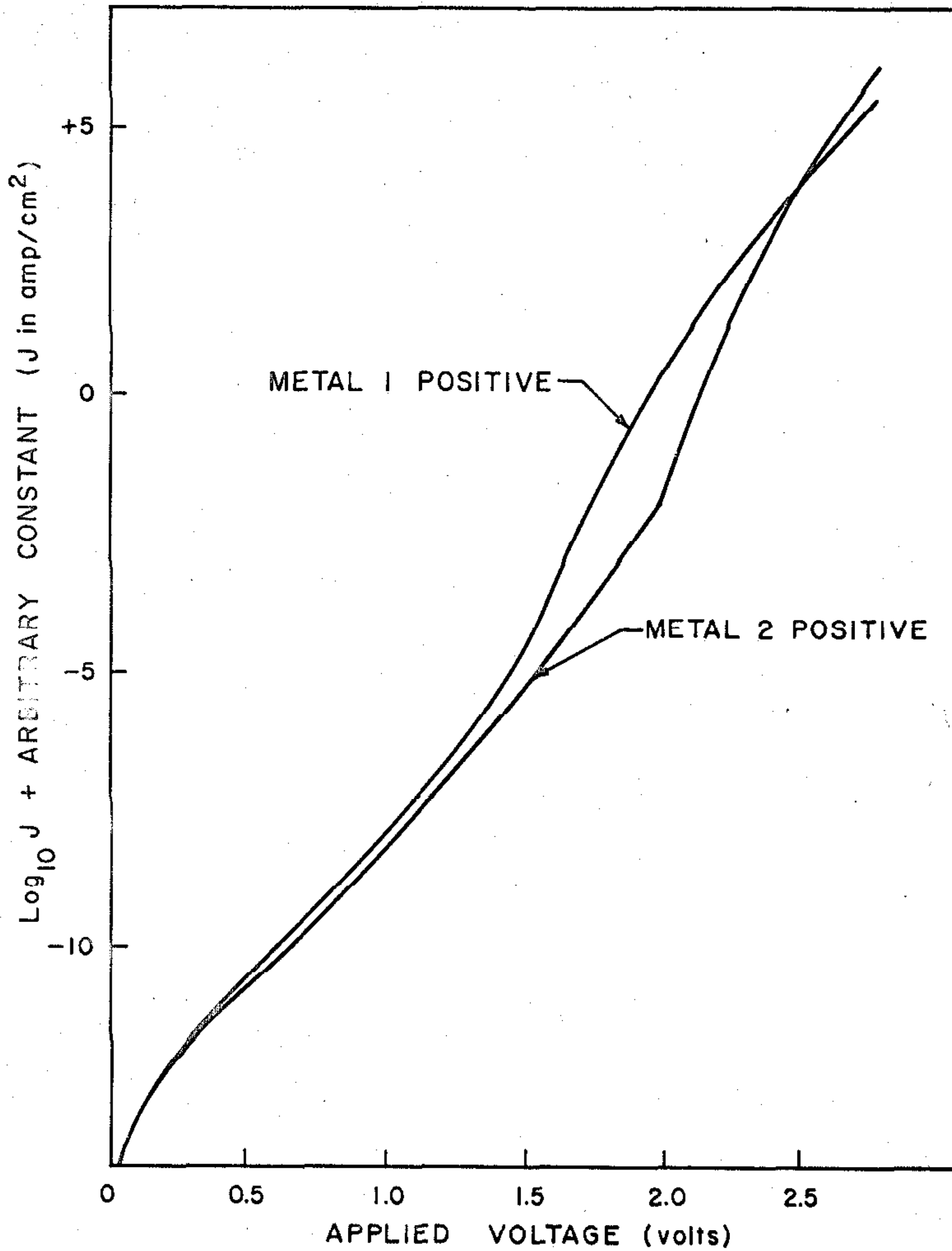

Figure 1.3 Zero temperature current voltage characteristic of thin film structure defined by a trapezoidal barrier with a parabolic energy momentum relationship. $\phi_1 = 1.5$ eV, $\phi_2 = 2.0$eV; $\alpha x_o = 25$; $m^*_{ins}/m = 1/4$.

Inspection of relations (1.29) and (1.30) will show that the coefficient $c(V)$ has a behavior which in principle allows the identification of the barrier heights associated with a trapezoidal barrier. For $V < \phi_{2,1}$, $c_{+,-}(V)$ is a slowly increasing function of voltage while for $V > \phi_{2,1}$, $c_{+,-}(V)$ is a decreasing function of voltage. The resulting cusps in the coefficient $c_{+,-}(V)$ occurring at voltages equal to $\frac{\phi_2}{e}$ and $\frac{\phi_1}{e}$ allow a verification of the barrier energies deduced from current voltage characteristics by measurement of the tunneling current temperature dependence.

Agreement with the model just described has been claimed for structures using Aluminum Oxide as the insulating layer; the basis of the agreement was the fitting of theoretical and experimental current voltage characteristics over a limited range of applied voltage with the use of plausible values for barrier energies, insulator thickness, and insulator effective mass.[12] Departures from agreement have also been observed in these same structures; barrier energies deduced from temperature measurements were not consistent with the observed current voltage characteristics.[13] The discrepancies have been interpreted as the result of the barrier deviating from a trapezoidal shape to an extent greater than that expected on the basis of image forces. Thus the coefficients $c(V)$ and $b(V)$, determined experimentally from the dependence of tunneling current on voltage and temperature, have been presented with the implication that some par-

ticular barrier shape could possibly account for the detailed dependence of these coefficients on voltage.[13]

The model involving a trapezoidal barrier characterized by a parabolic energy momentum relationship was found not to be applicable to the thin film structures investigated in the author's research. The data obtained implied that the inapplicability of the model was not the result of the barrier deviating from a trapezoidal shape but that of the energy momentum relationship within the insulator forbidden band being nonparabolic.

1.4 TRAPEZOIDAL BARRIER WITH ARBITRARY ENERGY MOMENTUM RELATIONSHIP[14]

The tunneling current voltage characteristic as it is determined by the tunneling probability is extremely sensitive to the insulator energy momentum relationship. In this section the implications of a semi-arbitrary but well behaved energy momentum relationship will be considered. It will be shown that even though current voltage characteristics acquire greater freedom certain relations between these characteristics and the insulator thickness are retained which provide a basis for determining whether or not a barrier is trapezoidal. Furthermore, these same relations provide a means for the experimental determination of the insulator energy momentum relationship once the barrier has been found to be trapezoidal.

1.4.1 Tunneling Current Equation.

The assumption of a parabolic energy momentum relationship defined by an effective mass m_m^* within both of the metals is retained. A well behaved and in this sense semi-arbitrary energy momentum relationship is assumed for the insulating region.

$$\frac{p_{INS}^2}{2m_i^*} = g(\phi_c - E) \tag{1.31}$$

$$Im\, p_{INS} = [2m_i^*]^{1/2}[g(\phi_c - E)]^{1/2} \tag{1.32}$$

This is to say that the function $g(\phi_c - E)$ does not depart too greatly from the usual $(\phi_c - E)$; it will be positive for $\phi_c > E$, negative for $\phi_c < E$, and equal to zero for $\phi_c = E$. As a result, the expression for the tunneling current (1.7) becomes

$$J = \frac{4\pi m_m^* e}{h^3} \int_0^\infty \{f_1(E) - f_2(E)\} \left\{ \int_0^E \exp\left(-\alpha \int_{x_1}^{x_2} \left[g(\phi_c - E) + \frac{m_m^*}{m_i^*} E_\perp\right]^{1/2} dx\right) dE_\perp \right\} dE \tag{1.33}$$

where $E_\perp$ is the transverse energy of the electrons incident within the metals. Again closed form integration is out of the question; thus the assumption is made that the tunneling probability drops off at a sufficiently rapid rate with increasing values of $(E_{fl} - E)$ and $E_\perp$ so that for sufficiently low temperatures only

electrons with energies in the vicinity of the fermi level of the appropriate metal and with transverse momenta essentially equal to zero need be considered in the integration of the expression for the tunneling current, and that the exponent of the tunneling probability need only be represented by the first two terms of an expansion about $E = E_{fl}$ and $E_{\perp} = O$.

$$-\ln P(E, E_{\perp}) = B + C(E_{fl} - E) + DE_{\perp} \tag{1.34}$$

Integrating (1.33) with respect to energy E and transverse energy $E_{\perp}$, a very familiar expression is obtained.

$$J = \frac{4\pi m_m^* e}{h^3} \left\{ 1 + \frac{\pi^2}{6}(cKT)^2 \right\} \frac{1 - \exp(-CeV)}{DC} \exp(-B) \tag{1.35}$$

if the inequalities $(C-D)eV + DE_{fl} \gg 1$, $(C-D)kT \ll 1$ and $ckT \ll 1$ are valid. The only difference between (1.35) and (1.21) is the existence of a new voltage dependent coefficient D(V). If the energy momentum relationship is parabolic, it can be easily shown that D(V) becomes equal to m^*_m/m^*_i C(V) and that this newly obtained expression becomes identical to that given by (1.21). The only reason for the use of different notation is to emphasize the fact that one set of coefficients corresponds to a parabolic energy momentum relationship while the other set corresponds to a semi-arbitrary energy momentum relationship.

1.4.2 The Coefficients B(V), C(V), D(V)

For an arbitrarily shaped barrier the coefficients are defined by

$$B(V) = \alpha \int_{x_1}^{x_2} \{ g(\phi_c(x) - E_{f_1}) \}^{1/2} dx \qquad (1.36)$$

$$C(V) = \frac{1}{2} \alpha \int_{x_1}^{x_2} \{ (-\frac{\partial g}{\partial E}) \Big|_{E=E_{f_1}} \} \{ g(\phi_c(x) - E_{f_1}) \}^{-1/2} dx \qquad (1.37)$$

$$D(V) = \frac{1}{2} \alpha \frac{m_m^*}{m_i^*} \int_{x_1}^{x_2} \{ g(\phi_c(x) - E_{f_1}) \}^{-1/2} dx \qquad (1.38)$$

where x_1 and x_2 are the turning points of the barrier. If the barrier is trapezoidal, the coefficients can be simply related to $\mathrm{Im}\, p_{ins}\ (\phi_c - E)$. For if $\frac{d\phi_c(x)}{dx}$ is independent of position within the insulator, the tunneling probability for $E_\perp = 0$ may be rewritten as

$$-\ln P(E, E_\perp, V) \Big|_{E_\perp = 0} = \frac{2}{\hbar} (x_2 - x_1) \frac{\int_{\phi_c(x_2,V) - E}^{\phi_c(x_1) - E} \mathrm{Im}\, p_{ins}(\phi_c - E)\, d(\phi_c - E)}{\phi_c(x_1) - \phi_c(x_2, V)} \qquad (1.39)$$

where the integral over position has been replaced by an integral over energy referenced to the conduction band edge of the insulator. The exponent of the tunneling probability is seen to be proportional to the product of the tunneling path length and the aver-

age value of $\mathrm{Im}\; p_{ins}$ encountered along a tunneling path, the average being taken over energy referenced to the conduction band edge of the insulator. When the tunneling path extends from the conduction band of one metal to the conduction of the opposite metal then the tunneling path length is equal to the insulator thickness and (1.39) becomes

$$-\ln P(E,0,V) = \frac{2}{\hbar}\, x_0\, \frac{\displaystyle\int_{\phi_2 + E_{f1} - eV - E}^{\phi_1 + E_{f1} - E} \mathrm{Im}\, p_{ins}(\phi_c - E)\, d(\phi_c - E)}{\phi_1 - \phi_2 + eV} \tag{1.40}$$

when $E < \phi_1 + E_{fl}$ and $E + eV < \phi_2 + E_{fl}$.

The variation of the tunneling probability with voltage is seen to be the result of $\mathrm{Im}\; p_{ins}$ being averaged over different ranges of energy referenced to the insulator conduction band edge. When the tunneling path connects the conduction band of one of the metals to the conduction band of the insulator, it is the tunneling path length which varies with voltage while $\overline{\mathrm{Im}\; p_{ins}}$ remains constant

$$-\ln P(E,0,V) = \frac{2}{\hbar}\, x_0\, \frac{\phi_1}{\phi_1 - \phi_2 + eV} \left\{ \frac{\displaystyle\int_0^{\phi_1 + E_{f1} - E} \mathrm{Im}\, p_{ins}(\phi_c - E)\, d(\phi_c - E)}{\phi_1 + E_{f1} - E} \right\} \tag{1.41}$$

when $E < E_{fl} + \phi_1$ and $E + eV > \phi_2 + E_{fl}$.

Setting $E = E_{fl}$ in (1.40) and (1.41), the coefficient $B(V)$ is obtained

$$B(V) = \frac{2}{\hbar} x_0 \frac{\int_{\phi_2 - eV}^{\phi_1} Im\, p_{INS}(\phi_2 - E)\, d(\phi_2 - E)}{\phi_1 - \phi_2 + eV} \quad \text{for } eV < \phi_2 \tag{1.42}$$

and

$$B(V) = \frac{2}{\hbar} x_0 \frac{\phi_1}{\phi_1 - \phi_2 + eV} \quad \frac{\int_0^{\phi_1} Im\, p_{INS}(\phi_2 - E)\, d(\phi_2 - E)}{\phi_1} \tag{1.43}$$

for $eV < \phi_2$.

B(V) can be directly related to Im p_{ins}

$$-\frac{d}{dV}\left\{\frac{(\phi_1 - \phi_2 + eV) B(V)}{e}\right\} = \frac{2}{\hbar} x_0 \left\{ Im\, p_{INS}(\phi_1) - Im\, p_{INS}(\phi_2 - eV) \right\} \tag{1.44}$$

$$\text{for } eV < \phi_2$$

Taking the derivative of (1.40) and (1.41) with respect to E_x and then setting $E_x = E_{fl}$ the coefficient C(V) is obtained.

$$C(V) = \frac{2}{\hbar} x_0 \frac{Im\, p_{INS}(\phi_1) - Im\, p_{INS}(\phi_2 - eV)}{\phi_1 - \phi_2 + eV} \quad \text{for } eV < \phi_2 \tag{1.45}$$

and
$$C(V) = \frac{2}{\hbar} x_0 \left(\frac{\phi_1}{\phi_1 - \phi_2 + eV}\right)\left(\frac{Im\, p_{INS}(\phi_1)}{\phi_1}\right) \tag{1.46}$$

For $eV < \phi_2$, C(V) is seen to be directly related to the energy momentum relationship of the insulator. In a similar way it can

be shown that D(V) is given by

$$D(V) = \frac{2}{\hbar} x_0 \frac{m_m^*/m_i^*}{\phi_1 - \phi_2 + eV} \int_{\mathrm{Im}\, p_{INS}(\phi_2 - eV)}^{\mathrm{Im}\, p_{INS}(\phi_1)} \frac{\partial[2m_i^*(\phi_c - E)]}{\partial[(\mathrm{Im}\, p_{INS})^2]} \, d\,\mathrm{Im}\, p_{INS} \quad (1.47)$$

for $eV < \phi_2$

and

$$D(V) = \frac{\phi_1}{\phi_1 - \phi_2 + eV} D(\phi_2) \quad (1.48)$$

for $eV > \phi_2$

The relationships between B(V), C(V), and Im p_{ins} are illustrated in Figure I.4. There it can be seen that C(V) is proportional to the difference between the initial and final values of Im p_{ins} encountered along the tunneling path appropriate to an incident electron with zero transverse momentum and energy equal to E_{fl} divided by the difference in initial and final energies referenced to the conduction band edge of the insulator. As long as the effective mass, defined by the reciprocal of the second derivative of energy with respect to momentum, is positive within the forbidden band, C(V) will increase with voltage until $V = \phi_2/e$ at which point the difference between initial and final values of Im $p_{x\ ins}$ becomes constant. For higher voltages C(V) becomes proportional to the decreasing tunneling path length. For more complicated energy momentum relationships, Figure I.4 can be used for a geometrical interpretation of the dependence of C(V) on voltage. However, in view of the fact

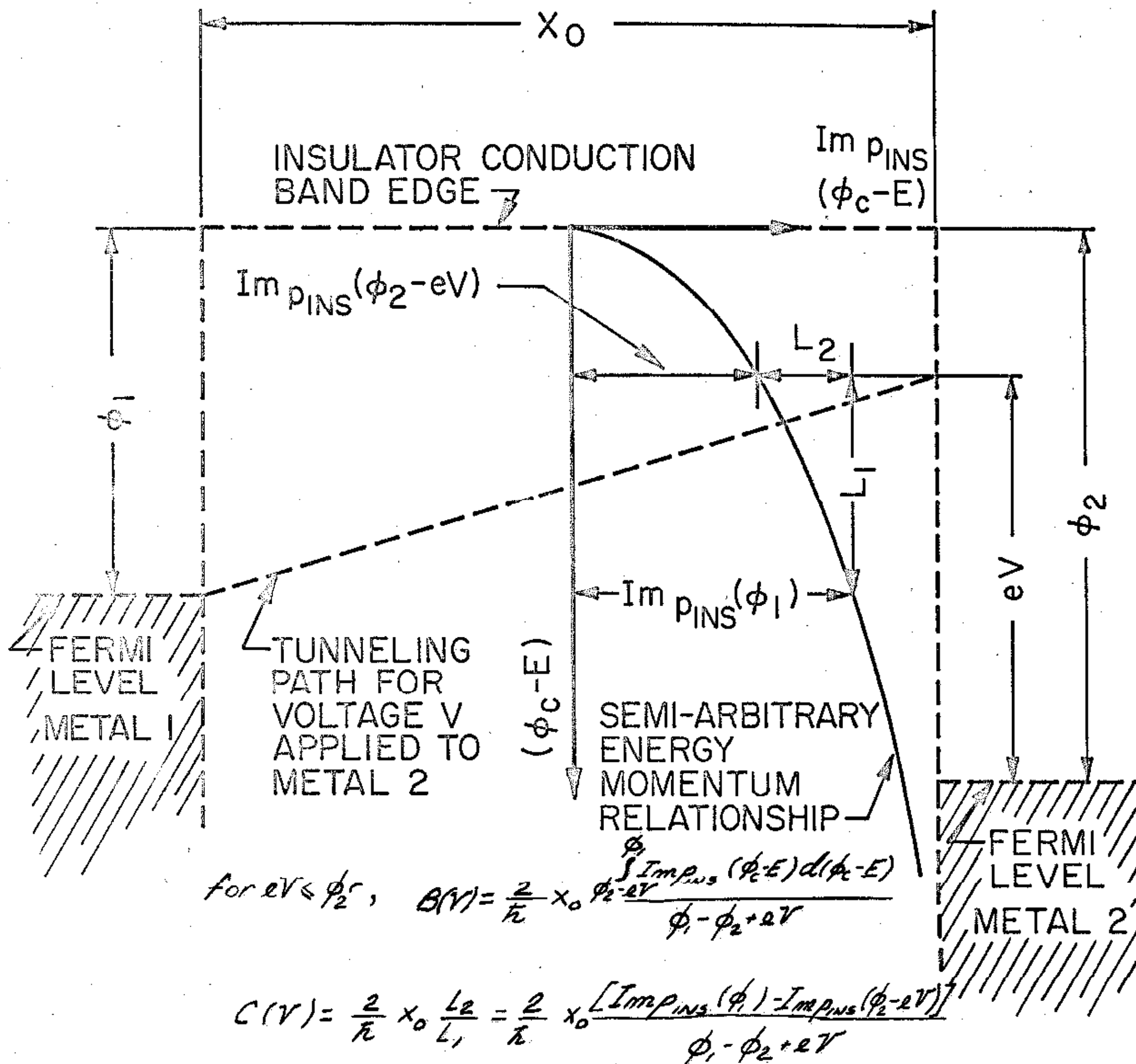

Figure 1.4 Geometrical representation of coefficients B(V) and C(V). Energy is referenced to insulator conduction band edge.

that the effective mass will certainly be positive in the vicinity of the insulator conduction band, $C(V)$ will be an increasing function of voltage for voltages just below ϕ_2/e. Consequently, $C(V)$ will have cusps at voltages equal to the barrier energies divided by the electron charge independent of the energy momentum relationship characterizing the forbidden band; the cusps are simply the effect of a transition from tunneling of electrons between the two metals to tunneling of electrons from a metal to the conduction band of the insulator.

The voltage dependence of the coefficient $B(V)$, for voltages in excess of the barrier heights, $V > \phi_2$ for $B_+(V)$ and $V > \phi_1$ for $B_-(V)$, is in a sense independent of the energy momentum relationship. For these voltages the average value of Im p_{ins} is constant and the variation of the coefficient is related to the variation of the tunneling path length which has only to do with the geometry of the trapezoidal barrier .

For voltages smaller than those of the barrier energies divided by the electron charge, the probability coefficient $B(V)$ will have a negative second derivative with respect to voltage if the effective mass is positive over the ranges of energy (referenced to the conduction band edge of the insulator) covered by the relevant tunneling paths. For more complicated energy momentum relationships all that can be said is that $B(V)$ is defined by (1.42).

Thus the current voltage characteristic corresponding to a trapezoidal barrier with an arbitrary energy momentum relationship can be summarized in the following way. The current increase, for voltages smaller than the energy spread of the tunneling electrons defined by the variation of the tunneling probability with energy, is approximately linear. This range of voltage is defined by $CeV \ll 1$. For higher voltage, or $C(V)eV \gtrsim 1$, the current will increase in the way dictated by the energy momentum relationship until $V = \phi_2/e$. Further increase in the current will then be determined by the variation of the tunneling path length.

1.4.3 Dependence of Characteristics on Insulator Thickness.

Once the thickness of the insulator is known it is possible in principle to construct an energy momentum relationship for the forbidden band of the insulator if it can be assumed that the barrier is indeed trapezoidal. This can be done with the use of temperature measurements, measurements of current at various voltages as a function of insulator thickness, and measurement of current voltage characteristics. But how is one assured that the characteristics of a particular structure are the effect of a non-parabolic energy momentum relationship or of a non-trapezoidal barrier? The dependence of the current voltage characteristics on insulator thickness serves as a means of removing this ambiguity.

For a trapezoidal barrier the average value of the imaginary component of x momentum encountered along a tunneling path is independent of the insulator thickness and only a function of voltage. Similarly, the variation of the tunneling path length to insulator thickness ratio for electrode to insulator tunneling is also independent of insulator thickness and only a function of voltage. Consequently, B(V) is proportional to the insulator thickness as are both the coefficients C(V) and D(V). The effect of this circumstance may be seen by rewriting the tunneling current for low temperatures in terms of three new coefficients; $B^*(V) = B(V)/x_o$, $C^*(V) = C(V)/x_o$, and $D^*(V) = D(V)/x_o$.

$$\ln J = \ln \left\{ \frac{4\pi m_m^* e}{h^3} \frac{[1-\exp(-C^* eV)]}{C^* D^* x_o^2} \right\} - B^* x_o \qquad (1.49)$$
$$\text{if } C^* x_o kT \ll 1$$

For voltages approaching zero, $C(V)eV \rightarrow 0$, it is easily shown that

$$\ln \frac{J x_o}{V G_1} = -B^*(0) x_o \qquad (1.50)$$
$$\text{where } G_1 = \frac{4\pi m_m^* e^2}{h^3 D^*}$$

and that

$$\frac{\partial \ln \frac{J x_o}{V G_1}}{\partial x_o} = -B^*(0) \qquad (1.51)$$

For higher voltages, $C(V)eV \gtrsim 1$, the current is given by

$$\ln \frac{J x_o^2}{G_2} = - B^*(V) x_o \tag{1.52}$$

$$\text{where } G_2 = \frac{4\pi m m_m^* e}{h^3 C^*(V) D^*(V)}$$

and consequently

$$\frac{\partial \left[\ln \frac{J x_o^2}{G_2} \right]}{\partial x_o} = - B^*(V) \tag{1.53}$$

If the derivatives defined by (1.47) and (1.51) are observed to be independent of thickness, then the conclusion can be made that the barrier is essentially trapezoidal. It is true that this thickness independence only guarantees a barrier describable by a specific function of the ratio x/x_o but the argument used is that the only physically plausible reasons for a barrier to deviate from a trapezoidal shape are edge effects at the metal insulator interfaces, for example image forces or physically non-abrupt transitions from metal to insulator. Edge effects certainly do not lead to arbitrary barrier shapes describable by specific functions of x/x_o. It is also to be noted that (1.51) and (1.53) provide a direct way of experimentally determining the coefficient $B^*(V)$ which, with the knowledge of the insulator thickness and with (1.44), can be used to obtain the insulator energy momentum relationship appropriate to a particular structure. One more approximate relation is given which emphasizes the fact that even though

the current voltage characteristics for voltages corresponding to electrode to electrode tunneling are arbitrary in the sense that the insulator energy momentum relationship may be arbitrary, certain relations exist between the shape of the current voltage characteristics and the insulator thickness. It can be shown that for $CeV \gg 1$ the current at a given voltage for a structure having a particular insulator thickness can be simply related to the current at the same voltage for a structure with a different insulator thickness if the variation of $\log_e C^*(V)D^*(V)$ with voltage is negligible in comparison to the variation of $B^*(V)x_o$ with voltage.

Consider the differential of the logarithm of the currents $J_1(V)$ and $J_2(V)$ for two structures having different insulator thicknesses x_{o1} and x_{o2} for voltages such that $C(V)eV \gg 1$ and low temperatures such that $CkT \ll 1$.

$$\frac{x_{o2}}{x_{o1}} d \ln J_1(V) = -\frac{x_{o2}}{x_{o1}} \left[\frac{\partial}{\partial V} \ln C^*(V) D^*(V) \right] dV - x_{o2} \left[\frac{\partial B^*(V)}{\partial V} \right] dV \tag{1.54}$$

$$d \ln J_2(V) = -\left[\frac{\partial}{\partial V} \ln C^*(V) D^*(V) \right] dV - x_{o2} \left[\frac{\partial B^*(V)}{\partial V} \right] dV \tag{1.55}$$

$$d \ln J_2(V) = \frac{x_{o2}}{x_{o1}} d \ln J_1(V) \left\{ 1 + \frac{\left[\frac{x_{o2} - x_{o1}}{x_{o2}} \frac{\partial}{\partial V} (C^* D^*) \right]}{\frac{\partial}{\partial V} \ln J_1(V)} \right\} \tag{1.56}$$

For regions of voltage where the second term in the parentheses is smaller than unity or where the variation of the tunneling probability with voltage greatly exceeds the variation of the effective number of tunneling electrons with voltage, the current flow through structure 2 may be related to the current flow through structure I in the following simple way

$$\ln J_2(V) = \text{constant} + \frac{X_{02}}{X_{01}} \ln J_1(V) \qquad (1.57)$$

The current for a structure with a thicker insulator when compared to the current through a structure with a thinner insulator is lower but its rate of increase with voltage is greater.

1.5 CONCLUSION

When it has been determined that the barrier appropriate to a thin film structure is trapezoidal by observing current exponentially dependent on insulator thickness as given by (1.51) and (1.53) and/or current voltage characteristics related to insulator thickness as by (1.57), there are in principle three methods of experimentally determining the barrier heights at the metal insulator interfaces and the insulator energy momentum relationship. If the temperature variation of the observed tunneling current can be attributed solely to the temperature variation of the Fermi-Dirac distribution within the metals then C(V) can be ob-

tained directly from temperature measurements (see 1.35). The cusps in C(V) define the barrier energies while the actual variation of C(V) with voltage defines the energy momentum relationship (see 1.45).

The second method involves the use of the observed current voltage characteristic. The coefficients B(V), C(V), and D(V) are all interrelated and in principle an energy momentum relationship and barrier geometry can be found which will correspond to the observed current voltage characteristic.

The last method involves the experimental dependence of current on insulator thickness. As can be seen from (1.51) and (1.53), this dependence leads directly to the coefficients $B^*_+(V)$ and $B^*_-(V)$. Differentiation of these experimentally determined coefficients with respect to voltage as by (1.44) leads to the energy momentum relationship. The difference between the barrier heights ϕ_2 and ϕ_1 is that which allows $B_+(V)$ and $B_-(V)$ to lead to the same energy momentum relationship. The actual values of ϕ_1 and ϕ_2 are given by those voltages V_1 and V_2 multiplied by the electron charge for which Im $p_{ins}(\phi_1 - eV_1)$ and Im $p_{ins}(\phi_2 - eV_2)$ are equal to zero.

It is concluded that an experimental investigation of electron tunneling in thin film structures requires the observation of currents not only as a function of voltage and temperature but

also as a function of insulator thickness. Such measurements allow the construction of a complete self-consistent model directly from experimental data. Measurement of current voltage characteristics for structures with only one particular insulator thickness can only lead to the verification or refutation of a <u>proposed</u> model.

CHAPTER II

SAMPLE PREPARATION AND MEASUREMENT PROCEDURES

Thin film structures composed of Aluminum as the base electrode, Aluminum Nitride as the insulating layer, and either Magnesium, Aluminum, or Gold as the counterelectrode were fabricated with the thickness of the insulating layer in the order of tens of Angstroms. This was the range of insulating layer thicknesses where the current density resulting from the tunneling of electrons was expected to be sufficiently large for experimental observation. The structures were obtained by the nitridization of a freshly vacuum deposited Aluminum film in a nitrogen glow discharge. Subsequent evaporation of counterelectrodes completed the sandwich structures.

The technique of reacting the surface of a film in a plasma was chosen in that it allowed a fairly accurate control of the insulator thickness. Variation of the barrier height at the counterelectrode insulator interface was attempted by using Magnesium, Aluminum, and Gold as counterelectrodes. These metals, listed in the above order, have successively higher work functions and values of electronegativity. It is the purpose of this chapter to describe in detail the procedures used in the fabrication of these structures and in the measurement of their properties.

2.1 SAMPLE PREPARATION

2.1.1 Substrate Preparation.

Microscope cover slides and commercially available ceramics having surfaces much smoother than that of the glass slides were tried as substrates. It was found that the characteristics of the samples were independent of the type of substrate used. This observation and the fact that better control over the thicknesses of the base and counterelectrodes could be achieved by visual observation of the optical transparency of the films during evaporation led to the dominant use of the microscope cover slides.

Several procedures for cleaning the substrates were compared. The simplest of these gave the best results. The substrate was dipped into an ordinary soap solution which was then rubbed over the surface by hand and finally removed by holding the substrate with a pair of tweezers under a running stream of distilled water. The remaining film of water was evaporated off by holding the slide in a stream of hot air. The corner used for holding the slide with the tweezers invariably had some residue left on it; this corner was broken off when the slide was placed into the vacuum system. Further cleaning was carried out in the vacuum system by initiating a nitrogen glow discharge over the substrate for a period of a few minutes.

This procedure also allowed a cleanup of the discharge cathode.

2.1.2 Evaporation of Base Electrode.

Following the cleanup provided by the glow discharge, the system was pumped down to a pressure of the order of 10^{-6} Torr and a film of Aluminum of the order of 1000 Angstroms was deposited onto the substrate. The purity of the Aluminum used for the evaporation was 99.99%. The geometry of the deposited film in relation to the geometry of the substrate is shown in Figure 2.1b. A mask was used to create an edge so that after nitridization of the Aluminum film counterelectrodes could be deposited which overlapped the film and the substrate. This procedure allowed soldered contacts to be made to the areas of the counterelectrodes over the clear substrate without causing damage to the nitrided Aluminum film.

2.1.3 Nitridization of the Base Electrode.

Immediately following the evaporation of the base electrode, the system was isolated from the diffusion pump and high purity nitrogen was allowed to enter. A constant flow of the gas through the system was established by the use of a zeolite trapped roughing pump. When the pressure had stabilized at some 200 microns of mercury, a glow discharge was initiated by applying a high voltage of approximately 1000 volts across two high purity Aluminum electrodes, the discharge cathode

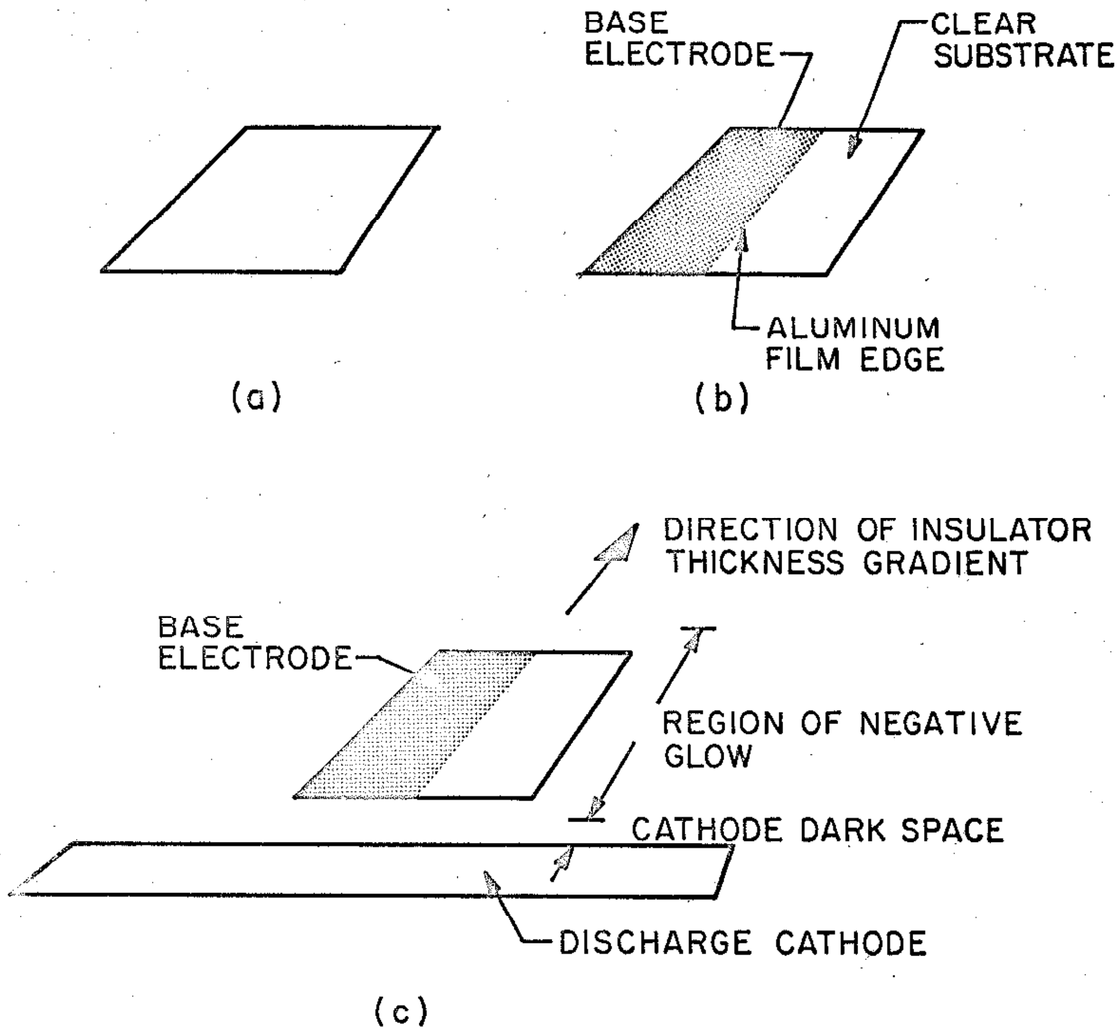

Figure 2.1 (a) Substrate geometry, (b) Geometry of deposited base electrode with respect to that of the substrate, (c) Geometry of discharge cathode with respect to that of the base electrode.

being in the vicinity of the Aluminum film to be nitrided.

No attempt was made to study the kinetics of the surface reaction taking place at the film plasma interface. As a matter of fact, it was not clear as to whether the layer of Aluminum Nitride that was obtained was the result of Aluminum being sputtered off the discharge cathode, reacting with the nitrogen plasma, and settling finally on the recently deposited base electrode or the result of a surface reaction. The geometry of the discharge cathode with respect to the film to be nitrided, the discharge voltage and current, the nitrogen pressure, and the time allowed for nitridization were all interrelated factors affecting the thickness of the layer of Aluminum Nitride obtained and the electrical characteristics of the completed structures. A great deal of time was spent in trying various combinations of these factors and correlating them to the characteristics of the structures so that an optimum nitridization procedure could be developed. This is not to say that the characteristics were tailored to fit the predictions of the models described in Chapter I. Rather, the range of results obtained with the structures were extended so that a greater degree of confidence could be placed in them.

It was noted in the early stages of this research that the variation in thickness of the Aluminum Nitride layer along the

surface of the base electrode could be correlated to the spatial variation in intensity of the visible radiation given off by the region of negative glow of the discharge. This observation led to an attempt at controlling the insulator thickness in a desired manner. As a result, a single nitrided film could be made to yield a large number of sandwich structures covering the entire range of desired insulator thicknesses. This method of studying the effect of insulator thickness on the characteristics of the structures was expected to be superior to that of fabricating a large number of samples each having a constant but different insulator thickness in that the effects of small variations in the procedures used in the preparation of different samples could be avoided.

For reasons that will soon become apparent, it was desired that the gradient in the thickness of the Aluminum Nitride lay in the direction parallel to the edge of the base electrode. This gradient was obtained by making the discharge intensity distribution essentially one dimentional along the surface of the substrate. The geometry of the discharge cathode was that of a long strip. For distances away from the cathode small compared to the length of the strip and away from the ends of the strip the discharge intensity distribution was radial. By positioning the substrate in this region with the edge of the base electrode perpendicular to the discharge cathode the desired direction of the insulator

thickness gradient could be obtained. The geometry of the discharge cathode with respect to the base electrode is shown in Figure 2.lc.

The dimentions of the substrate used limited the length of the base electrode edge to approximately one inch. Within this distance the thickness of the nitrided layer of Aluminum could typically be made to vary by a factor of two. Deposition of small area counter electrodes on this layer thus yielded a large number of sandwich structures with the thickness of the insulator varying from one to three percent from structure to structure.

Many attempts were made at nitriding Aluminum films before samples could be obtained which contained a relatively small number of faulty structures characterized by short circuits or by current voltage characteristics with unusually high values of current. The faults could be placed into two categories; those which extended over very small areas of the nitrided film and those which extended over fairly large areas of the nitrided film.

Faults, when found to be randomly distributed, could be attributed to "pinhole" imperfections usually arising from excessive sputtering of the discharge cathode, sputtering of material in the vicinity of the glow discharge, or a dirty substrate. Excessive sputtering from the discharge cathode was evidenced by sparking and an erratic discharge current; it could be controlled by setting a limit to the discharge current for

the nitrogen pressure used. Sputtering from material in contact with the glow discharge was reduced by exposing nothing but Aluminum or glass to the plasma and by keeping the surface areas of these materials to a minimum.

Use of very low discharge currents, high nitrogen pressures, and correspondingly long nitridization times, while minimizing the problems arising from sputtering, did not allow the formation of thinner layers of Aluminum Nitride in the region of the Aluminum film furthest away from the discharge cathode. This effect was evidenced by an unusual increase in current density for structures located in the outer regions of the substrate in plots of the logarithm of the current density at low applied voltages (of the order of 50 mv) as a function of insulator thickness. The structures located in the regions of the substrate closer to the discharge cathode defined an approximately linear dependence of the logarithm of the current density on insulator thickness which was not followed by the structures located in the outer regions of the substrate. Use of a higher discharge current, a lower nitrogen pressure, and a correspondingly shorter nitridization time, not only tended to eliminate this inconsistency but also reduced the current density for all applied voltages in all of the structures. Consequently, the lower limit on the thickness of a formed layer of Aluminum Nitride which led to structures having

current voltage characteristics consistent with each other over the whole range of insulator thicknesses was set by the maximum discharge current that could be used without running into the problems associated with excessive sputtering.

The discharge current finally chosen for the nitridization of the base electrode was of the order of ten milliamperes; the values of the surface area of the discharge cathode and the nitrogen pressure were approximately 43 cm^2 and 200 microns of mercury. Nitridization times ranging from two to three minutes, depending on the exact area of the discharge cathode, the discharge current, the nitrogen pressure, and the geometry of the discharge cathode in relation to that of the substrate, allowed the formation of Aluminum Nitride layers having a minimum thickness of approximately thirty Angstroms.

2.1.4 Counterelectrodes.

The thickness of the insulator separating the base and counter electrodes was determined by the measurement of the structure capacitance. The relationship used to obtain the insulator thickness is given below

$$X_o = \frac{A \epsilon_o k_s}{C'} \qquad (2.1)$$

where:

A = Area of counter electrode
ϵ_o = Permitivity of free space
k_s = Static dielectric constant of insulator
C' = Structure capacitance

Several considerations were involved in the choice of a practical counterelectrode area: 1) the dimension of counter-electrode has to be such as to cover only a small range of the insulator thickness; 2) the area had to be kept small enough so that the probability of a counterelectrode encompassing a pinhole imperfection remained at a reasonably low value; 3) the area had to be large enough to allow its accurate measurement. Use of counterelectrode areas of approximately 5×10^{-4} cm^2 was mainly the result of the second consideration.

A commercially available mesh having openings whose areas varied less than 1 % about a nominal value was used as a mask for the deposition of counterelectrodes thus eliminating the need for measuring the variations in area from structure to structure. As a result the values of insulator thickness for structures of a particular sample were related to the inverse capacitance of these structures by one proportionality constant. The value of this proportionality constant involved the measured area of the counterelectrodes on that sample and the use of 8.5 as the value of the insulator static dielectric constant. Figure 2.2a shows the geometry of the deposited counterelectrodes.

Contact to the base electrode was made by soldering a lead to the Aluminum film with Indium. Contact to the counter-electrodes having areas wholly on the nitrided film was made with a probe consisting of a 3 mil copper wire mounted on a

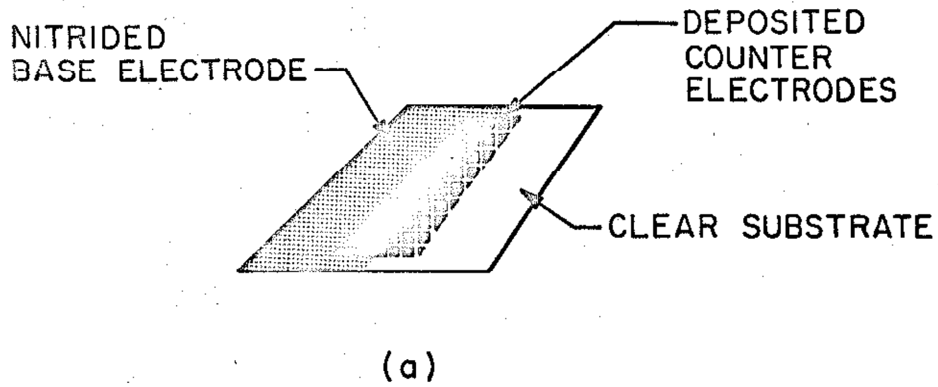

(a)

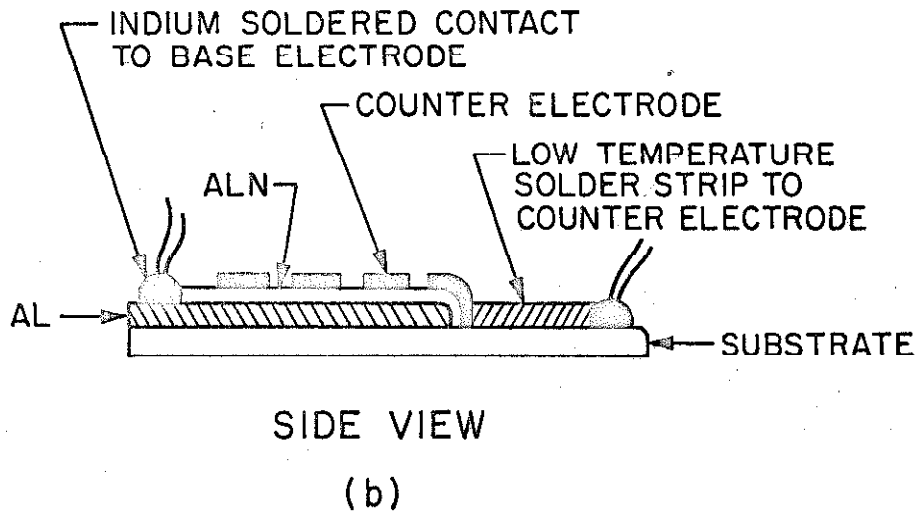

SIDE VIEW

(b)

Figure 2.2 (a) Fabricated sample, (b) Cross-section of nitrided Aluminum film showing procedure used for making contact to base and counterelectrodes.

three dimensional micropositioner. This thickness of wire allowed enough stiffness for the penetration of the oxide layers forming on the Magnesium and Aluminum counterelectrodes within a few days after the fabrication of the sample.

Low temperature measurements required that mechanically rigid contacts be made to the counterelectrodes. Attachment of a connection by soldering or by the use of a conductive epoxy to an electrode wholly on the nitrided film always resulted in the destruction of the structure. However, mechanically rigid contacts to counterelectrodes overlapping the nitrided film and the substrate could be made. Low temperature solder was used to run a conducting strip from the edge of the counterelectrode on the clear substrate to somewhere in the middle of the substrate where a wire could be attached to the strip by soldering with Indium. This procedure is illustrated in Figure 2.2b.

Measurement of the insulator thickness and counterelectrode area of structures having an overlapping counterelectrode was carried out in the following manner. Because of the nitridization procedure used, the thickness of the nitride layer did not vary in the direction perpendicular to the film edge. Thus the insulator thickness of a structure having an overlapping counterelectrode was assumed to be the same as that of the structure having a non-overlapping counterelectrode next to it in the direction perpendicular to the film edge. The ratio of the two structure capaci-

tances multiplied by the area of the non-overlapping counter-electrode gave the area of the overlapping counterelectrode. This procedure was justified by using pairs of structures for which the ratio of counterelectrode areas thus obtained was approximately equal to the ratio of currents observed for an arbitrary applied voltage.

For some samples the whole fabrication was carried out in one vacuum system; following the nitridization of the Aluminum film the flow of nitrogen was stopped and the system was evacuated to a pressure of 10^{-6} Torr so that evaporation of the counter-electrodes could take place. This procedure was found to be inconvenient in that it required a great deal of apparatus for accurate positioning of masks. Furthermore, deposition of Gold and Magnesium required removal of these metals from the structures supporting the discharge cathode and the substrate following the preparation of each sample. Consequently, a procedure was tried whereby after the nitridization of the base electrode the substrate was removed from one system and placed into another allowing the surface of the nitrided film to come in contact with room atmosphere for a time period of less than a minute. Deposition of counterelectrodes was then carried out in this second system. The characteristics of the samples prepared in this manner did not vary from those prepared completely within one vacuum station. The greater simplicity associated with the use

of one station for the deposition and subsequent nitridization of the base electrode and a second one for the deposition of counter-electrodes led to the dominant use of this second procedure for the fabrication of the thin film structures.

2.2 MEASUREMENT PROCEDURES

The current as a function of voltage, temperature, and insulator thickness was measured in the thin film structures. The arrangement for the measurement of the current voltage characteristics involved a variable voltage supply and an ammeter in series with the structure. For measurement of small current variations (in the order of 10%) with temperature, the voltage supply consisted of a battery and potentiometer made up of fixed value resistors assuring the same values of applied voltage for measurements taken during different intervals of time.

Dewars were used for low temperature measurements. When placed in the evacuated region of a dewar, the sample substrate assumed a temperature near that of the liquid in the dewar. Liquid Helium, Nitrogen, Methane, and Ethylene were used to achieve temperatures near 4^0K, 77^oK, 111^oK, and 169^oK. A second dewar was used to achieve temperatures not obtainable with liquids. The sample substrate was connected thermally to a reservoir of liquid nitrogen through a cylinder of teflon having a length of approximately 1/4 inch. The heat flow through the

teflon cylinder which determined the temperature drop across the length of the cylinder was controlled by a heater situated at the face of the cylinder nearest the sample. Nichrome wire wound in slots at the face of the cylinder served as the heater.

Capacitance measurements were carried out with a bridge providing a 100 KC sine wave of approximately 50 millivolts amplitude to the structures.

CHAPTER III

PRESENTATION OF EXPERIMENTAL RESULTS

Currents through thin film structures obtained by the methods described in Chapter II were measured as a function of voltage, temperature, and insulator thickness to determine whether these currents could indeed be attributed to electron tunneling through the forbidden band of a trapezoidal barrier with the exponent of the tunneling probability proportional to the product of the tunneling path length and the average value of the x component of the imaginary value of momentum encountered along a tunneling path.

The currents observed were interpreted as the sum of two independent currents both exponentially dependent on thickness and independent of temperature. Only one of these currents fitted the predictions of the models presented in Chapter I and consequently will be termed the tunneling current. The second current will be referred to as the excess current.

For structures with Magnesium counterelectrodes the tunneling current was dominant over a sufficiently large range of insulator thicknesses as to allow its identification. The barrier appropriate to these structures was found to be approximately rectangular; the energy momentum relationship was found not to be parabolic over the energy range relevant to tunneling but was consistent with the barrier energies being an appreciable fraction

of the forbidden energy gap.

The current through structures with Aluminum and Gold counterelectrodes could be identified as that resulting from electron tunneling only for those structures with the thinnest insulating regions. The current through structures with thicker insulating regions could clearly be seen as a combination of a tunneling current and an excess current.

3.1 PROPERTIES OF STRUCTURES WITH MAGNESIUM COUNTERELECTRODES

Current voltage characteristics measured at various temperatures for structures with Magnesium counterelectrodes and various insulator thicknesses will be presented in this section. It will be shown that for structures with the thinner insulating regions, the observed current could be considered as that resulting from electron tunneling through a trapezoidal barrier since the dependence of this current on insulator thickness and voltage could be interpreted in terms of the second model in Chapter I. The procedures used in determining the barrier energies and the insulator energy momentum relationship will be presented along with the results obtained therewith.

3.1.1 Current Voltage Characteristics.

It has been shown in Chapter I that for low voltages, $CeV \ll 1$, the tunneling current is expected to vary linearly with voltage. Multiplying the low voltage resistance by the structure capacitance

results in an expression which does not contain the insulator thickness in the preexponential term and which is independent of counterelectrode area.

$$\ln\left(\frac{V}{J \cdot A} \cdot \frac{A k_s \epsilon_0}{x_0 t_0}\right) = \ln \frac{RC'}{t_0} = \ln \frac{h^3 k_s \epsilon_0 B^*(0)}{4\pi m_m^* e^2 t_0} + B^*(0) x_0 \quad (3.1)$$

where:

A = counterelectrode area

R = low voltage resistance $= \frac{V}{JA}$ as $V \to 0$

C' = structure capacitance $= \frac{A k_s \epsilon_0}{x_0}$

t_0 = 1 second

The expected exponential dependence of the resistance capacitance product on insulator thickness was observed. This dependence is shown in Figure 3.1 where $\log_{10} RC'$ for structures picked at random from a fabricated sample (sample A) is plotted as a function of insulator thickness. The values of the insulator thickness were deduced from the measurement of structure capacitance and counterelectrode area assuming a static dielectric constant of 8.5. The value of counterelectrode area was assumed to be the same for all structures on a given sample; a deviation in this area from structure to structure of approximately 1% from the nominal value assumed accounts for the scatter seen in Figure 3.1. The deviation seen for insulator thicknesses in excess of 50 Å cannot be accounted for by variations in counterelectrode area; however, at lower temperatures the low voltage resistance of the structures with these thicker insulating regions increased and

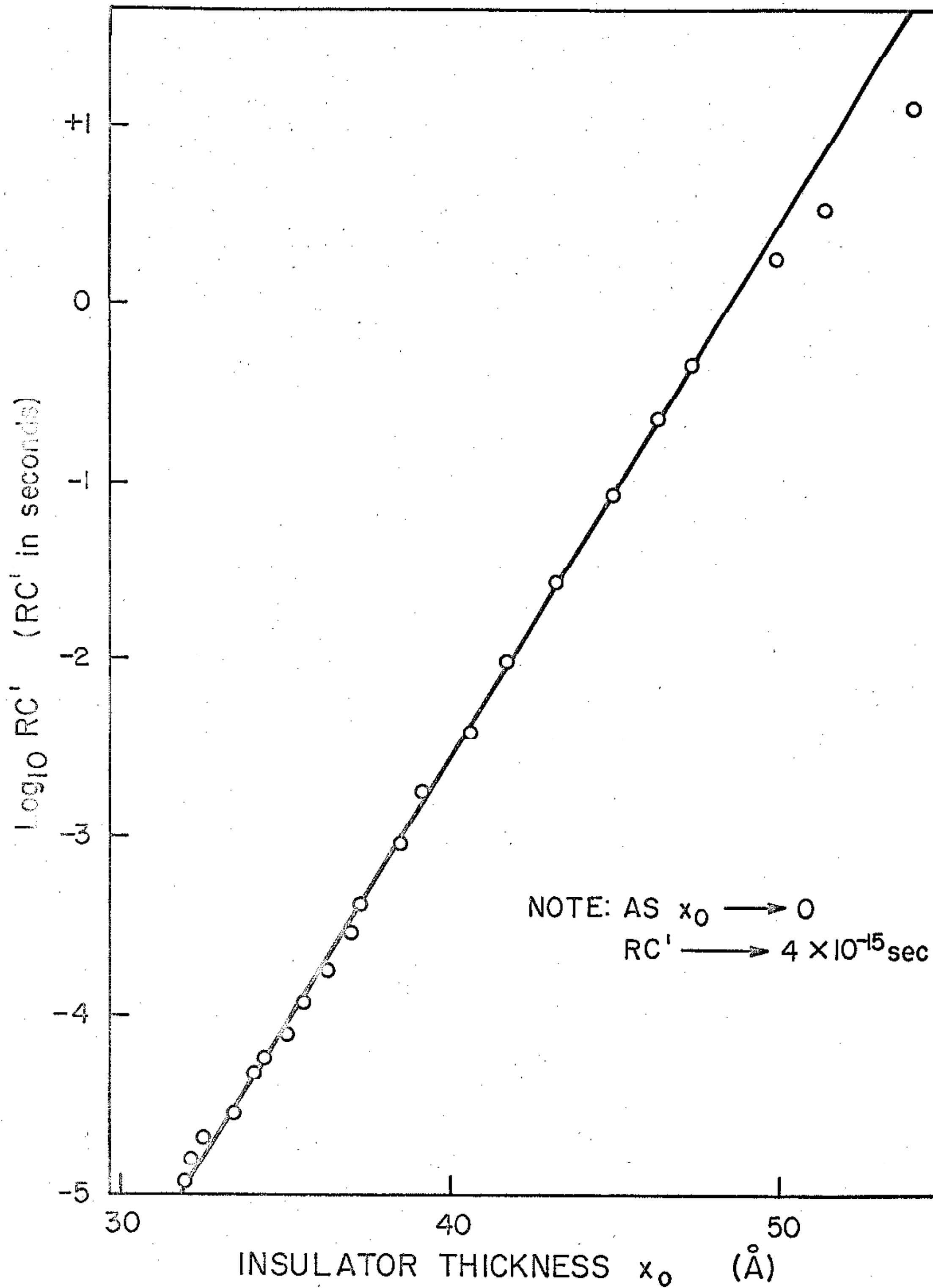

Figure 3.1 RC' of Al-AlN-Mg structures versus insulator thickness; R measured at 300°K. (sample A).

RC' followed the same exponential dependence on thickness as the structures with thinner insulating regions.

The zero thickness intercept of $\log_{10}$ RC' versus x_o is related to the energy momentum relationship within the insulator forbidden band through the coefficient $D^*(0)$. A comparison of the experimentally observed value of the zero thickness intercept, RC' $= 4 \times 10^{-15}$ seconds, with that based on the experimentally determined insulator energy momentum relationship will be carried out later in this section.

The current voltage characteristics for five structures taken from one sample (sample B) with insulator thicknesses ranging from some 32 to 48 Angstroms are shown in Figure 3.2. The characteristics were measured at room temperature (300°K) with a positive voltage applied to the counterelectrode. It can be seen that the characteristics have the general features expected from an insulator energy momentum relationship with a positive effective mass over the energy ranges relevant to tunneling. At low voltages, the current is linearly dependent on voltage, while at higher voltages the current increases with voltage at a faster than exponential rate. Voltages greater than $\frac{\phi_e}{e}$ could not be applied without causing damage to the structures evidenced by irreversible changes in the current voltage characteristics.

It has been pointed out in Chapter I that independent of the

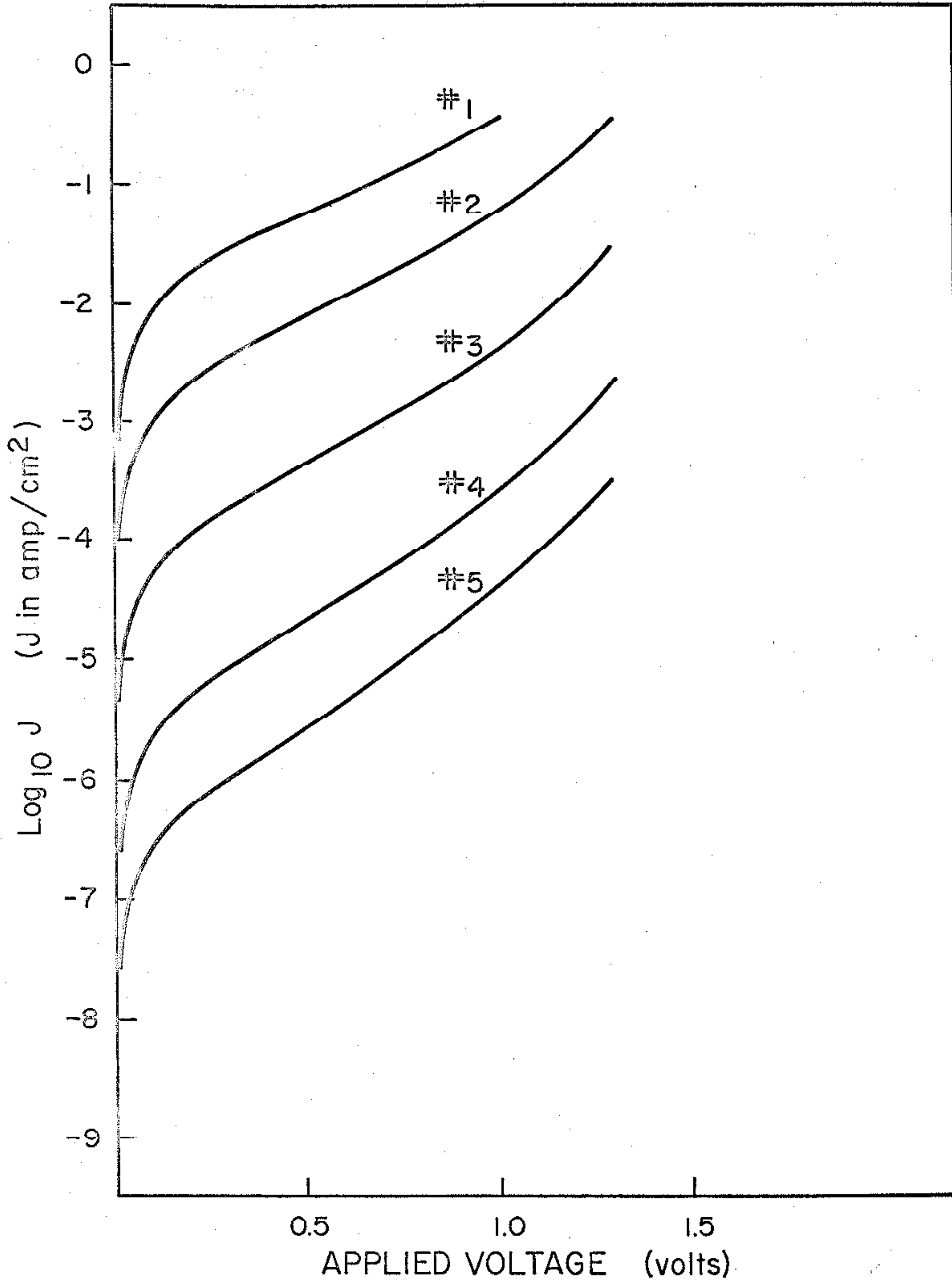

Figure 3.2 300°K J(V) versus V, counterelectrode positive, of Al-AlN-Mg structures with insulator thicknesses from 32 to 48 Å (sample B).

insulator energy momentum relationship, the current through a structure with a particular insulator thickness can be related in a simple way to the current through a structure with a different insulator thickness if the barrier is indeed trapezoidal (see I.56). For voltages where the voltage variation of the effective number of tunneling electrons is small when compared to the voltage variation of the tunneling probability, the logarithm of the current corresponding to a structure with insulator thickness x_{oa} when plotted against the logarithm of the current corresponding to a structure with insulator thickness x_{ob} for the same applied voltage should yield a straight line with the slope equal to the ratio of the two insulator thicknesses or x_{oa}/x_{ob}. The current voltage characteristics shown in Figure 3.2 are thus compared in Figure 3.3 using the logarithm of the current through structure 2 ($\log_{10} J_2(V)$) as a reference. It can be seen that the expected linear relation between the logarithms of currents of structures with different insulator thicknesses does indeed exist. The slopes of these plots are correlated to the insulator thickness in Figure 3.4. It is evident that for voltages greater than some 0.3 volts all of the observed characteristics can be described by a function

$$J \propto \exp[-B(V)x_o] \tag{3.2}$$

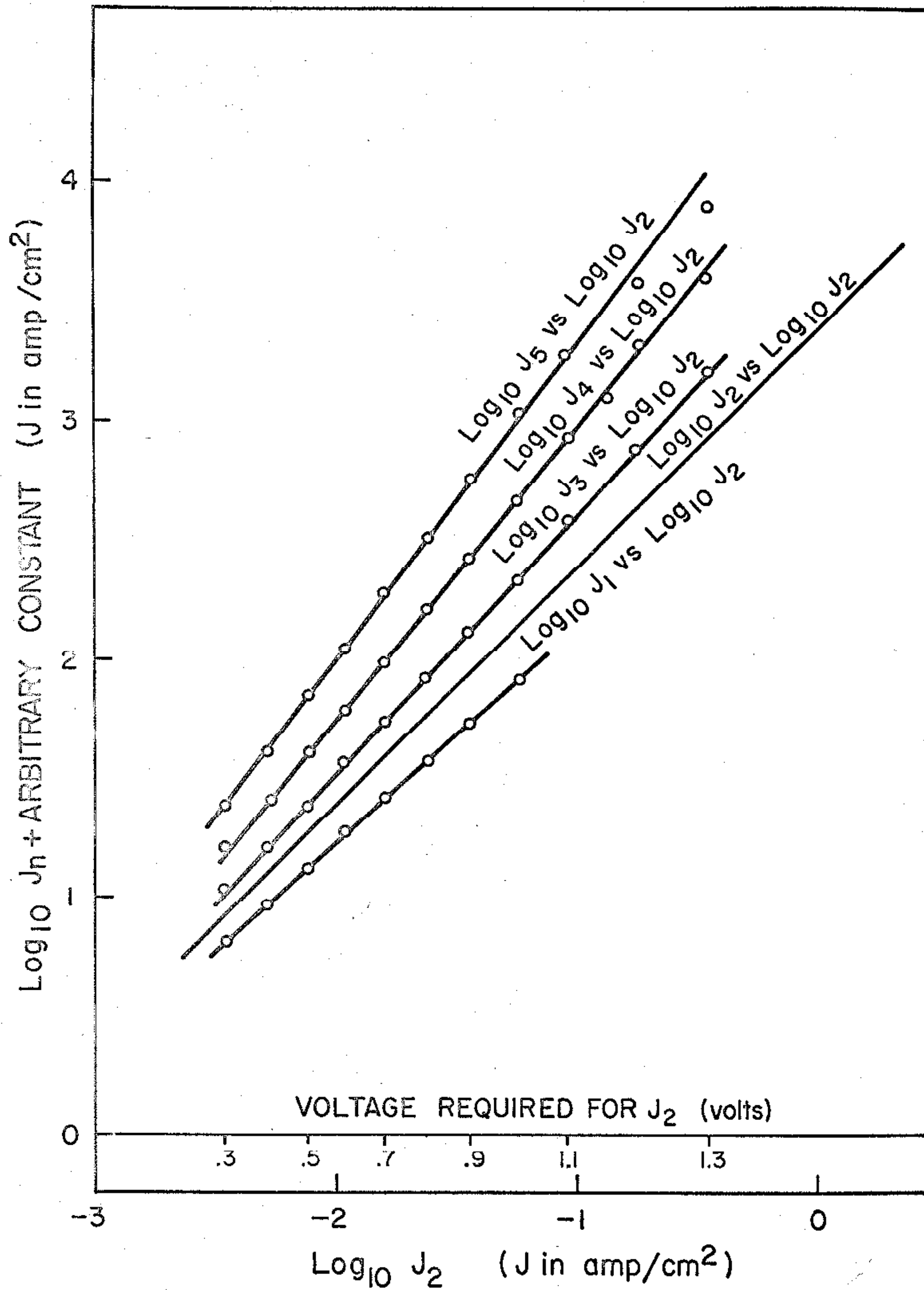

Figure 3.3 $\log_{10} J_n$ versus $\log_{10} J_2$ plots corresponding to characteristics shown in Figure 3.2.

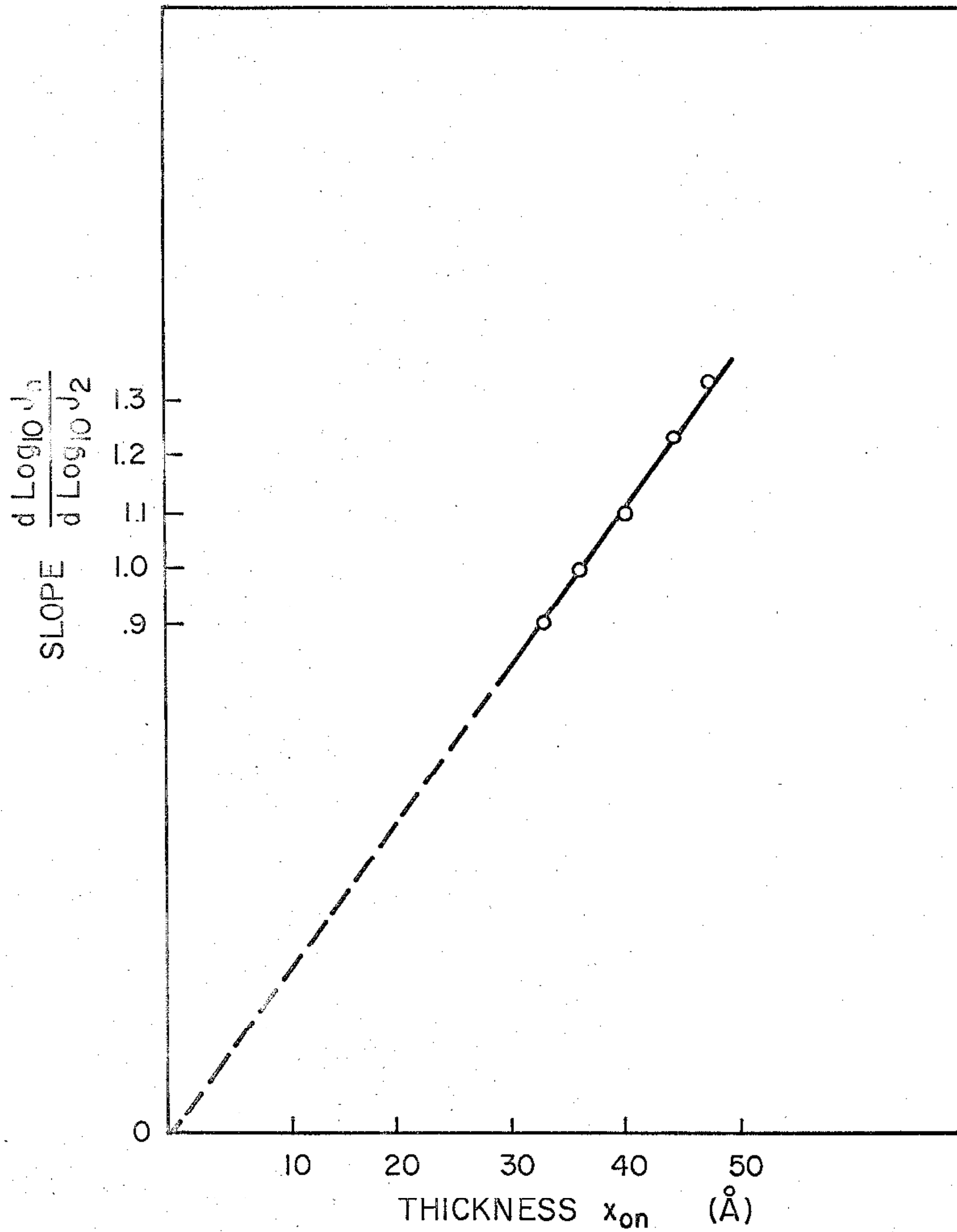

Figure 3.4 Slopes of $\log_{10}J_n$ versus $\log_{10}J_2$ plots of Figure 3.3 as a function of insulator thickness x_{on}.

where B(V) is a decreasing function of voltage. This functional dependence of current on insulator thickness and voltage is very strong evidence that the observed currents were the result of electron tunneling through a trapezoidal barrier with the tunneling probability proportional to the product of the tunneling path length and the average value of the x component of imaginary momentum encountered along a tunneling path.

Measurements carried out at room temperature allowed the observation of currents for only a narrow range of applied voltage. The maximum value of positive and negative voltages that could be safely applied to the counterelectrodes were 1.3 volts and 0.9 volts respectively. It was found that the structures could sustain much higher voltages at low temperatures. Figures 3.5 through 3.9, although involving structures from a different sample, are essentially a repetition of Figures 3.1 through 3.4. However, the information within them is broader in scope in that it is based on 77°K current voltage characteristics taken over wider ranges of applied voltage of both polarities. Consequently, the experimental determination of the geometry of the trapezoidal barrier and the insulator energy momentum relationship appropriate to thin film structures with Magnesium counterelectrodes will be based on these low temperature measurements.

Figure 3.5 relates $\log_{10}$ RC' of five structures (sample A) to their insulator thickness with R measured at 77°K. Since the

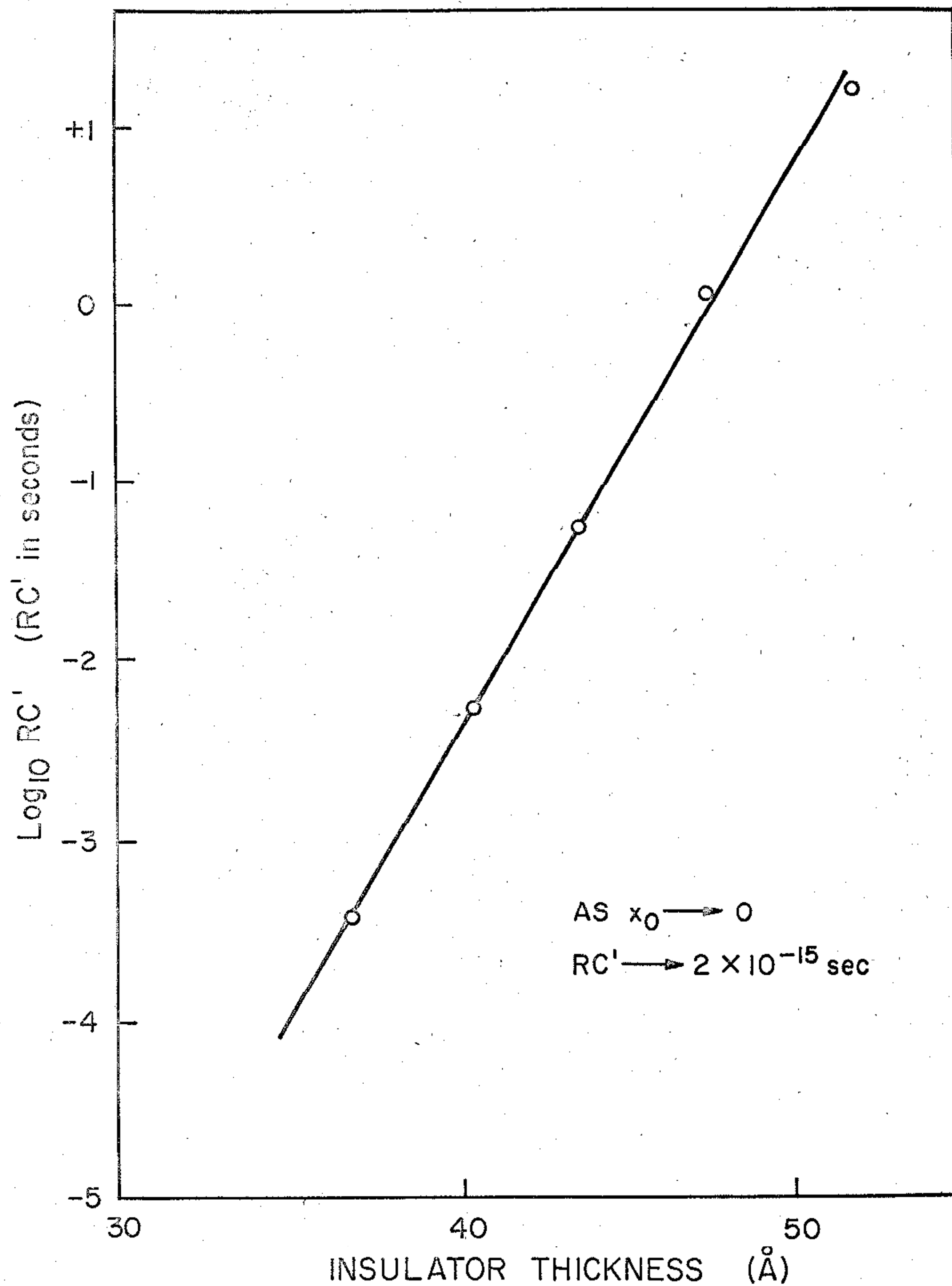

Figure 3.5 RC', R measured at 77°K, of five Al-AlN-Mg structures versus insulator thickness (sample A).

structures used for the plots given in Figures 3.1 and 3.5 came from the same sample, the exponential dependence of the resistance capacitance product on insulator thickness can be considered valid at least over a six decade variation in RC'. It must be added that good reproducibility between structures was obtained; the zero thickness intercept of $\log_{10}$ RC' was essentially the same for all samples with the slope of the plot varying by no more than 5% from sample to sample. It is felt that the major part of the variation in slope could be accounted for by the undetectable variation of counterelectrode area from sample to sample leading to an incorrect identification of insulator thickness deduced from the counterelectrode area and structure capacitance. Magnesium was found to be a difficult metal to work with in that the deposited areas did not necessarily correspond to those defined by the geometry of the mask; apparently, Magnesium has a tendency to travel over the surface of the substrate over which it is deposited.

The current at 77°K for the five structures used in Figure 3.5 is plotted as a function of applied voltage of both polarities in Figure 3.6. The plots of $\log_{10}$J versus $\log_{10}$J appropriate to these current voltage characteristics are shown in Figures 3.7 and 3.8. It can be seen that the current at intermediate voltages for structures with thicker insulating regions is greater than that expected on the basis of currents in structures with thinner in-

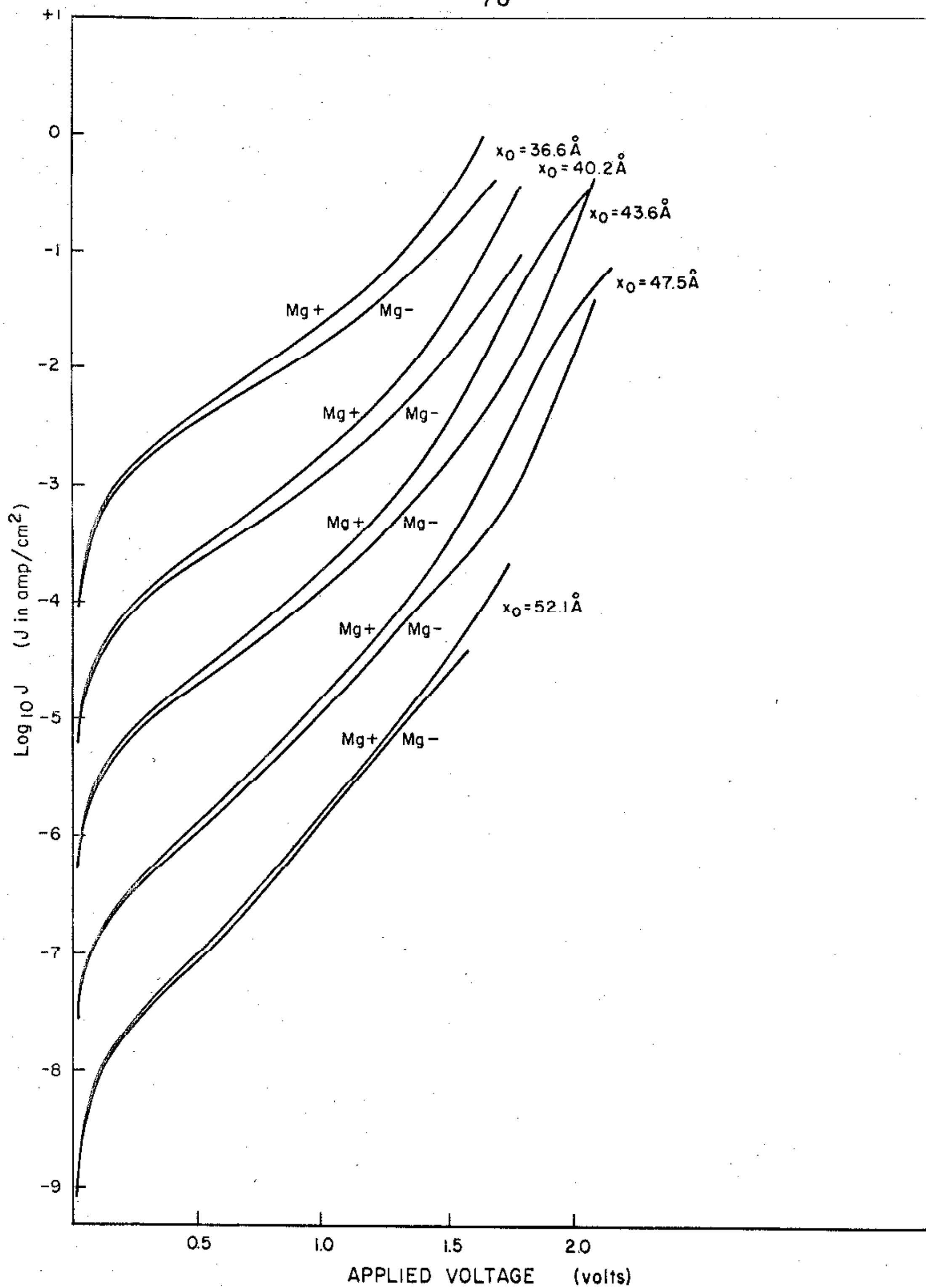

Figure 3.6 77°K J(V) versus V for 5 Al-AlN-Mg structures with insulator thicknesses from 36 to 52 Å (sample A). Mg+ corresponds to a positive voltage applied to counterelectrodes.

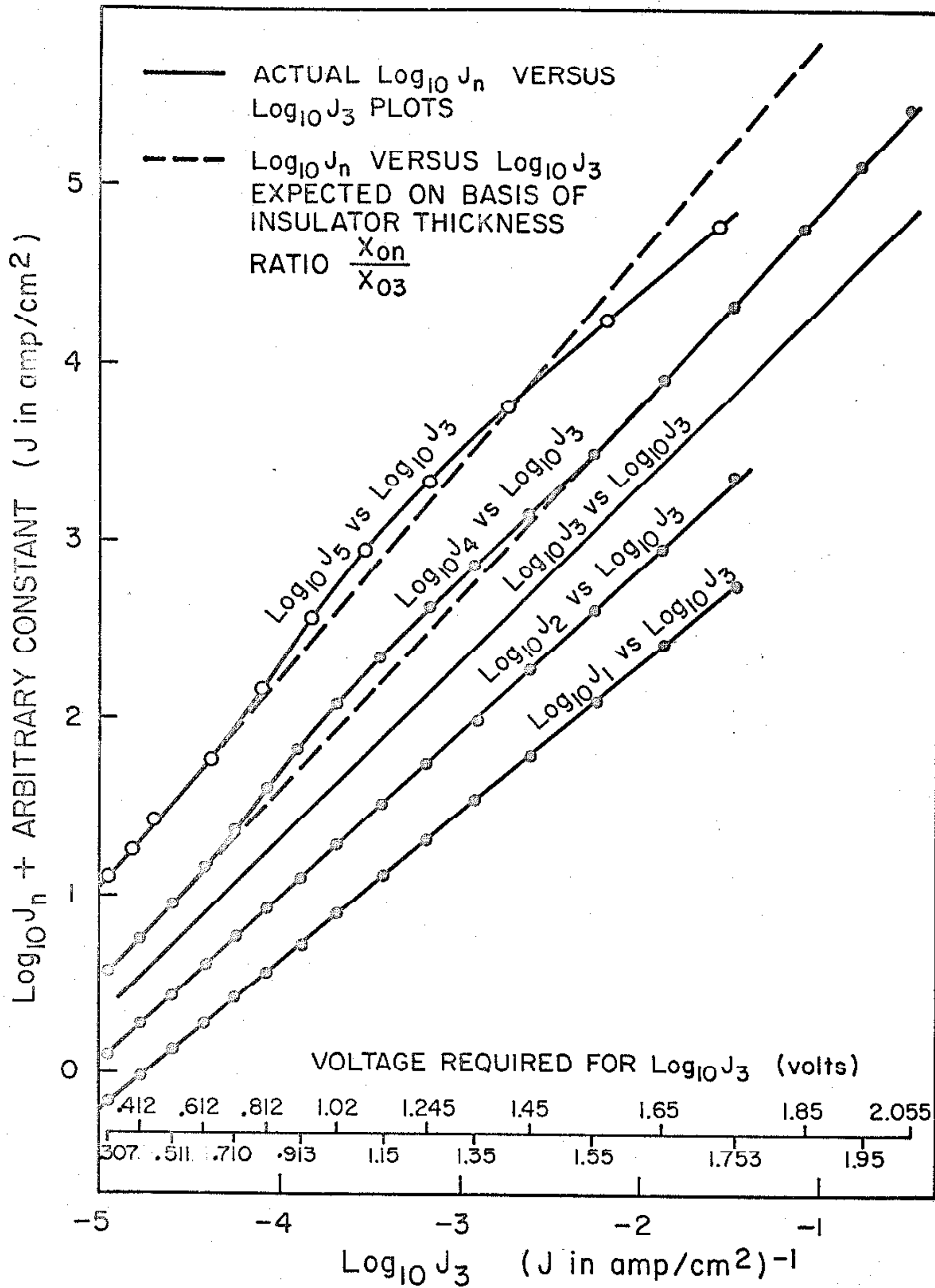

Figure 3.7 $\log_{10} J_n(V)$ versus $\log_{10} J_3(V)$ plots of characteristics shown in Figure 3.6 (counterelectrodes positive).

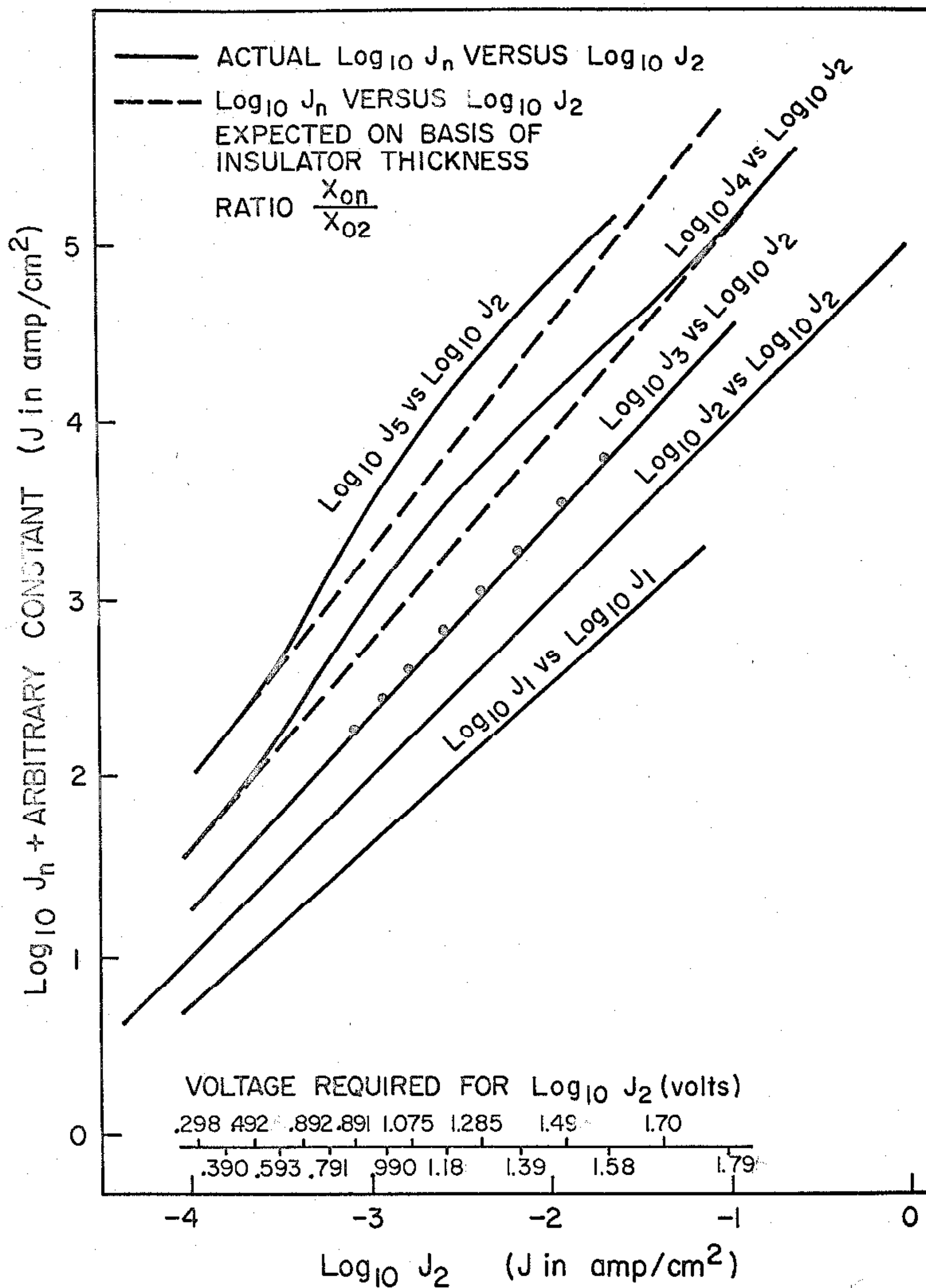

Figure 3.8 $\log_{10}J_n(V)$ versus $\log_{10}J_3(V)$ plots of characteristics shown in Figure 3.6 (counterelectrodes negative).

sulating regions. Furthermore there is some evidence to indicate that for higher applied voltages the current for these thicker structures is equal or smaller than that expected on this basis (see plots $\log_{10} J_5$ and $\log_{10} J_4$ versus $\log_{10} J_3$ in Figure 3.7). These deviations from expected behavior are more prominent in structures with Aluminum counterelectrodes and will be considered in the section dealing with these structures.

It must be noted that the results obtained at a temperature of 77°K are not in disagreement with those obtained at room temperature. The deviations seen in Figures 3.7 and 3.8 are associated with structures having thicker insulating regions than those associated with Figure 3.4.

No noticeable change in the current voltage characteristics was observed between 4°K and 77°K.

The slopes of the $\log_{10} J$ versus $\log_{10} J$ plots shown in Figures 3.7 and 3.8 are correlated to the insulator thickness in Figure 3.9. The meager number of points in this correlation is the main reason for the presentation of room temperature characteristics.

It is evident from the data just presented that the current through thin film structures with Magnesium counterelectrodes and with insulator thicknesses smaller than 48 Angstroms is that expected on the basis of electron tunneling through the forbidden band

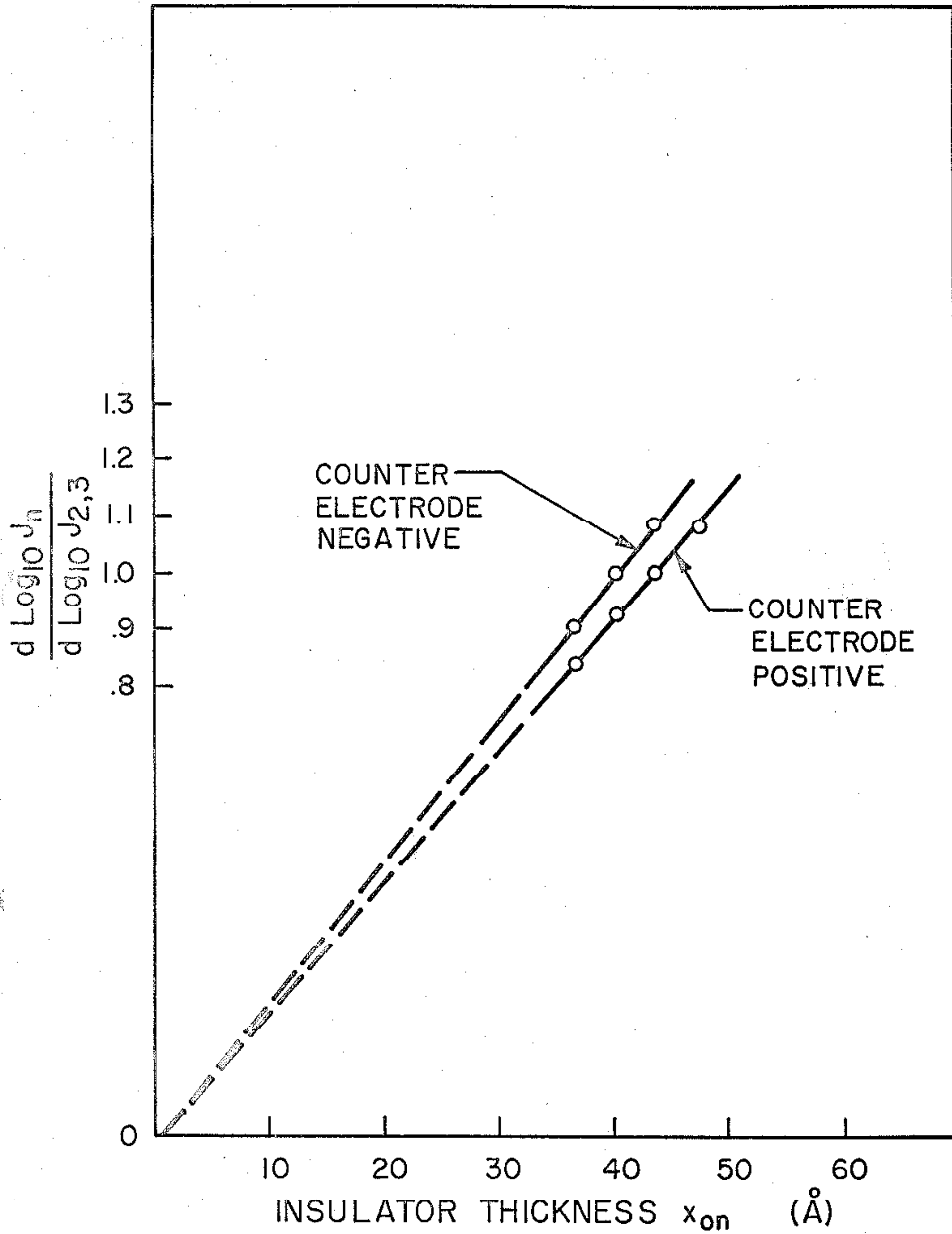

Figure 3.9 Slopes of $\mathrm{Log}_{10} J_n$ versus $\mathrm{Log}_{10} J_{2,3}$ plots shown in Figures 3.7 and 3.8 as a function of insulator thickness.

of a trapezoidal barrier. The current at all voltages is exponentially dependent on insulator thickness; furthermore, the functional dependence of the current on thickness and voltage at higher voltages is that given by (3.2). All that remains now is the experimental determination of the barrier geometry and the insulator energy momentum relationship appropriate to thin film structures Al-AlN-Mg from the data just presented.

3.1.2 Barrier Geometry and Insulator Energy Momentum Relationship.

There are in principle three methods of obtaining the barrier geometry or barrier heights at the metal insulator interfaces and the energy momentum relationship characterizing the insulator forbidden band. The first two methods involve the determination of the coefficient B(V) either from the dependence of current on insulator thickness (see (1.51) and (1.53)) or, from the current voltage characteristic of a particular structure, and the use of (1.44) which relates B(V) to the insulator energy momentum relationship. The third method involves the determination of the coefficients C(V) from measurement of the temperature dependence of the tunneling current and the use of (1.45). The application of these three methods will be considered in this section. The subscripts "+" and "-" will be used to differentiate the coefficients and currents corresponding to positive and negative voltages applied to the counterelectrodes.

3.1.2a Dependence of Current on Insulator Thickness.

Consider the current voltage characteristic of structure 2, sample A, with insulator thickness x_{o2}. The low voltage conductance per unit area is given by

$$\frac{J_2}{V} = \frac{4\pi m_m^* e^2}{h^3 D^*(0) x_{o2}} \exp[-B^*(0) x_{o2}] \qquad (3.3)$$

(The temperature dependent component of the tunneling current in the above and following expressions is ignored since the current voltage characteristics to which they will be applied were found to be temperature independent). The low voltage conductance per unit area for structure 1, sample A, with insulator thickness x_{o1} is given by

$$\frac{J_1}{V} = \frac{4\pi m_m^* e^2}{h^3 D^*(0) x_{o1}} \exp[-B^*(0) x_{o1}] \qquad (3.4)$$

Dividing (3.3) by (3.4) the following result is obtained.

$$B^*(0) = \frac{\ln \left\{ \frac{x_{o1}}{x_{o2}} \frac{J_1/V}{J_2/V} \right\} \Big/_{V \to 0}}{x_{o2} - x_{o1}} \qquad (3.5)$$

It can be shown in a similar way that for higher voltages, $eCV \geq 1$

$$B^*(V) = \frac{\ln \left\{ \frac{x_{o1}^2}{x_{o2}^2} \frac{J_1}{J_2} \right\}}{x_{o2} - x_{o1}} \qquad (3.6)$$

The relations between $B^*_\pm(V)$, the insulator energy momentum relationship Im p_{ins} (ϕ_c – E), and the barrier heights ϕ_1 and ϕ_2 were derived in Chapter I and for convenience will be re-stated here.

$$\frac{d}{dV}\left[\left(\frac{\phi_1-\phi_2+eV}{e}\right)B^*_+(V)\right]=\frac{2}{\hbar}\,Im\,p_{ins}(\phi_2-eV) \quad (3.7)$$

$$\frac{d}{dV}\left[\left(\frac{\phi_2-\phi_1+eV}{e}\right)B^*_-(V)\right]=\frac{2}{\hbar}\,Im\,p_{ins}(\phi_1-eV) \quad (3.8)$$

The difference between the barrier energies $(\phi_1-\phi_2)$ is that value which when used with (3.7) and (3.8) allows $B^*_+(V)$ and $B^*_-(V)$ to yield identical energy momentum relationships. The barrier heights ϕ_1 and ϕ_2 are given by the product of the electron charge and those values of voltage V_1 and V_2 for which Im p_{ins} $(\phi_1 - eV_1)$ and Im p_{ins} $(\phi_2 - eV_2)$ become equal to zero.

The coefficients $B^*(0)$ and $B^*_\pm(V)$ obtained with the use of (3.5) and (3.6) and the current voltage characteristics of structures 1 and 2, sample A, are shown in Figure 3.10. The differentiations of $B^*_\pm(V)$ required by (3.7) and (3.8) were performed and the resulting energy momentum relationship is illustrated in Figure 3.11 by a plot of $\left(\frac{2}{h}\text{ Im } p_{ins}\right)^2$ as a function of

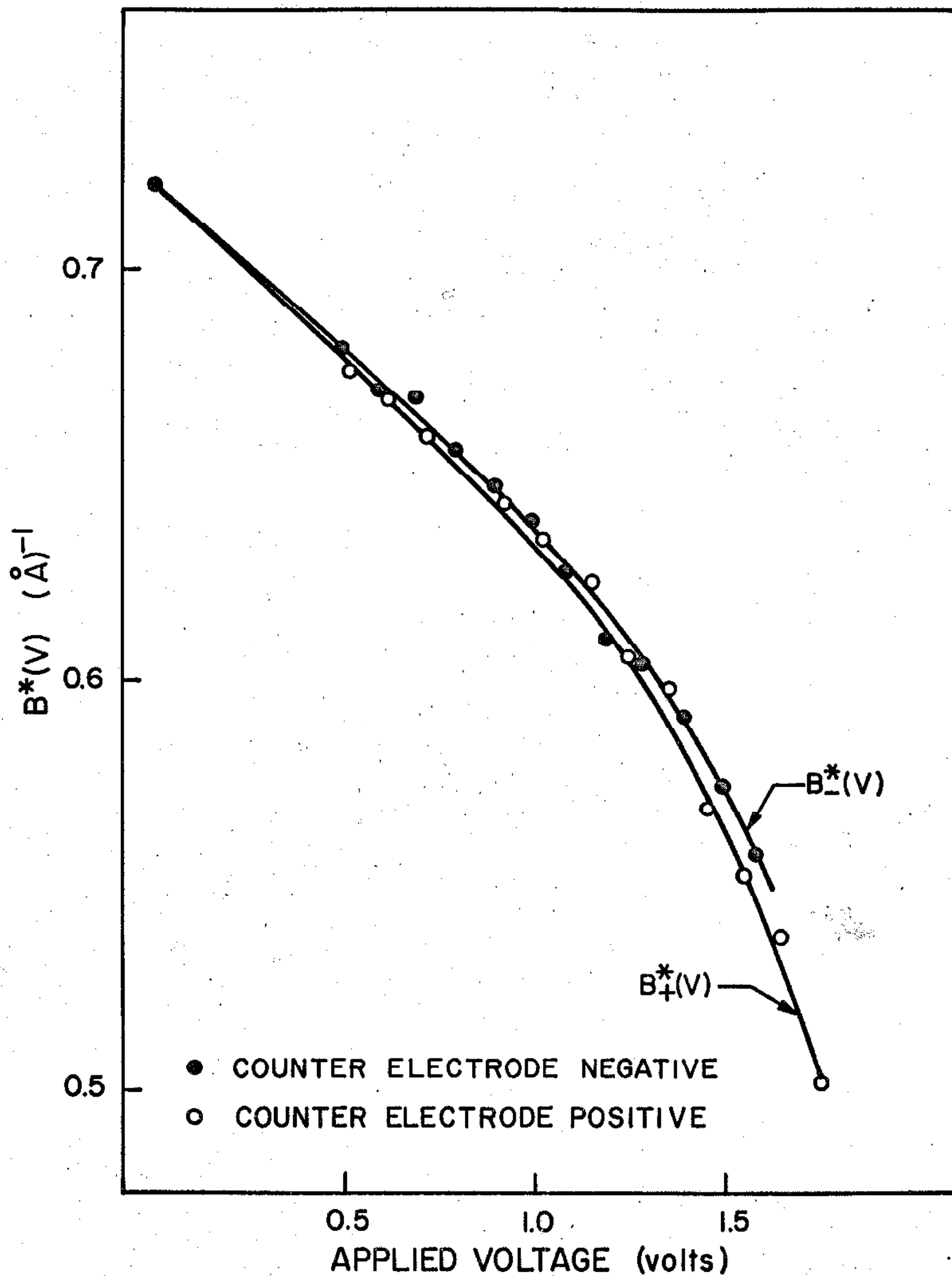

Figure 3.10 $B^*(V)$ for Al-AlN-Mg structures obtained from dependence of current on insulator thickness.

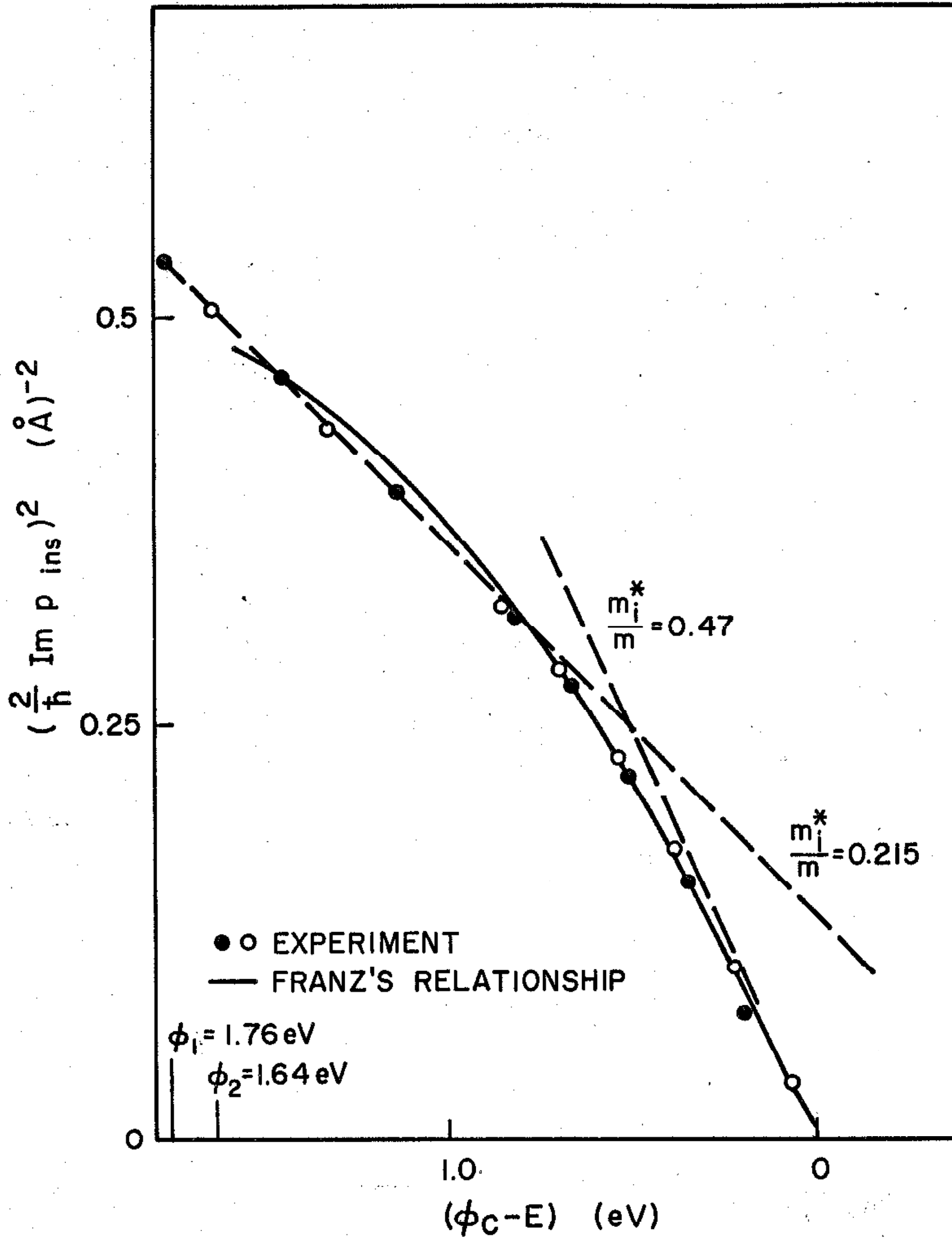

Figure 3.11 Insulator energy momentum relationship. ● and ○ represent relationships obtained from $B_-^*(V)$ and $B_+^*(V)$ in Figure 3.10. Solid line is best fit of Franz's relationship.

energy referred to the conduction band edge of the insulator. The barrier energies were found to be ϕ_1 = 1.77 eV and ϕ_2 = 1.64 eV. It is evident that the energy momentum relationship over the ranges of energy relevant to tunneling is not describable by a simple parabolic equation of the form

$$p_{INS}^2 = 2m_i^* [E - \phi_c] \tag{3.9}$$

The plot in Figure 3.11 is not a straight line.

Is this a surprising result? The answer is in the negative. The energy momentum relationship is expected to be parabolic only in the vicinity of the conduction and valence band edges. Thus for energies near the valence band edge the following expression should be valid.

$$p_{INS}^2 = 2m_{iv}^* [\phi_v - E] \tag{3.10}$$

where ϕ_v is the valence band edge energy and m^*_{iv} is the effective mass of holes with energies in the vicinity of this edge. Consequently, $(\mathrm{Im}\ p_{ins})^2$ is expected to increase linearly with decreasing energy referenced to the conduction band edge, bend over and linearly decrease towards zero at an energy corresponding to the insulator valence band edge. Equation (3.9) is expected to be useful in the determination of the tunneling probabil-

ity only if the height of the barrier separating the two metal electrodes is a very small fraction of the insulator forbidden energy gap.

It is quite possible that Figure 3.11 represents an experimental observation of the effect of the insulator valence band on the energy momentum relationship. The observed barrier height is approximately 1.7 eV while the forbidden band gap of AlN is reported in the literature as 4.2 eV[15].

Franz[16] has proposed an empirical energy momentum relationship within the forbidden band of an insulator. For equal effective masses near the valence and conduction band edges

$$p_{ins}^2 = 2m_i^*[E-\phi_c][1-\frac{(\phi_c-E)}{E_g}] \qquad (3.11)$$

Here, E_g is the insulator forbidden energy gap. An attempt to fit this relationship to the experimental result is shown in Figure 3.11. E_g was assumed to equal 4.2 eV. The best fit obtained was with the use of an effective mass to free electron mass ratio of 0.47. It is evident that (3.11) describes the observed energy momentum relationship quite well down to some 1.5 eV below the insulator conduction band edge.

For a narrow range of energies near 1.7 eV below the insulator conduction band edge, Im $p_{ins}(\phi_c - E)$ behaves as if

the energy momentum relationship were parabolic with an effective mass to free electron mass ratio of 0.215 and as if the barrier energies were ϕ_1 =2.36 eV and ϕ_2 = 2.24 eV (see Figure 3.11). This circumstance allows the calculation of $D^*(0)$ and thus the expected value of the zero thickness intercept of RC' (see 3.1). The theoretical value of this zero thickness intercept becomes 3.3×10^{-15} seconds and compares favorably with the value of 4×10^{-15} seconds deduced experimentally from the data shown in Figure 3.1.

3.1.2b Current Voltage Characteristic.

The second method of obtaining the coefficient $B^*(V)$ involves the use of the current voltage characteristic of a particular structure. Consider the current for structure 3, sample A, with insulator thickness x_{o3}.

$$\ln J_3 = \ln \frac{4\pi m m^* e}{h^3 D^*(0) C^*(0) x_{o3}^2} + \ln[1 - \exp(x_{o3} C^* e V)] - \ln \frac{C^*(V) D^*(V)}{C^*(0) D^*(0)} - x_{o3} B^*(V) \qquad (3.12)$$

For voltages approaching 0

$$x_{o3} B^*(0) = \ln \frac{J_0 C^*(0) e V x_{o3}}{J_3} \qquad (3.13)$$

For higher voltages $CeV \gg 1$

$$x_{03}\,B^*(V) = \ln \frac{J_0}{J_3} - \ln \frac{C^*(V)\,D^*(V)}{C^*(0)\,D^*(0)} \qquad (3.14)$$

where $$J_0 = \frac{4\pi m_m^* e}{h^3 D^*(0) C^*(0)\, x_{03}^2}$$

The second term in (3.14) is small in comparison to $\log_e \frac{J_0}{J_3(V)}$. However, this term may not be neglected since it has some effect in the determination of the energy momentum relationship for energies near the insulator conduction band edge.

The existence of the coefficient $C^*(0)$, $D^*(0)$, $C^*(V)$, and $D^*(V)$ in (3.13) and (3.14) is unfortunate in that knowledge of their values implies knowledge of $B^*(V)$. It is possible in principle to obtain expressions involving only $B^*(V)$ and J_3 with the use of the relations connecting $B^*(V)$, $C^*(V)$, and $D^*(V)$ developed in Chapter I. Unfortunately these expressions are complicated and considerable effort would be required for their solution. Since the purpose of the following discussion is to show that the current voltage characteristic of a particular structure is that expected on the basis of the current dependence on thickness, the small correction term $\log_e \frac{C^*(V)D^*(V)}{C^*(0)D^*(0)}$ was computed using $C^*(V)$ and $D^*(V)$ obtained from the energy momentum relationship shown in Figure 3.11. Figure 3.12 illustrates $B^*_1(V)$ obtained with the use of the

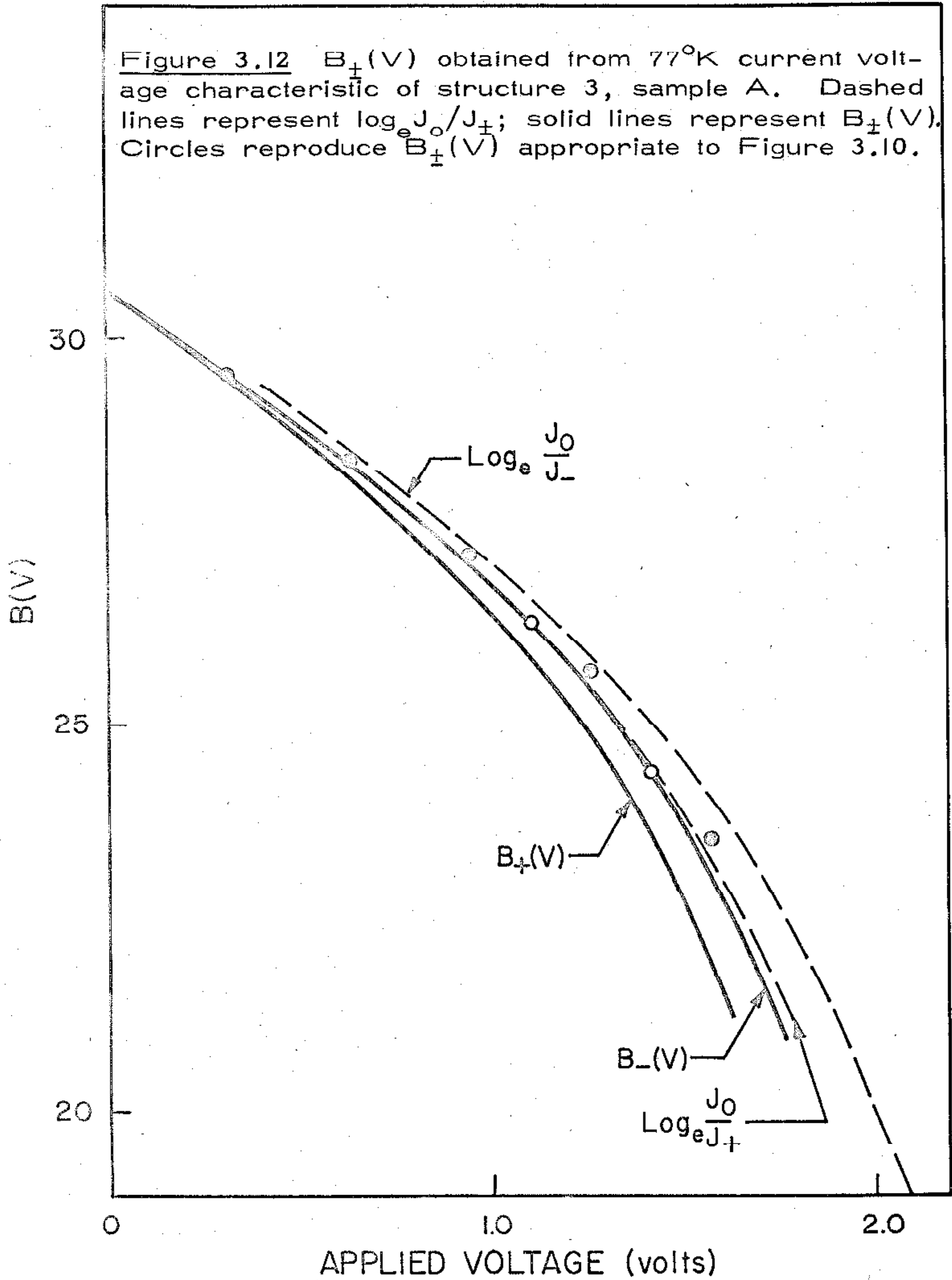

Figure 3.12 $B_\pm(V)$ obtained from 77°K current voltage characteristic of structure 3, sample A. Dashed lines represent $\log_e J_o/J_\pm$; solid lines represent $B_\pm(V)$. Circles reproduce $B_\pm(V)$ appropriate to Figure 3.10.

current voltage characteristic of structure 3, sample A, and (3.13) and (3.14). The dashed lines represent the term $\log_e \frac{J_o}{J_3}$ The difference between the dashed line and $B^*_\pm(V)$ gives a feeling for the magnitude of the term, $\log_e \frac{C^*_\pm(V)\, D^*_\pm(V)}{C^*(0) D^*(0)}$ which is independent of insulator thickness. Relatively good agreement is seen to exist between the coefficients $B^*_\pm(V)$ obtained in this manner and those obtained from the dependence of current on insulator thickness. The detailed discrepancy seen in this comparison can easily be attributed to a very small shift in the current voltage characteristics of either structure I or 2, sample A, occurring during the measurement of current as a function of applied voltage. Such a small shift would have a negligible effect in $B_\pm(V)$ obtained from a particular current voltage characteristic.

The insulator energy momentum relationship and barrier geometry obtained from $B^*_\pm(V)$ corresponding to the current voltage characteristic of structure 3, sample A, is presented in Figure 3.13 and is seen to be slightly different from that shown in Figure 3.11. The barrier heights become ϕ_1 = 1.68 eV and ϕ_2 = 1.53 eV while the best fit of Franz's empirical relationship to the data, assuming a forbidden energy gap of 4.2 eV, requires an effective mass to free electron mass ratio of 0.446. Once again for energies more than 1 eV below the insulator conduction band edge the energy momentum relationship is seen to be parabolic with an effective mass to free electron mass ratio of

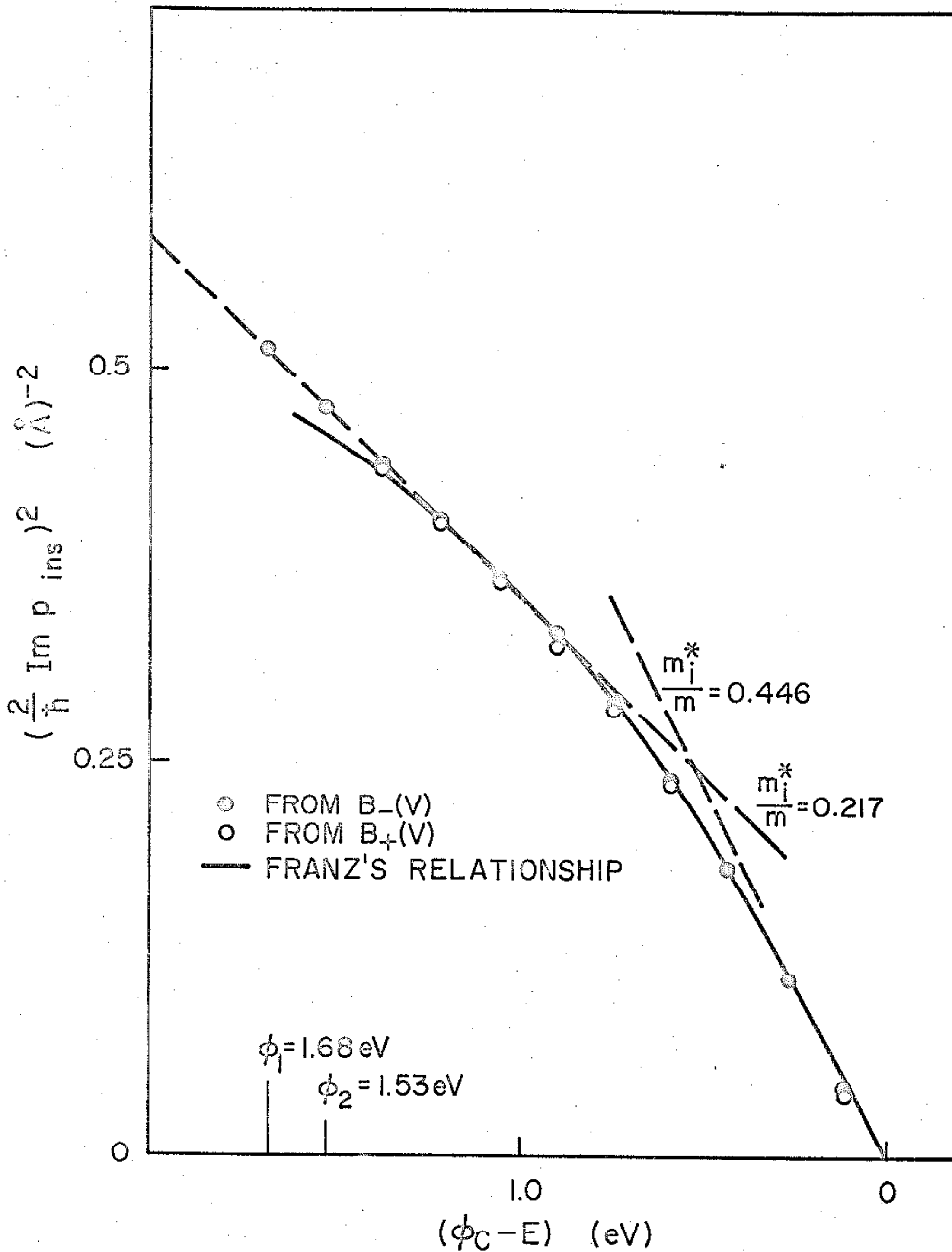

Figure 3.13 Insulator energy momentum relationship obtained from $B_\pm(V)$ in Figure 3.12. Solid line represents best fit of Franz's relationship; circles represent experimentally determined relationship.

o.217.

The energy momentum relationship shown in Figure 3.13 is undoubtedly more accurate than that shown in Figure 3.11. The use of $C^*(V)$ and $D^*(V)$ corresponding to the variation of current on insulator thickness in the evaluation of the energy momentum relationship from the current voltage characteristic introduces only a negligible error into the result obtained.

3.1.2c Tunneling Current Temperature Dependence.

The third method of experimentally determining the insulator energy momentum relationship and barrier geometry appropriate to a particular structure involves a measure of the temperature dependence of the tunneling current. Referring to (1.35) it can be seen that

$$\frac{6}{\pi^2}\frac{1}{J(V,0)}\frac{\partial J(V,T)}{\partial[(kT)^2]} = [C^*(V)x_o]^2 \qquad (3.15)$$

Restating (1.45), simple relations between $C^*(V)$, the barrier heights, and the insulator energy momentum relationship are seen to exist.

$$\frac{2}{\hbar}\{Im\, p_{INS}(\phi_1) - Im\, p_{INS}(\phi_2 - eV)\} = (\phi_1 - \phi_2 + eV)C_1^*(V) \qquad (3.16)$$

$$\frac{2}{\hbar}\left\{ \mathrm{Im}\, p_{INS}(\phi_2) - \mathrm{Im}\, p_{INS}(\phi_1 - eV) \right\} = (\phi_2 - \phi_1 + eV)\, C_{-}^{*}(V) \quad (3.17)$$

Use of (3.16) and (3.17) is greatly facilitated by the fact that the barrier heights ϕ_1 and ϕ_2 should in principle be identifiable by the cusps generated by the experimentally determined coefficients $C_{\pm}^{*}(V)$. It must be added that this procedure for determining the insulator energy momentum relationship is valid only as long as the temperature dependence of the tunneling current can be attributed solely to the temperature variation of the Fermi-Dirac distributions within the metals.

Temperature measurements indicated that the derivative of current with respect to T^2 was constant but only up to temperatures in the order of 200°K and only for structures with insulating regions thinner than 43 Å.

In Figure 3.14 $C_{+}^{*}(V)$, obtained experimentally with the use of (3.15), is plotted as a solid line and seen to be too large when compared to $C_{+}^{*}(V)$ expected on the basis of the energy momentum relationship shown in Figure 3.11. However, $C_{+}^{*}(V)$ based on temperature measurements has cusps at voltages close to those of the barrier height ϕ_2 predicted by the current voltage characteristics of Al-AlN-Mg structures and the dependence of current through these structures on insulator thickness. The experimentally observed cusps in Figure 3.14 occur in the vicin-

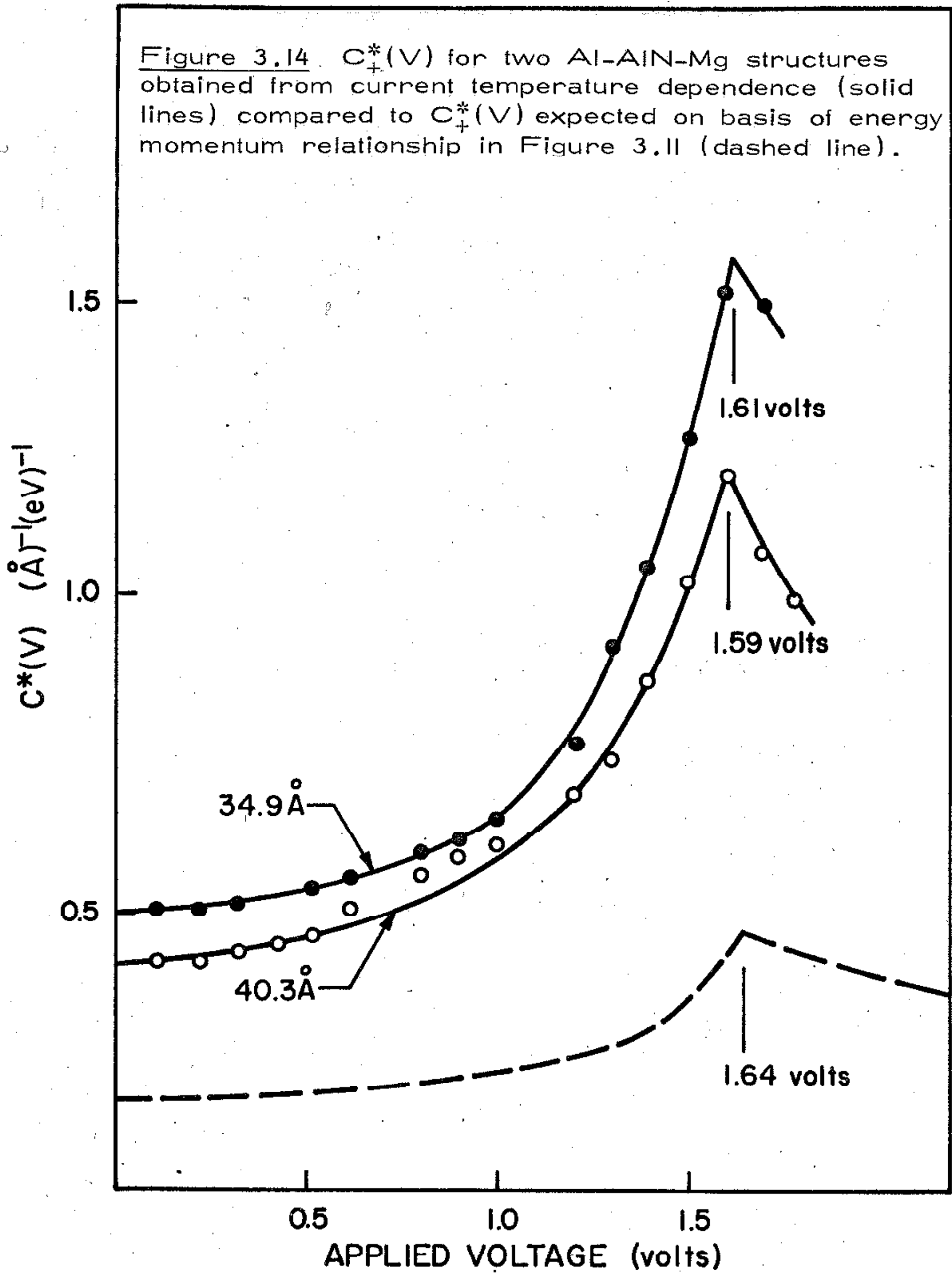

Figure 3.14 $C_+^*(V)$ for two Al-AlN-Mg structures obtained from current temperature dependence (solid lines) compared to $C_+^*(V)$ expected on basis of energy momentum relationship in Figure 3.11 (dashed line).

ity of 1.60 volts while the values for the barrier height ϕ_2 associated with Figures 3.11 and 3.13 are 1.64 eV and 1.53 eV. A cusp for $C_-^*(V)$ could not be obtained; samples with currents which were stable with time at high negative voltages were not available. Consequently, high negative voltage currents for different temperatures could not be compared. At lower values of negative voltage applied to the counterelectrode, the temperature dependence was less pronounced than that for positive applied voltages.

It is very doubtful that the observed increase in current with temperature can be attributed solely to the temperature variation of the Fermi-Dirac distributions within the metals. It is quite conceivable that the energy momentum relationship characterizing the forbidden band of the insulator varies in such a way as to lead to increasing tunneling probabilities with increasing temperatures. Measurements of barrier heights in thin film structures using Aluminum Oxide insulating regions indicate a decrease of barrier height with increasing temperature[17]. A similar effect in the thin film structures used in this research could explain the observation that $C_+^*(V)$, obtained with (3.15) and the temperature dependence of the tunneling current, was greater than that expected on the basis of other data by a factor of approximately 2. The following simple model illustrates this point.

Consider a trapezoidal barrier with an energy momentum relationship independent of temperature and barrier heights given by

$$\phi_{1,2} = \overline{\phi}_{1,2} - \eta (kT)^2 \tag{3.18}$$

As a result, the coefficients $B^*(V)$, $C^*(V)$, and $D^*(V)$ are all dependent on temperature. The total current is thus given by

$$J(V,T) = \exp[-B^*(V,T)x_0] \frac{4\pi m_m^* e \{1 + \frac{\pi^2}{6}[C^*(V,T)x_0 kT]^2\}\{1 - \exp[-C^*(V,T)x_0 eV]\}}{h^3 C^*(V,T) D^*(V,T) x_0^2} \tag{3.19}$$

If the temperature variation of the coefficient C^* and D^* in the expressions defining the effective number of tunneling electrons is ignored it can be shown that

$$\frac{1}{J(V,0)} \left. \frac{d\,J(V,T)}{d\,[(kT)^2]} \right|_{\text{as } kT \to 0} = \frac{\pi^2}{6}[C^*(V,0)x_0]^2 + \eta C^*(V,0)x_0 \tag{3.20}$$

The model yields a tunneling current which at low temperature may be considered to have a temperature dependent component proportional to $(kT)^2$. Furthermore, the proportionality coefficient, equal to the expression on the right hand side of (3.20), is expected to have a maximum at a positive voltage equal to ϕ_2/e or ϕ_1/e depending on whether this voltage is applied to the

counter or base electrode. It is of interest to note that for Al-AlN-Mg structures with insulator thicknesses in the vicinity of 35 Å, η need only be equal to approximately $9(eV)^{-1}$ for the contributions of the barrier height variations and the Fermi-Dirac distribution variations to the temperature dependence of the tunneling current to be equal ($\eta = \frac{\pi^2}{6} C^*(V,0)x_o$).

The low temperature variation of insulator forbidden energy gaps is known to follow the following relation at low temperatures[18].

$$E_g(T) = E_{go} - \eta_g (KT)^2 \tag{3.21}$$

where η_g is usually in the order of $10^{+2}(eV)^{-1}$. If $10^{+2}(eV)^{-1}$ is a representative value for η in the above model it is not surprising that the observed temperature dependence of the tunneling current was greater than that expected on the basis of the temperature variation of the Fermi-Dirac distributions within the metals.

3.2 PROPERTIES OF STRUCTURES WITH ALUMINUM COUNTERELECTRODES

The current voltage characteristics of Al-AlN-Al structures with the thinnest insulating regions were consistent with the insulator energy momentum relationship shown in Figure 3.13. The currents through structures with thicker insulating regions were complicated by the presence of an excess current. Even

though this excess current was exponentially dependent on thickness and essentially independent of temperature it could not be interpreted as the result of electron tunneling with the exponent of the tunneling probability proportional to the product of $\overline{\mathrm{Im}\ \chi_{ins}}$ and the tunneling path length.

3.2.1 Barrier Geometry and Insulator Energy Momentum Relationship.

The 77°K current voltage characteristic of an Al-AlN-Al structure with an insulator thickness of 39.5 Å was inserted in (3.13) and (3.14) for the determination of the insulator energy momentum relationship and barrier energies appropriate to these structures.

The coefficients $C^*(V)$ and $D^*(V)$ inserted in (3.13) and (3.14) were those obtained from the energy momentum relationship shown in Figure 3.13; the parabolic dependence exhibited by this relationship at energies more than 1.0 eV below the insulator conduction band edge was extrapolated towards lower energies and barrier energies $\phi_1 = 1.68$ eV and $\phi_2 = 2.0$ eV were arbitrarily assumed.

The resulting coefficients $B_{\pm}(V)$ based on the current voltage characteristic of an Al-AlN-Al structure and the insulator energy momentum relationship deduced from the current voltage characteristic of an Al-AlN-Mg structure, are shown in Figure 3.15. $\mathrm{Log}_e \frac{J_o}{J_{\pm}}$ are represented by dashed lines while

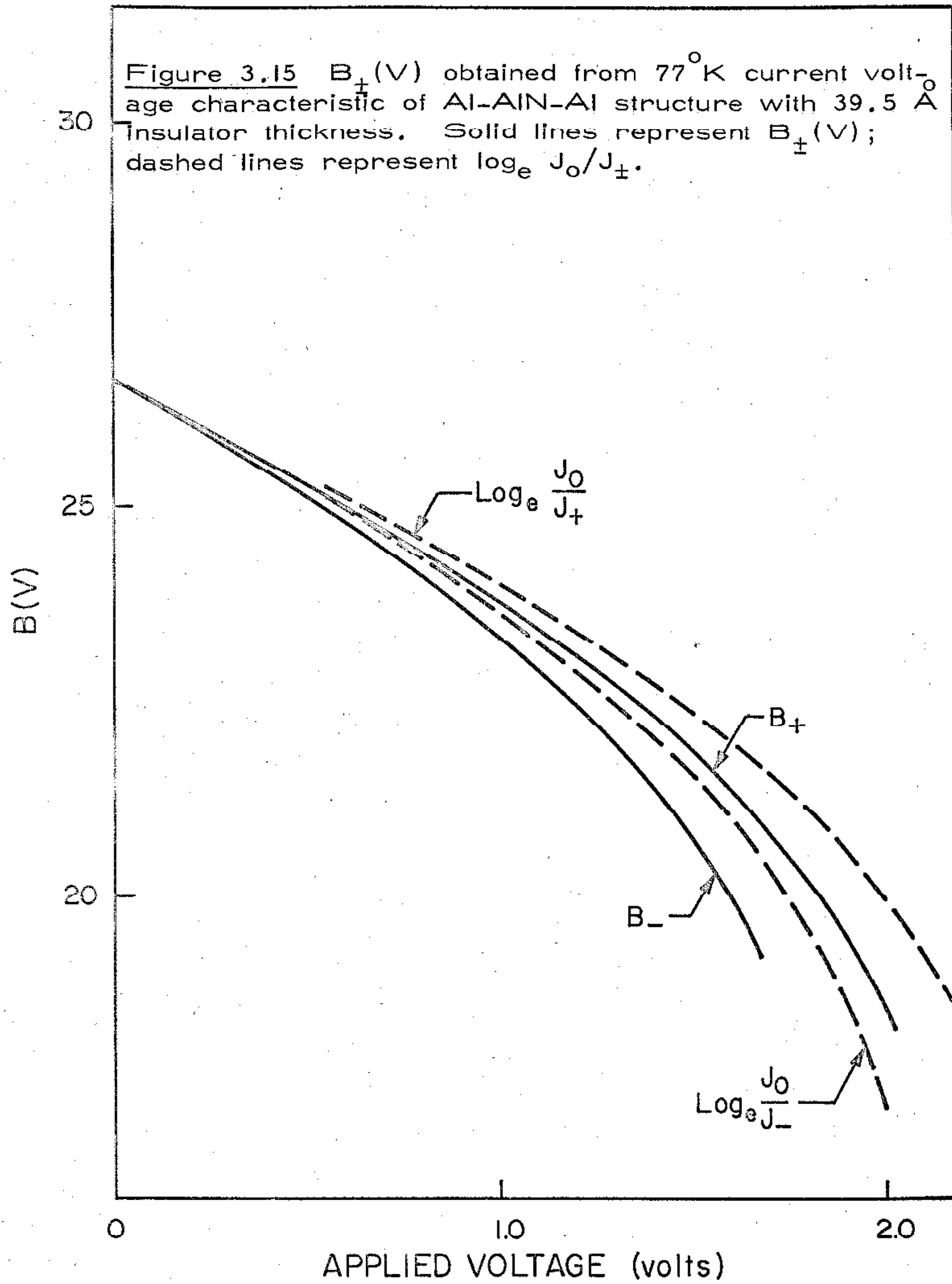

Figure 3.15 $B_{\pm}(V)$ obtained from 77°K current voltage characteristic of Al-AlN-Al structure with 39.5 Å insulator thickness. Solid lines represent $B_{\pm}(V)$; dashed lines represent $\log_e J_o/J_{\pm}$.

$B_{\pm}(V)$ are represented by solid lines. The presentation of these two terms allows a visualization of the magnitude of $\log_e \frac{C^*(V)D^*(V)}{C^*(0)D^*(0)}$.

The differentiation of the coefficients $B_{\pm}(V)$ as by (3.7) and (3.8) led to the insulator energy momentum relationship shown in Figure 3.16. It is seen that the energy momentum relationship is the same as that shown in Figure 3.13. Furthermore the barrier heights determined by this procedure were ϕ_1 = 1.67 eV and ϕ_2 = 2.01 eV. Thus the assumptions made in the evaluation of the term $\log_e \frac{C^*(V)D^*(V)}{C^*(0)D^*(0)}$ are justified.

The fact that the Al-AlN-Mg insulator energy momentum relationship (Figure 3.13) had to be scaled down by a factor of 1.2 to match the Al-AlN-Al energy momentum relationship (Figure 3.16) is an insignificant discrepancy. The fabrication procedure used guaranteed all structures on a given sample to have identical areas not necessarily equal to those on different samples. However, because of the difficulty involved in the definition of counterelectrode areas no attempt was made to measure the sample to sample variations; structure areas on all samples were assumed equal. Since $B_{\pm}(V)$ for $V < \phi_{2,1}$ involves the product of the insulator thickness and $\overline{\text{Im } p_{ins}}$, an error in the assumed structure area for a given sample results in an error in the scale used for x_o and thus in the scale used for $\text{Im } p_{ins}$. The necessity of scaling down the Al-AlN-Mg energy momentum re-

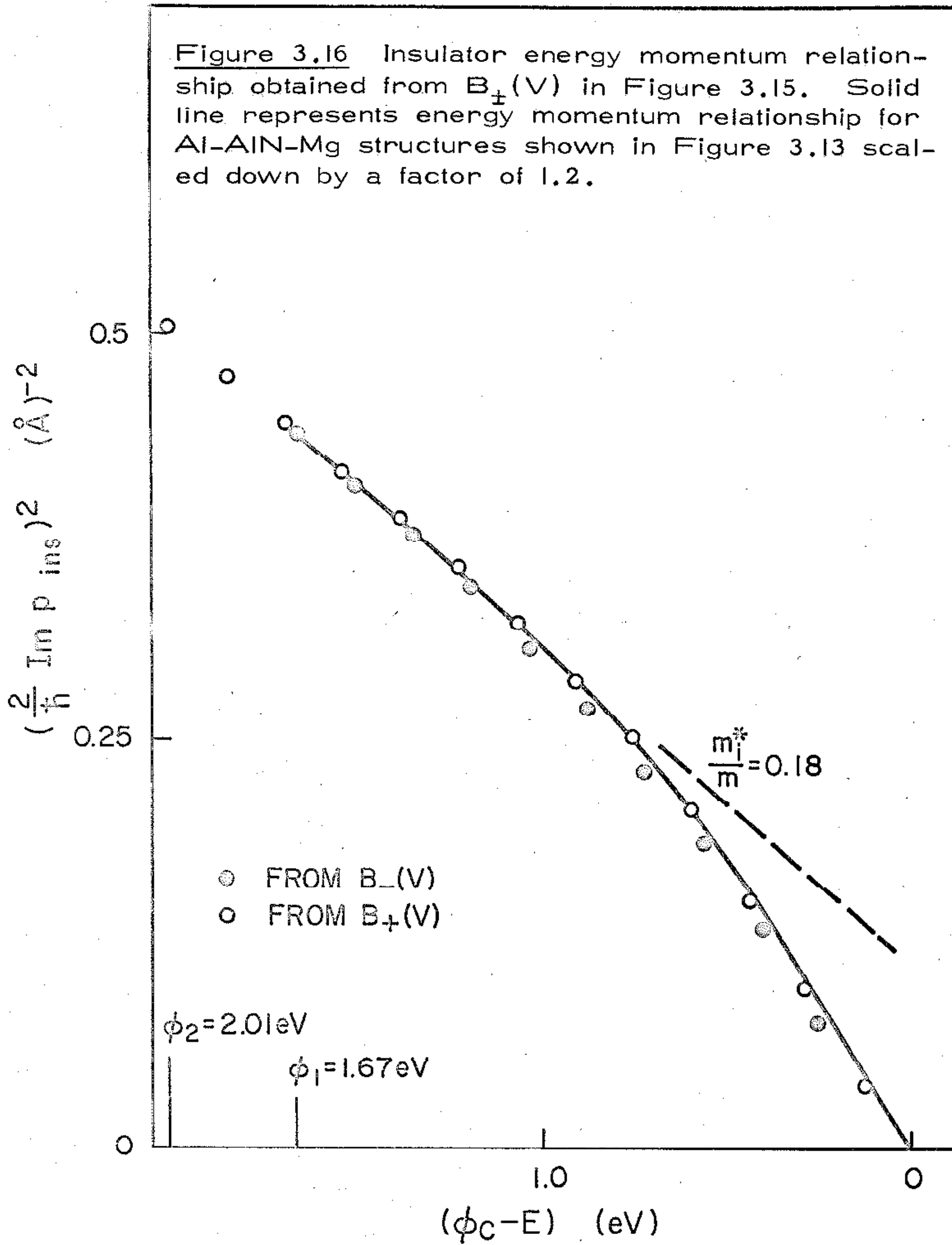

Figure 3.16 Insulator energy momentum relationship obtained from $B_{\pm}(V)$ in Figure 3.15. Solid line represents energy momentum relationship for Al-AlN-Mg structures shown in Figure 3.13 scaled down by a factor of 1.2.

lationship by a factor of 1.2 implies a difference of 5% in the counterelectrode dimentions of the two samples used for the determination of the energy momentum relationship.

The important conclusions to be drawn from the data presented in Figure 3.16 are:

1) The insulator energy momentum relationship is valid in the sense that it describes the tunneling current voltage characteristics in both the structures Al-AlN-Mg and Al-AlN-Al.

2) The barrier at the counterelectrode insulator interface is not fixed by surface states since an increase in ϕ_2 was observed in going from Magnesium to Aluminum counterelectrodes. The increase was approximately 0.5 eV; this value agrees quite well with that expected from the difference between the electronegativities or work functions of the two metals.

3) Franz's empirical relationship accurately describes the observed insulator energy momentum relationship only down to some 1.5 eV below the insulator conduction band edge.

3.2.2 Excess Current Voltage Characteristics.

The excess current was found to be an exponentially decreasing function of thickness; however, the dependence was less pronounced than that of the tunneling currents. As a result, the observed current in structures with thicker insulating regions was

a combination of the tunneling current and the excess current while that observed in structures with the thickest insulating regions was primarily the excess current.

The procedure used to separate the excess current from the observed current in structures with thinner insulators will be described in this section. In addition the current voltage characteristics obtained in this manner will be presented and interpreted along with those appropriate to structures with the thickest insulating regions.

77°K current voltage characteristics of six Al-AlN-Al structures taken from one sample (sample C) and with insulator thicknesses ranging from some 35 to 55 Å are shown in Figure 3.17; the low voltage resistance capacitance product associated with these structures is plotted as a function of insulator thickness in Figure 3.18.

Examination of Figure 3.17 will show that the shapes of the current voltage characteristics depart from those expected on the basis of the insulator energy momentum relationship as the insulator thickness of the structures increases; the logarithm of the current for structures with thicker insulating regions acquires a negative second derivative with respect to voltage at higher voltages. Plots of $\log_{10} J_n(V)$ versus $\log_{10} J_l(V)$ found in Figures 3.19 and 3.20 serve to emphasize this irregularity; approximately straight lines expected on the basis of the tunneling

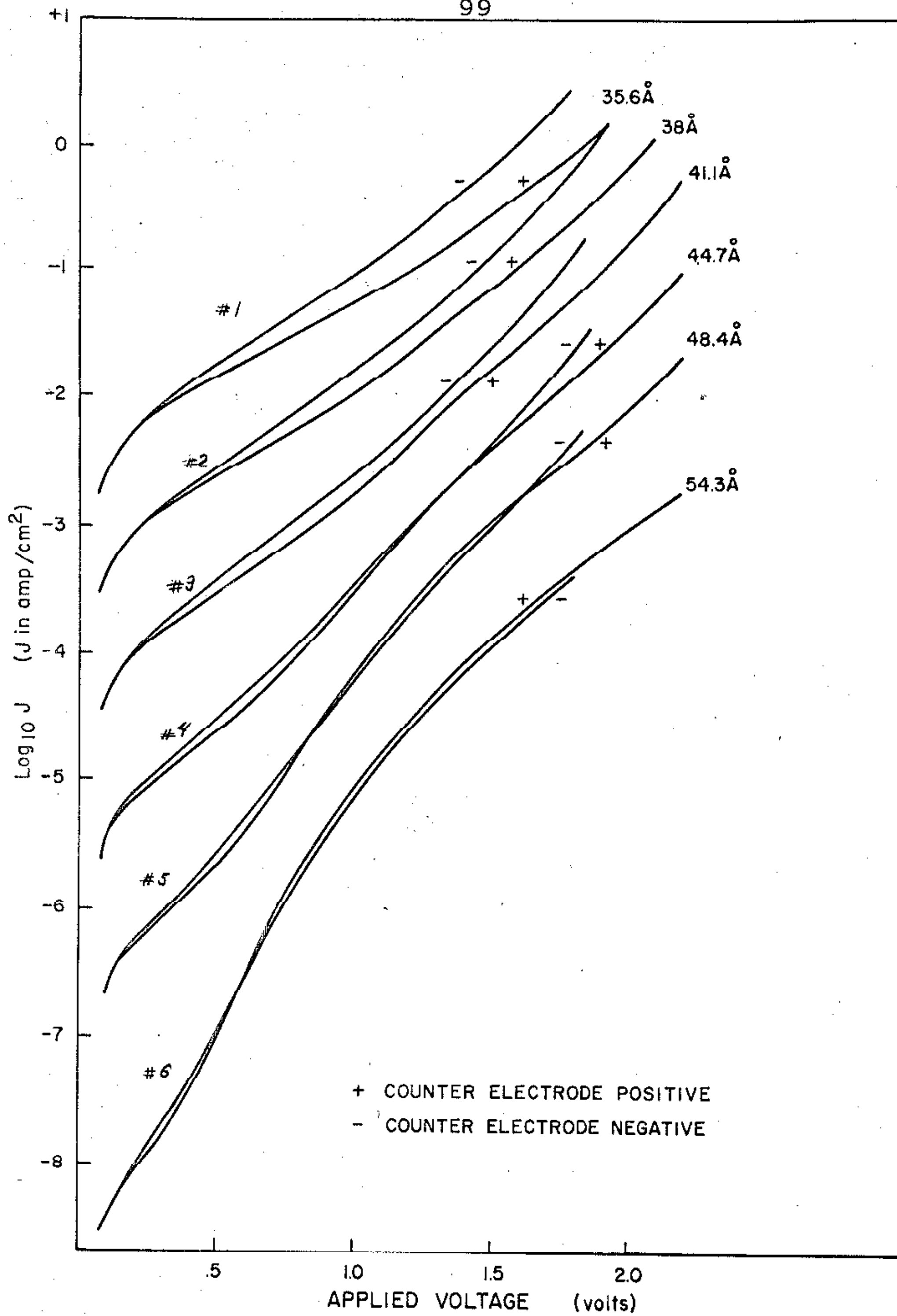

Figure 3.17 77°K current voltage characteristics for six Al-AlN-Al structures with insulator thicknesses ranging from 36 to 54 Å.

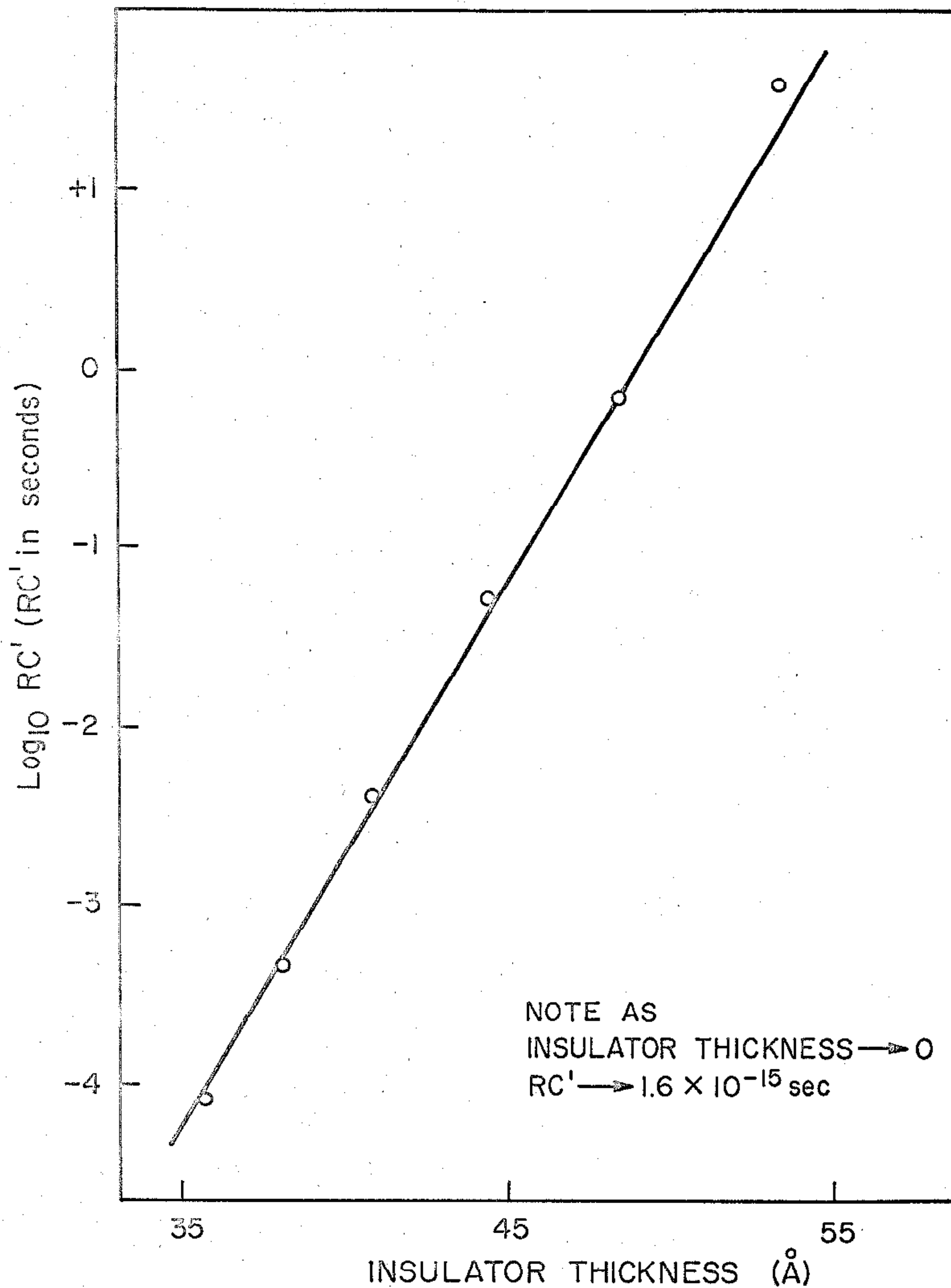

Figure 3.18 RC' versus insulator thickness for Al-AlN-Al structures with characteristics shown in Figure 3.17. (R measured at 77°K.).

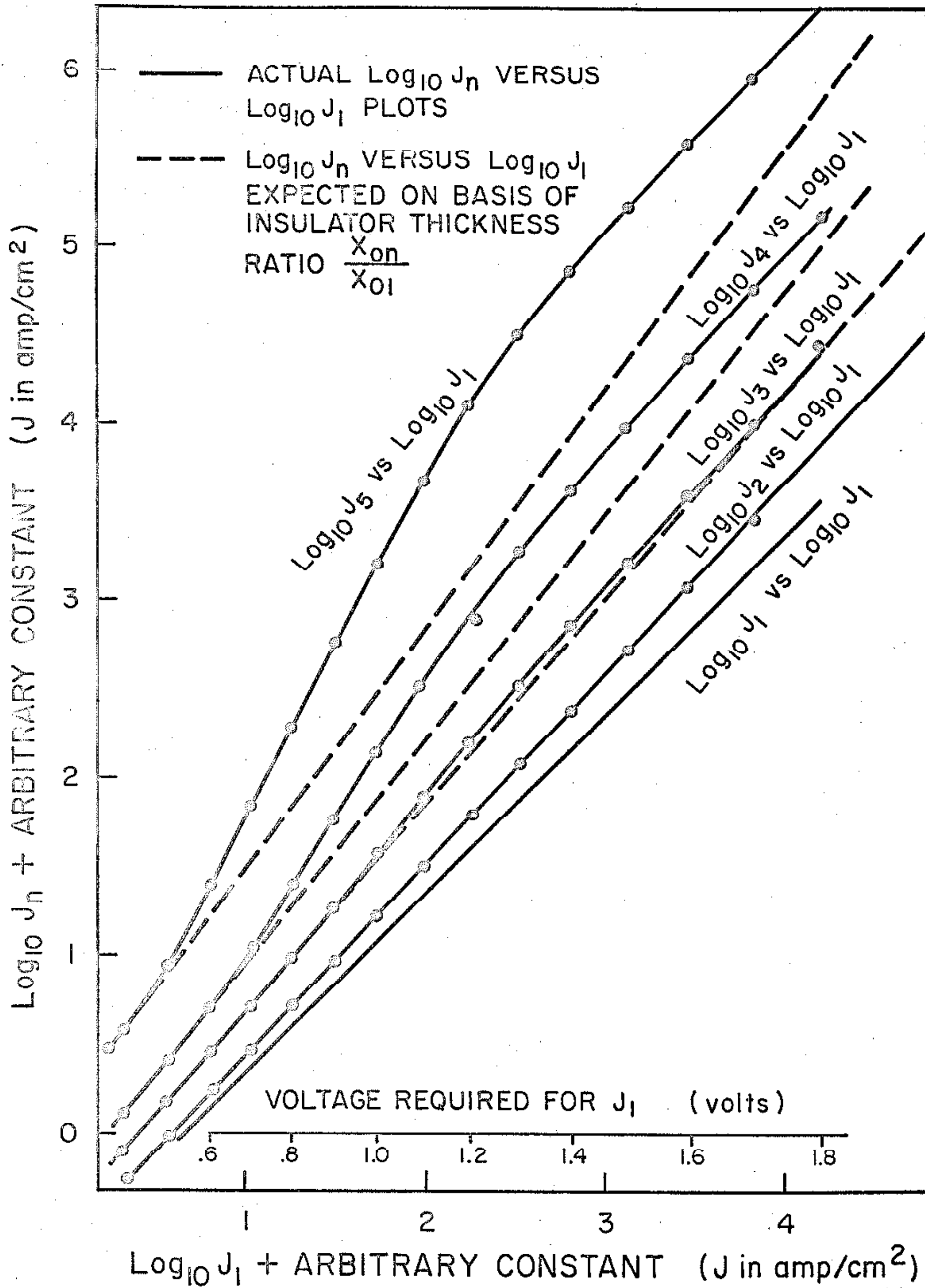

Figure 3.19 $\log_{10}J_n(V)$ versus $\log_{10}J_1(V)$ plots, counterelectrodes negative, for characteristics shown in Figure 3.17.

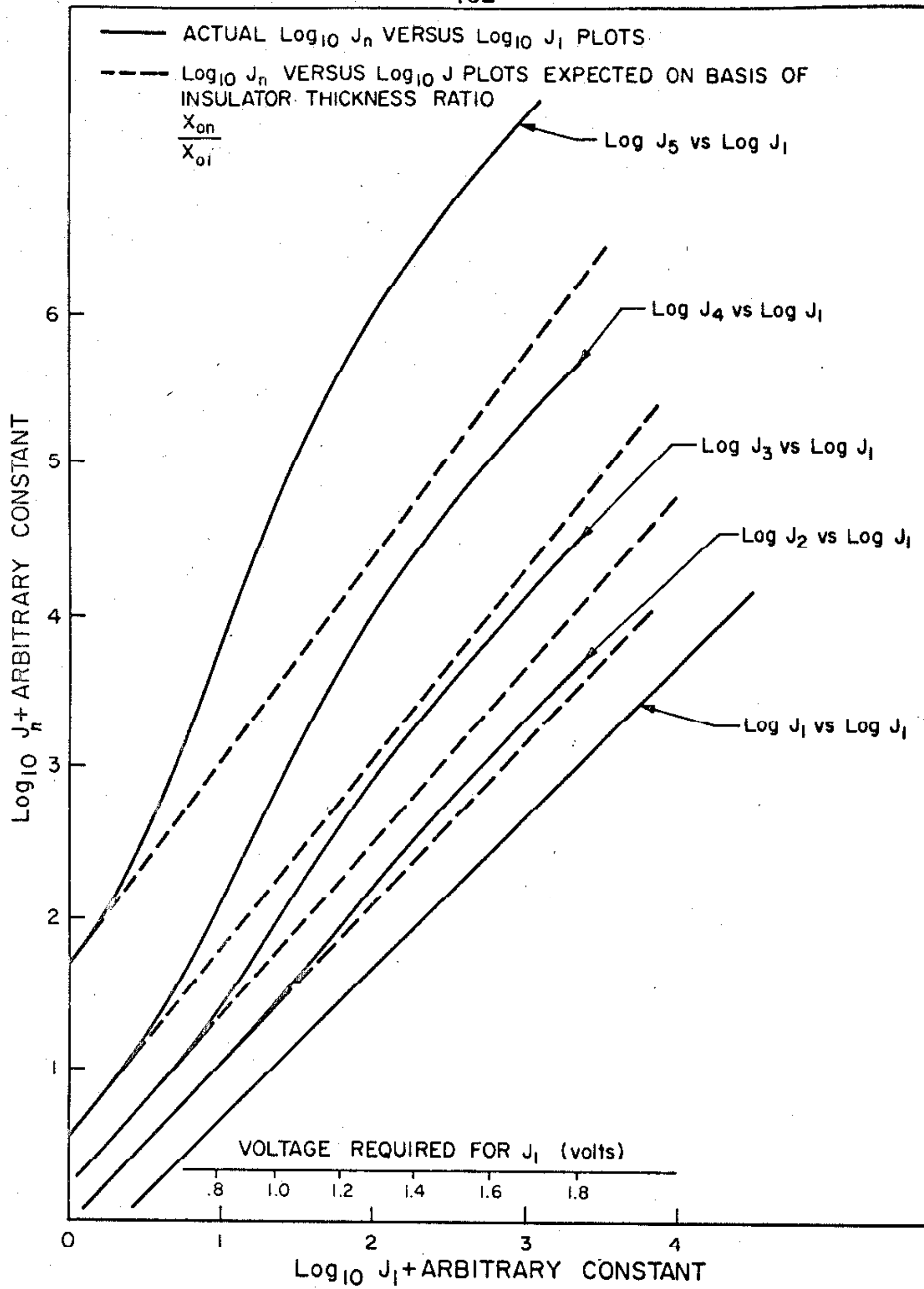

Figure 3.20 $\log_{10} J_n(V)$ versus $\log_{10} J_1(V)$ plots, counter-electrode positive, for characteristics shown in Figure 3.17.

theory are not obtained.

Two conclusions can be drawn from the data presented in Figures 3.17 through 3.20:

1) At low voltages, the current in all six structures is the result of electron tunneling since the low voltage resistance capacitance product of these structures follows an exponential dependence of insulator thickness with a zero thickness intercept very close to that expected on the basis of the insulator energy momentum relationship.

2) The current through the structure with the thinnest insulating region is the expected tunneling current for the range of voltages considered.

Acceptance of these two conclusions leads to a simple procedure for obtaining an estimate of the expected tunneling current at higher voltages for structures with thicker insulating regions. This procedure, based on (1.57) is illustrated in Figures 3.19 and 3.20. Straight lines with slopes $\frac{x_{on}}{x_{ol}}$ were drawn in to match the observed relations $\log_{10} J_n(V)$ versus $\log_{10} J_l(V)$ at low voltages. The values of current defined by these straight lines were considered to be those of the expected tunneling currents. Subtraction of the currents thus obtained from those observed led to the excess current voltage characteristics shown in Figures 3.21 and 3.22. Also shown in Figure 3.22 is the

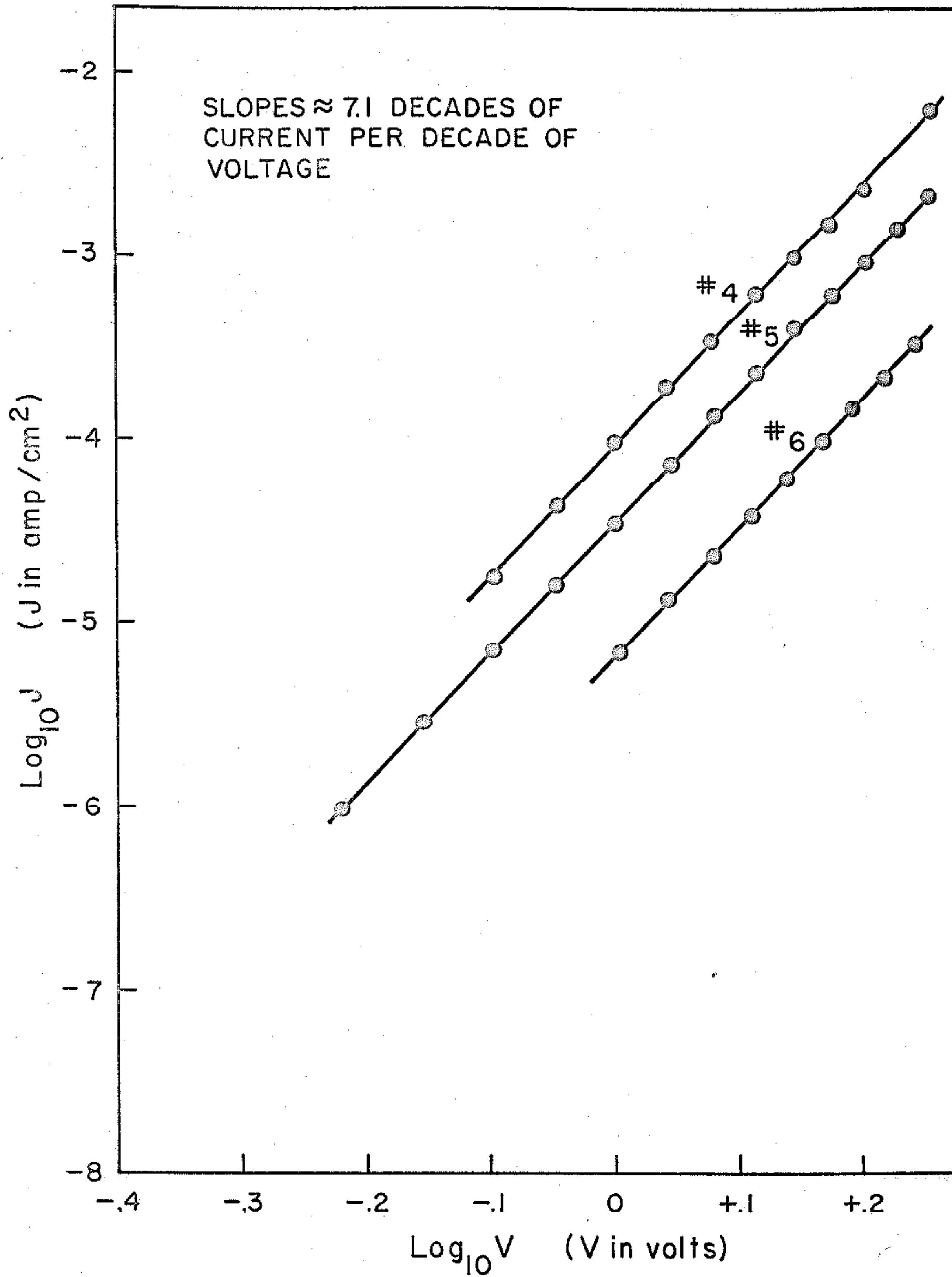

Figure 3.21 77°K excess current in Al-AlN-Al structures. (counterelectrode negative).

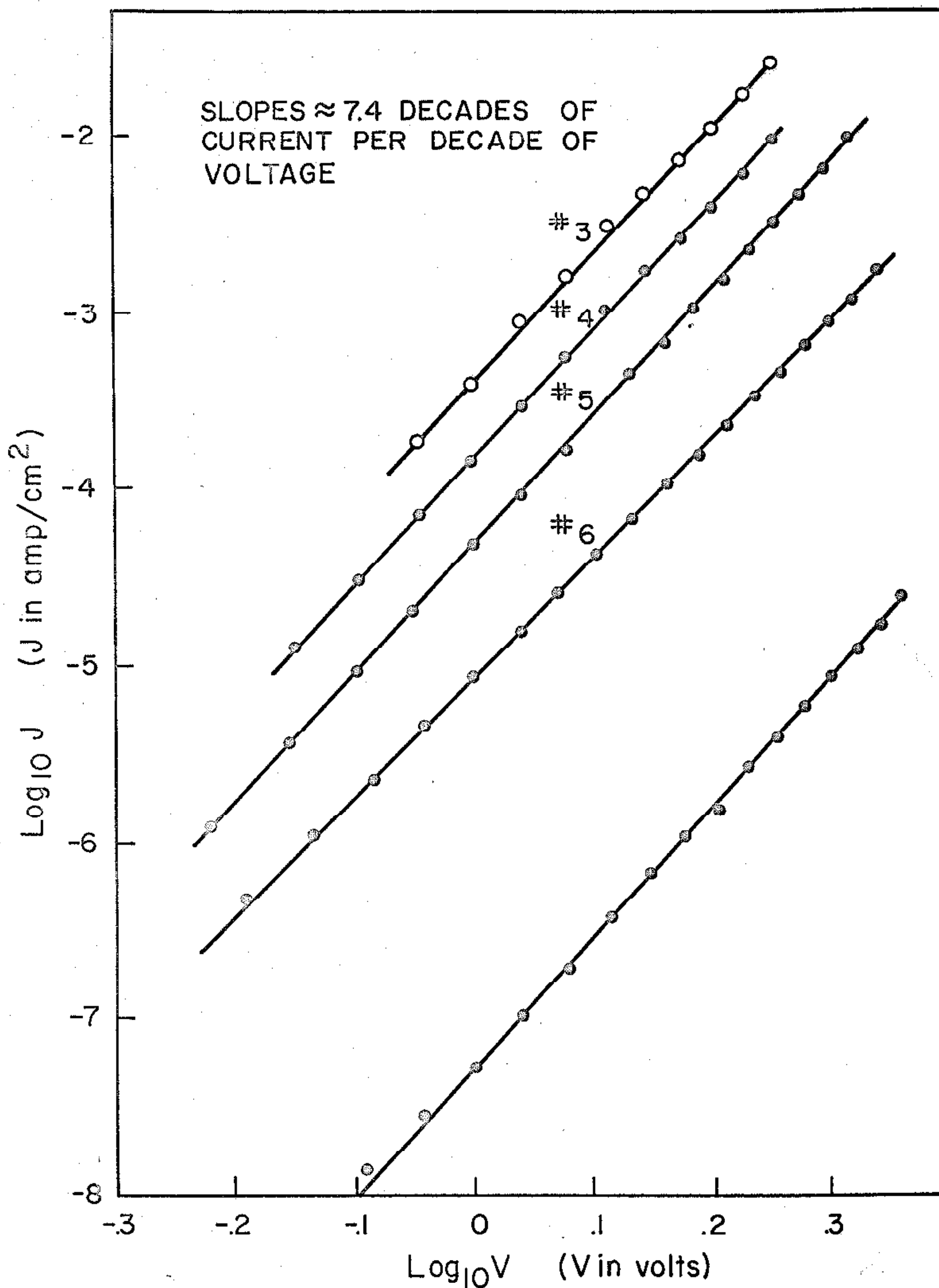

Figure 3.22 77°K excess current in Al-AlN-Al structures. (counterelectrode positive).

77°K current voltage characteristic for an Al-AlN-Al structure with an insulator thickness of 70 Å. This last characteristic, obtained by direct measurement, is seen to be consistent with those obtained by the substracting procedure.

The excess current at 77°K is seen to be related to applied voltage by a power law

$$J_{excess} \propto V^n = \exp[n \ln V] \tag{3.22}$$

where n is independent of insulator thickness and equal to approximately 7.4 and 7.1 for positive and negative voltages applied to the counterelectrode.

The temperature dependence of the excess current was found to be relatively small being more pronounced for low voltages. The current increase between 77°K and 300°K was in the order of a few hundred percent while that between 4°K and 77°K was only in the order of a few percent. At 300°K the characteristic was found to have changed sufficiently so that it could not be accurately represented by a relation of the form given by (3.22). 300°K current voltage characteristics of structures with insulator thicknesses sufficiently large for the direct observation of the excess current are shown in Figure 3.23. It is seen that the current is accurately represented by the relation of the form given by

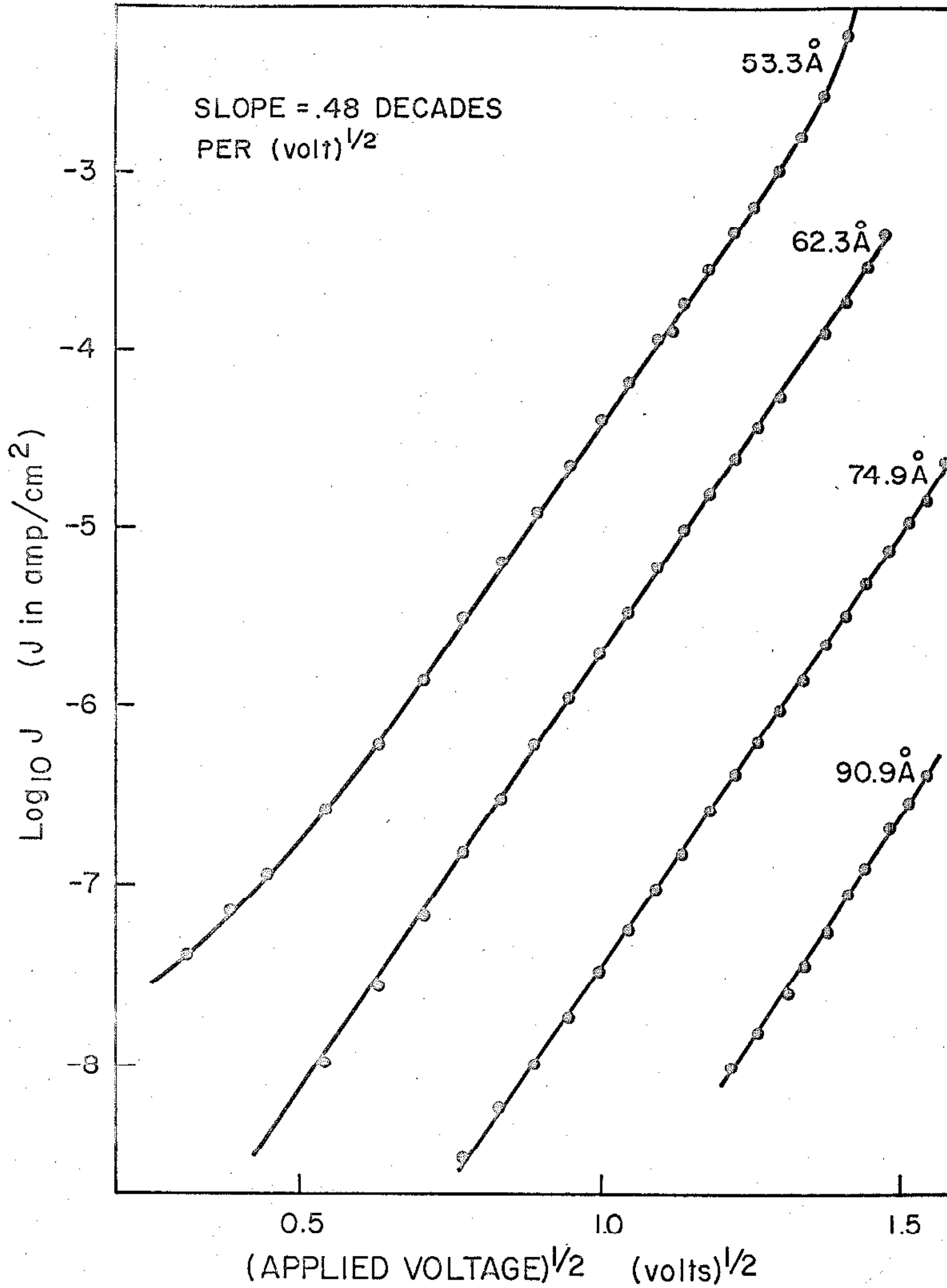

Figure 3.23 300°K excess current in Al-AlN-Al structures with various insulator thicknesses (counterelectrode positive).

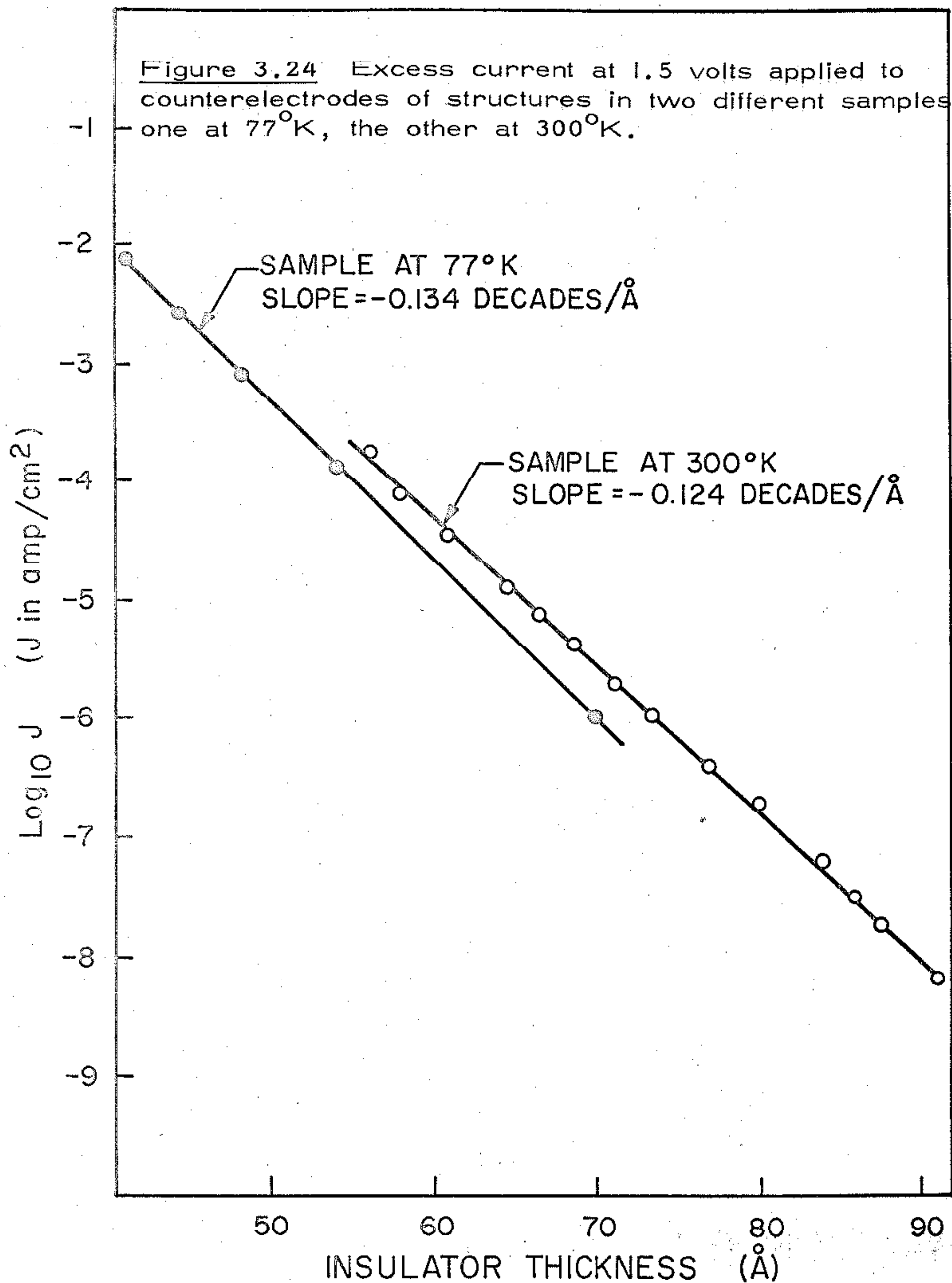

Figure 3.24 Excess current at 1.5 volts applied to counterelectrodes of structures in two different samples one at 77°K, the other at 300°K.

$$J_{excess} \propto e^{\mu V^{1/2}} \tag{3.23}$$
$$\mu = 1.11\ (\text{volts})^{-1/2}$$

where μ is independent of insulator thickness.

The dependence of the excess current on thickness was found to be exponential. Figure 3.24 contains a plot of the current at 300°K and 77°K for 1.5 volts applied to the counter-electrode as a function of insulator thickness.

The striking feature of the excess current is not its detailed dependence on applied voltage but its dependence on insulator thickness. The current is describable by a relation of the form

$$J_{excess} \propto e^{-\delta x_0 + h(V)} \tag{3.24}$$

where δ is independent of voltage. Thus the excess current cannot be attributed to a tunneling process with the tunneling probability exponent proportional to the product of the tunneling path length and $\overline{\text{Im}\ p_{ins}}$ since δ obviously cannot be related to $\overline{\text{Im}\ p_{ins}}$. Nor can the current be attributed to thermionic emission; this process would require a current temperature dependence much greater than that observed.

Undoubtedly the excess current involves tunneling of electrons through the forbidden band since the observed temperature insensitivity implies that non-thermal electrons are responsible for the process. However, the factors affecting the tunneling probability are not understood.

It is also doubtful that the excess current was the result of a sudden variation in the barrier geometry for structures with thicker insulating regions. At sufficiently high voltages the tunneling current was again seen to exceed the excess current. The tunneling current voltage relationship corresponding to negative voltages applied to the counterelectrode such that $eV > \phi_2$ is related to the variation of the tunneling path length with voltage and consequently is a sensitive measure of the barrier shape. The expected relationship is

$$\ln\left[J\left(\frac{\phi_2}{\phi_2-\phi_2+eV}\right)^2\right] = \ln J_0^* - x_0 B^*(\phi_1)\frac{\phi_2}{\phi_2-\phi_2+eV} \qquad (3.25)$$

$$\text{where} \quad J_0^* = \frac{4\pi m_m^* e}{h^3 D^*(\phi_1) C^*(\phi_2) x_0^2}$$

The 77°K current voltage characteristic for an Al-AlN-Al structure with an insulator thickness of 55 Å for high negative voltages applied to the counterelectrode in pulse form (pulse width 50 us) is plotted in a manner appropriate to (3.25) in Figure 3.25. The values used for ϕ_1 and ϕ_2 were those obtained in the determination of the insulator energy momentum relation.

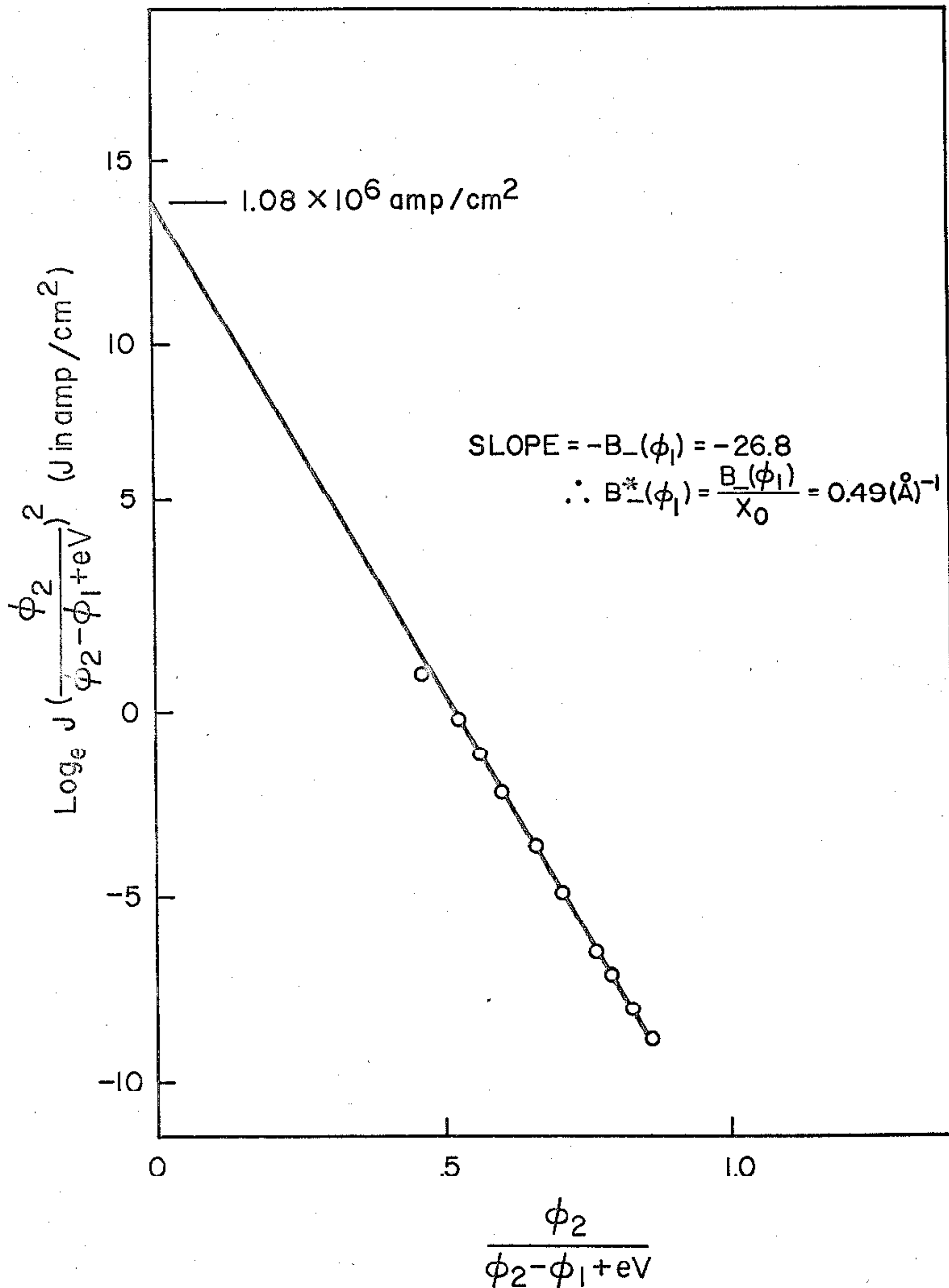

Figure 3.25 77°K current for high negative voltages applied to the counterelectrode of an Al-AlN-Al structure with insulator thickness 55 Å. (ϕ_1 = 1.67 eV; ϕ_2 = 2.01 eV).

It is evident that (3.11) does indeed describe the observed current. The slope of the plot, proportional to $B^*(\phi_1)x_o$, agrees quite well with that expected on the basis of the energy momentum relationship; the extrapolated value for J_o^* is less than a factor of ten smaller than the value expected on this basis.

Current voltage characteristics for high positive voltages applied to the counterelectrode could not be obtained. Indeed the data presented in Figure 3.25 was not easily reproducible. This is easily understood when it is realized that the voltages used for these measurements led to fields within the insulator approaching 10^7 volts per centimeter.

3.3 PROPERTIES OF STRUCTURES WITH GOLD COUNTERELECTRODES

The current voltage characteristics of Al-AlN-Au structures were consistent with those observed in structures having Magnesium and Aluminum counterelectrodes. The tunneling current was dominant in structures with the thinnest insulating regions; the excess current was dominant in structures with thicker insulating regions.

However, a peculiar effect was observed. The capacitance of the structures with the thinnest insulating regions decreased with time. A change of approximately 20% occurred within an hour after fabrication. Further decrease of the capacitance

was negligible. The effect could not be correlated to the variation of the insulator thickness since the magnitude of the tunneling currents through these structures remained essentially constant. Consequently, values of insulator thickness assigned to these structures were rather arbitrary in that they were based on capacitance measurements taken immediately after fabrication.

Figure 3.26 presents the 77°K current voltage characteristic for a structure with an insulator thickness of 52 Å for positive voltages applied to the counterelectrode. A power law is evident

$$J_{excess} \propto V^{n} \tag{3.26}$$

where n = 7.4. It is to be noted that this is the same value of n appropriate to the power law exhibited by excess currents in Al-AlN-Al structures.

The tunneling current voltage characteristics could certainly not be interpreted in terms of a parabolic energy momentum relationship; the current was resistive up to applied voltages of approximately 1 volt (see Figure 3.27). This behavior is, however, consistent with the energy momentum relationship expected within a finite forbidden energy gap.

On the basis of previous data and the difference in work

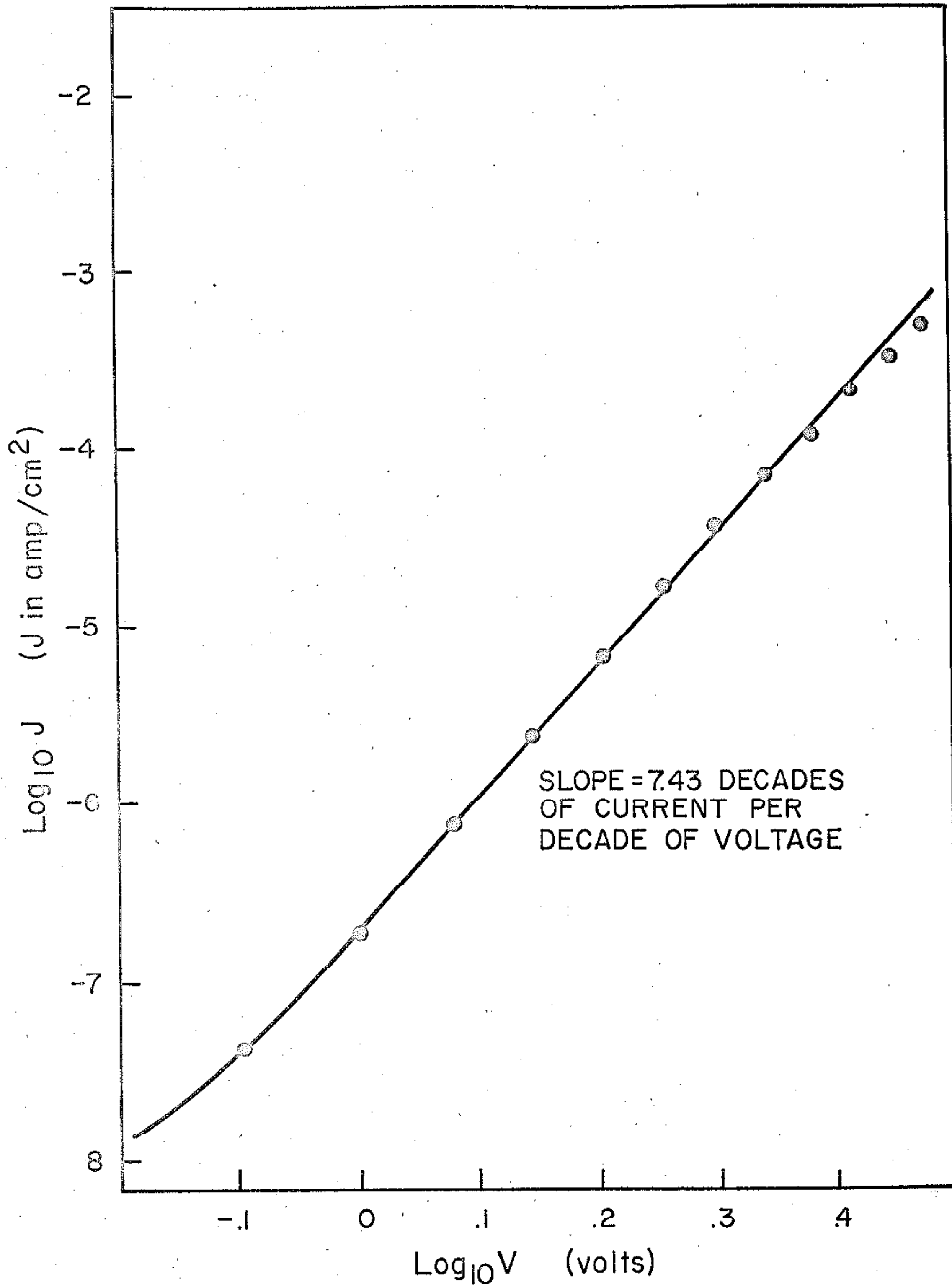

Figure 3.26 77°K excess current in Al-AlN-Al structures with insulator thickness of 52 Å (counterelectrode positive).

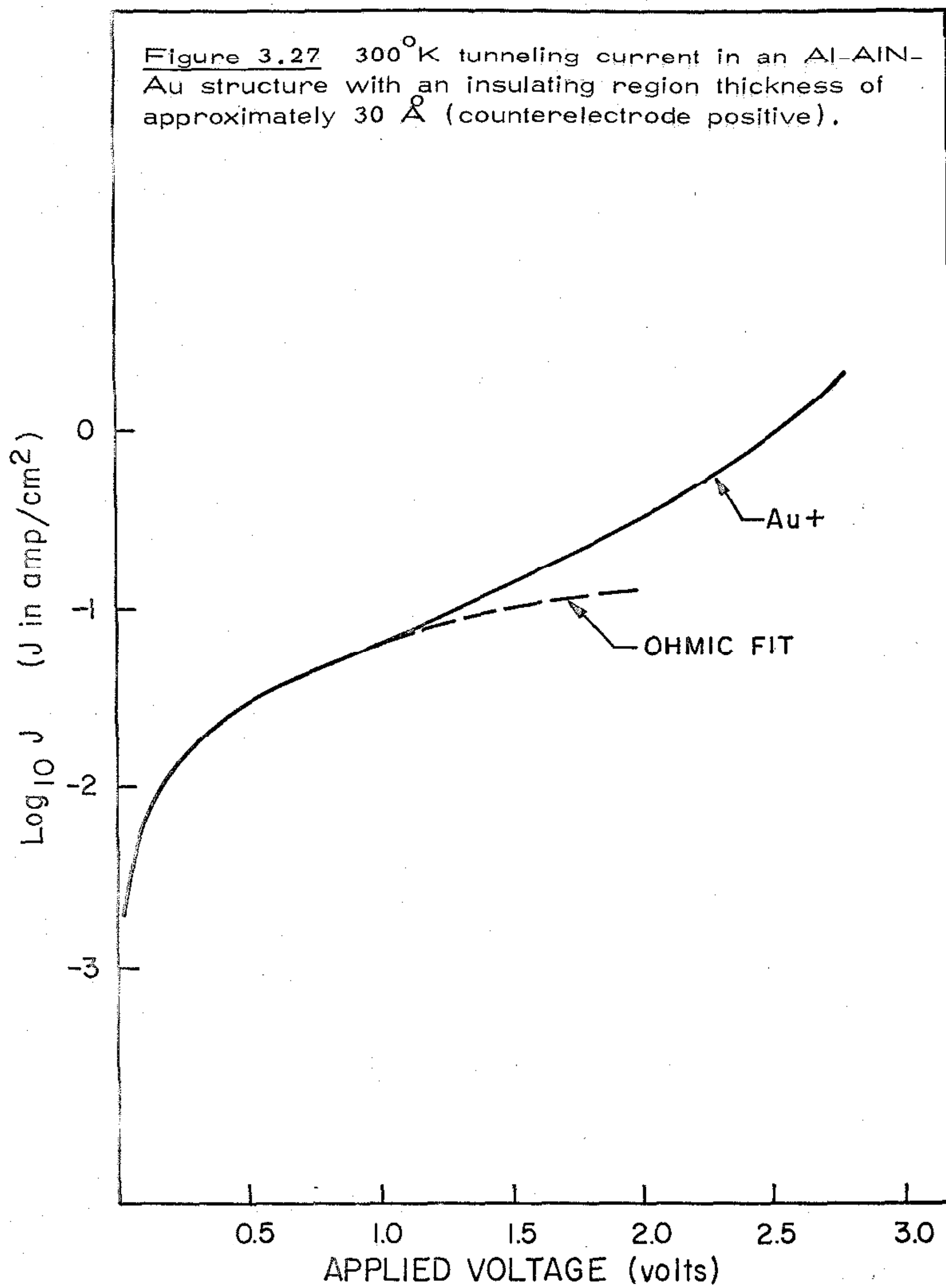

Figure 3.27 300°K tunneling current in an Al-AlN-Au structure with an insulating region thickness of approximately 30 Å (counterelectrode positive).

functions and electronegativities for Gold and Aluminum, ϕ_1 is expected to retain its value of 1.67 eV and ϕ_2 is expected to be in the vicinity of 2.7 eV. Thus the tunneling path corresponding to low applied voltages covers energies ranging from 2.7 to 1.67 eV below the insulator conduction band edge. Since the forbidden energy gap of AlN is 4.2 eV, Im p_{ins} will at these energies be either independent of energy or decreasing towards a zero value at the insulator valence band edge. The tunneling probability, proportional to the tunneling path length and $\overline{\mathrm{Im}\ p_{x\ ins}}$ encountered along a tunneling path, is thus expected to be independent of voltage until the tunneling path starts to cover energy ranges where Im p_{ins} decreases with increasing energy.

The observation that the tunneling current was resistive up to applied voltages of approximately 1 volt is consistent with this picture.

3.4 CONCLUSION

Currents through insulating layers of Aluminum Nitride were identified as those resulting from electron tunneling not on the basis of fitting experimentally observed current voltage characteristics to those predicted on the basis of some arbitrary model but rather on the basis of the dependence of these characteristics on insulator thickness. The characteristics themselves were used to obtain some specific information about the energy momen-

tum relationship within the forbidden band of Aluminum Nitride. It was found that the effective mass to free electron mass ratio at the conduction band edge was 0.40 ± 10%. Evidence that $(\text{Im}\ p_{ins})^2$ became independent of energy below that halfway between the valence and conduction band edges indicated that the effective mass to free electron mass ratio at the valence band edge was greater than that at the conduction band edge. The different values for ϕ_2 obtained with the use of various counterelectrode metals indicated that surface states played a minor role in determining the barrier energy at the counter-electrode insulator interface.

REFERENCES

1. Morse and Feshbach, Methods of Theoretical Physics (McGraw-Hill, New York, 1953), pp. 1092-1106.

2. W.A. Harrison, Phys. Rev., 123 , 85, (1961).

3. M.Aven,C.A.Mead,App. Phys. Lett., Vol. 6 No. 6, 103, (1965).

4. W.C.Spitzer, C.A. Mead, Phys. Rev. 134 A. 712, (1964).

5. W.R. Smythe, Static and Dynamic Electricity (McGraw-Hill, New York, 1950), Chapt.5.

6. H.K. Henisch, Rectifying Semiconductor Contacts (Oxford at the Clarendon Press, 1957) p.171.

7. W. Schottky, Z. Physik, 15, 872, (1914).

8. J. Lagrenaudie, J. Chim. Phys., 53, 222, (1956)

9. F. Keffer, A.M. Portis, Jour. Chem. Phys., 27, 675 (1957)

10. R.Stratton, J. Phys. Chem. Solids, 23 1177 (1962).

11. J.G. Simmons, J.App. Phys., 34, 2581, (1963).

12. D. Meyerhofer, S.A. Ochs, J. App. Phys., 34 2535.

13. J.E. Hartmann, J. App. Phys., 35, 3283, (1964).

14. R. Stratton, G.W. Lewicki, C.A. Mead, J. Phys. & Chem. Solids, (To be published)

15. N. Sclar, J. App. Phys., 33, 2999, (1962).

16. W. Franz, Handbuch der Physik (Edited by Flugge, S.) Volume 17, p. 155., Springer, Berlin (1962).

17. Morris, Braunstein, J. App. Phys., (To be published).

18. Hannay, Semiconductors (Reinhold Publishing Corporation,

New York, 1959), p.450.